Relaxation Analysis of Cathode Materials for Lithium-Ion Secondary Battery

Imsul Seo

Graduate School of Energy Science

Kyoto University

2013

Relaxation Analysis of Cathode Materials for Lithium-Ion Secondary Battery

Imsul Seo

Department of Fundamental Energy Science

Graduate School of Energy Science

Kyoto University

2013

Table of Contents

CHAPTER 1

INTRODUCTION

1.1 Battery

The battery is generally defined as a device system containing an electric cell or series of electric cells storing energy that can convert energy from chemical potential into electrical power. Batteries are divided into the primary battery and secondary or rechargeable battery, here the former is designed to be used once and discarded, otherwise the latter is able to be recharged with electricity and reused for much more cycle time. The first commercialized primary battery is zinc-carbon battery (manganese drycell, the first dry cell). It consists of a manganese dioxide cathode, a zinc anode and acidic aqueous electrolyte mixed with ammonium chloride (NH_4Cl) and zinc chloride ($ZnCl_2$), which provides a voltage of 1.43V.

$$Zn(s) + 2MnO_2(s) + 2\ NH_4Cl(aq) \rightarrow ZnCl_2 + Mn_2O_3(s) + 2NH_3(aq) + H_2O$$

Until the late 1950s the zinc-carbon battery continued to be a popular primary cell battery (The zinc-carbon battery is still manufactured today.), but it exhibits relatively low battery life. In the end of 1950s, the alkaline batteries with alkaline electrolyte of potassium hydroxide (KOH) instead of the acidic ammonium chloride or zinc chloride electrolyte in existing zinc-carbon battery, were invented, which features higher energy density and longer shelf-life than those of zinc-carbon battery, even with the same voltage (1.43V). Since the commercialization of 3V level primary batteries by the application of the lithium metal to the anode in the 1970s, the performance of primary battery was made considerably advanced progress.

The first rechargeable battery, lead-acid battery was invented in 1859, which consists of a lead anode and a lead dioxide cathode immersed in sulphuric acid. In the discharged state both the positive and negative plates become lead (II) sulfate ($PbSO_4$) and the electrolyte loses much of its dissolved sulfuric acid and becomes primarily water.

The total reaction can be written:

$$Pb(s) + PbO_2(s) + 2H_2SO_4(aq) \rightarrow 2PbSO_4(s) + 2H_2O(l)$$

Despite exhibiting a very low energy-to-weight ratio and a low energy-to-volume

ratio, their ability to supply high surge currents means that the batteries maintain a relatively high power-to-weight ratio (2V/cell). These performances, along with their low cost, make them attractive for application to motor vehicles to provide the high current required by automobile starter motors.

In 1946, the nickel and cadmium battery (Ni/Cd battery), a rechargeable alkaline battery that had nickel and cadmium electrodes in a potassium hydroxide solution was commercialized, which is the first battery to use an alkaline electrolyte. At this point in time, however, its use is limited due to environmental impact by use of toxic heavy metal and memory effect occurring voltage depression, etc. [1]

Recently, nickel–metal hydride batteries (Ni-MH, 1.2V) and lithium secondary batteries (3-4V level) have become commercially more available and cheaper. Ni-MH batteries commercialized in the early 1990 tend to have longer lifespan than Ni/Cd batteries, even in recent they have been interested about the potential of lifespan increase by the application of new alloys and less damaging to the environment. [2, 3]

Lithium ion secondary batteries are currently the most common in consumer electronics such as mobile phones, laptops and tablets, etc. and electric vehicles (EVs) due to high energy density with 3-4V (This point makes LIBs applied not only to the portable electronic devices, but also to EVs), no memory effect (however, recent new studies have shown signs of memory effect in LIB [4]) and only a slow loss of charge when not in use during relaxation time.

1.2 Lithium ion battery

During a little over 200 years of battery history, there were two epoch-making progresses in battery technology. The one is advancing from the primary battery system to the secondary battery system and another is increase of operation voltage to 3V level. Recently, the lithium secondary batteries became one of typical battery leading technology innovation compared with any other existing well-known batteries, in realizing the most outstanding energy density with light weight and 3.7V of high average operation voltage by utilizing the lithium ion as charge carrier between electrode and electrolyte.

The secondary batteries require a system construction that can repeatedly carry out charge/discharge process between cathode and anode.

1. To be easy for ion as charge carrier to insertion and extraction in cathode and anode

2. For the insertion and extraction, the structure of electrode materials must be maintained stably.

3. Electrolyte to perform the charge transfer without unnecessary side reaction.

Figure 1-1 shows the schematic diagram of construction for the typical lithium secondary battery. During discharge process, lithium ions Li^+ carry the current from the negative electrode to the positive electrode through the non-aqueous electrolyte and separator.[5] During charge process, an external charging circuit applies an over-voltage than voltage produced by the battery, forcing the current to flow in the reverse direction. Then, the lithium ions migrate from cathode to anode in a process known as electrochemical insertion or intercalation. Therefore, the electrode materials and the kind of ion migrated as charge carrier are main factor to determine the amount of electric energy saved in battery, the lithium ions play that role in the lithium secondary battery.

Under standard conditions, the lithium is the lightest metal element, even with the lowest standard reduction potential (E^o). When applied to a typical lithium ion battery, that is, approximately 3V of electromotive force (2.1V for lead-acid or 1.5V for zinc-carbon batteries) can be generated, which means that they have the high energy density per unit weight and unit volume. The lithium secondary batteries typically use non-aqueous electrolytes with mixture of organic carbonates because they are usually under the condition of higher operation voltage than water splitting voltage. For the electrode materials, oxide and graphite system with lattice structure favorable for lithium insertion or extraction are generally used as cathode and anode material, respectively. Since the lithium exists as a part of lattice structure in cathode material and is extracted as a type of ion at charge process, transition metal oxide with high structural stability has taken center stage. Lithium ion secondary batteries (LIBs) and lithium ion polymer batteries (LIPBs) are adopting liquid electrolyte and polymer electrolyte, respectively.

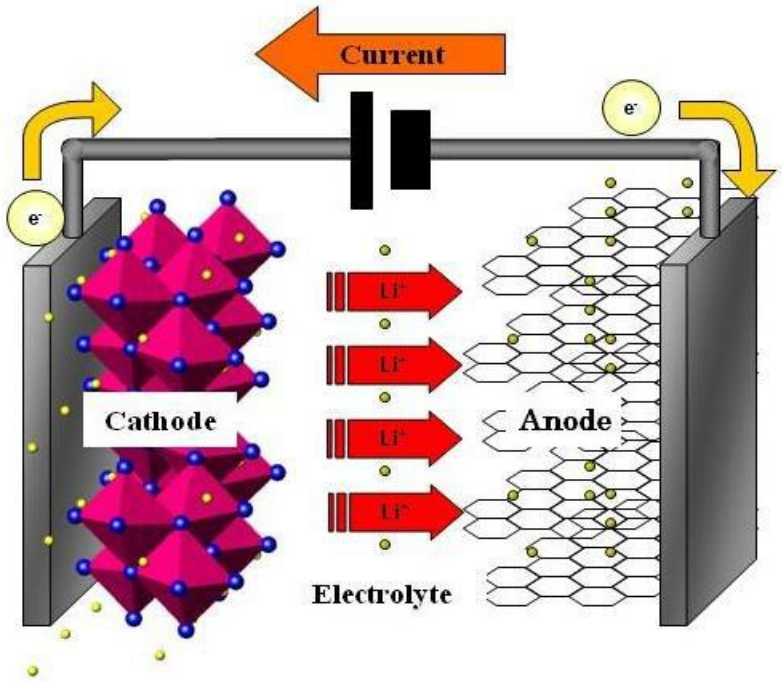

Figure 1-1. Schematic diagram of construction for lithium secondary battery

1.2.1 Cathode

In order for cation as charge carrier to perform high rate charge/discharge with reversibly wide oxidation-reduction (redox) potential range and to minimize crystal structure change of electrode material, small ion radius and low valence (weak bonding force with active material) is essential. In that regard, lithium ion is the most suitable cation as charge carrier for secondary battery. Though beryllium ion has smaller radius than that of lithium ion, considerably improper to increase operating voltage of battery in that its standard reduction potential (-1.847V) is much higher than that of lithium ion (-3.040V).

3d transition metal as cation in cathode materials features higher electrode potential, relatively light and small size than 4d and 5d transition metal, which provides important advantage in capacity properties. Since the lithium exists as a part of lattice structure in cathode material and is extracted as a type of ion at charge process, transition metal oxide with structural stability has taken center stage.

Cathode materials for LIBs generally require following properties.

1. Maintaining reversible reaction and flat potential (plateau) change over wide range of lithium constant to increase energy efficiency during charge/discharge process.

2. Light and consolidated structure for high energy density per unit weight and unit volume, high electronic and ion conductivity for high power

3. High cycle efficiency. Side reactions regardless of lithium ion circulation between cathode and anode raise fade cycle property.

4. Irreversible phase transition in crystal structure that is one of main reason of capacity fading, do not occur during charge/discharge process.

5. Chemical, electrochemical and thermal stability to avoid reaction with electrolyte.

Since the commercialization of LIBs with $LiCoO_2$ cathode and carbon anode in 1991, various research study on cathode materials for LIBs, such as layered structure $LiMO_2$ with lithium transition metal oxide, spinel structure LiM_2O_4, olivine structure $LiMPO_4$, etc. have been performed. Most recent handheld electronics adopt LIBs based on

lithium cobalt oxide ($LiCoO_2$) system, which offers high energy density, but have well-known safety concerns, especially when damaged.[2, 6, 7] Lithium manganese oxide (LMO), lithium nickel manganese cobalt oxide (NMC) and lithium iron phosphate (LFP) offer lower energy density, but longer lifespan and inherent safety. NMC in particular is a leading contender for automotive applications. Lithium nickel cobalt aluminum oxide (NCA) and lithium titanate (LTO) are specialty designs aimed at particular niche roles.[8-10] Figure 1-2 shows the relationship between the potential and capacity of common cathode and anode for LIBs. [3]

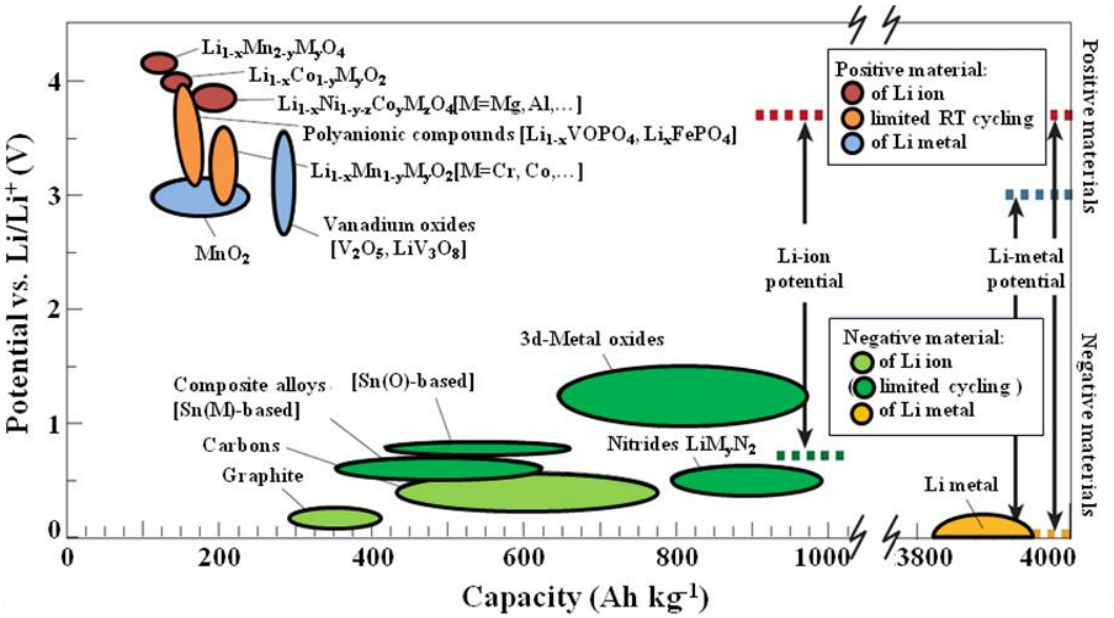

Figure 1-2. Relationship between potential and capacity of common cathode and anode for LIBs. [3]

1.2.1.1 Spinel structure cathode

Electrode materials with the spinel type LiM_2O_4 (M=Ti, V, Mn) structure are attractive for LIB, because the spinel structure is a thermodynamically highly stable, and many compounds in nature exist with this structure. In LiM_2O_4 compound with spinel structure of cubic system, oxygen occupy 32e sites of crystallographic position with face centered cubic (FCC) of ABCABC frame, as indicated figure 1-3. The cation in 16d octahedral sites and the oxide ions act as a spinel M_2O_4 host with a three dimensional interstitial space of 16c octahedral and 8a tetrahedral sites.[11]

Typical spinel cathode is $LiMn_2O_4$ suggested by Goodenough et al. in 1983. In spinel $LiMn_2O_4$, lithium, manganese and oxygen ions occupy the tetrahedral 8a sites, octahedral 16d sites and 32e sites in crystallographic position with the $Fd\bar{3}m$ space group respectively, showing the three dimensional diffusion paths for the lithium ions, as shown in figure 1-4. [12]

The spinel phase in $Li_xMn_2O_4$ exhibits two distinguishable regions in the potential- Li content curve vs Li as shown in figure 1-5, a plateau at around 4.2V in the range $0<x<0.5$ and a continuous, gradual change at around 4.0V in the lithium content range $0.5<x<1$. The 4.2V plateau is due to the coexistence of two spinel phases, one with lithium in octahedral sites and the other with lithium ordered at 8a sites on the face centered cubic arrays. The Li^+ ions occupy the 8a sites randomly in the 4.0V range. [12, 14-16] Amatucci et al. have reported that the capacity fade in the 4V range of $Li_{1-x}Mn_2O_4$ occurs mainly at the end of discharge process. [17]

Although the spinel $LiMn_2O_4$ exhibits great potential possibility, given its low-cost, good electronic and lithium ion conductivity, and three-dimensional structure with a good structural stability, but shows a poor cycling behavior at elevated temperature, e.g., 50°C~80°C.[13,18,19] The main factors for the cyclablity failure in 4V region at elevated temperature are as follows.

1. Dissolution of MnO induced by HF formed by the reaction of fluorinated anions and residual H_2O.

2. Phase transition from cubic to tetragonal by Jahn-Teller distortion

3. Oxygen deficiency. [20-22]

The poor cycle performance can be improved by cation or anion substitution and surface modification of electrode material. [23-25]

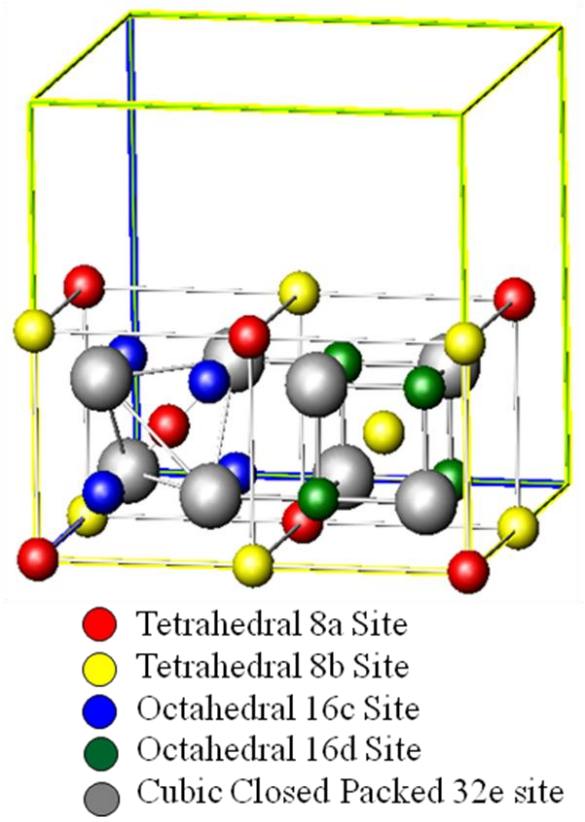

Figure 1-3. Two quadrants of $Li[M_2]O_4$ spinel structure

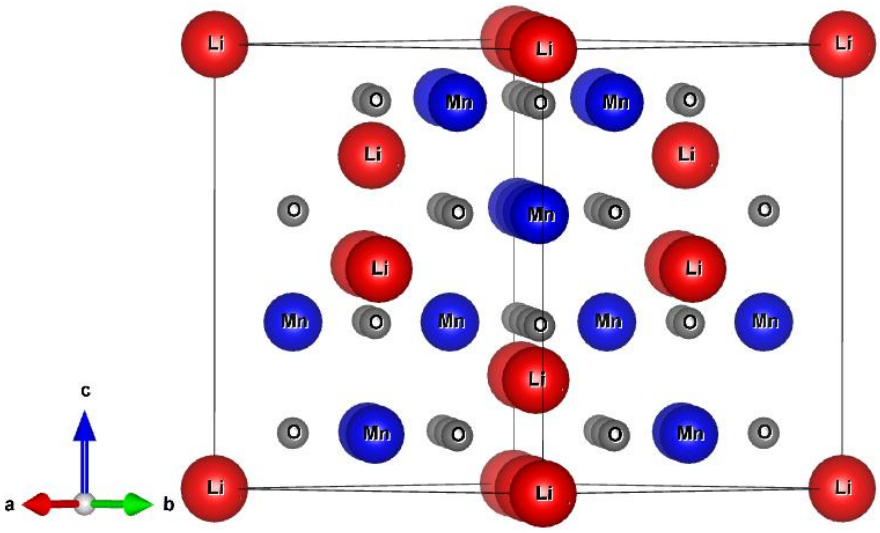

Figure 1-4. Three-dimensional octahedron arrangement in $Fd\bar{3}m$

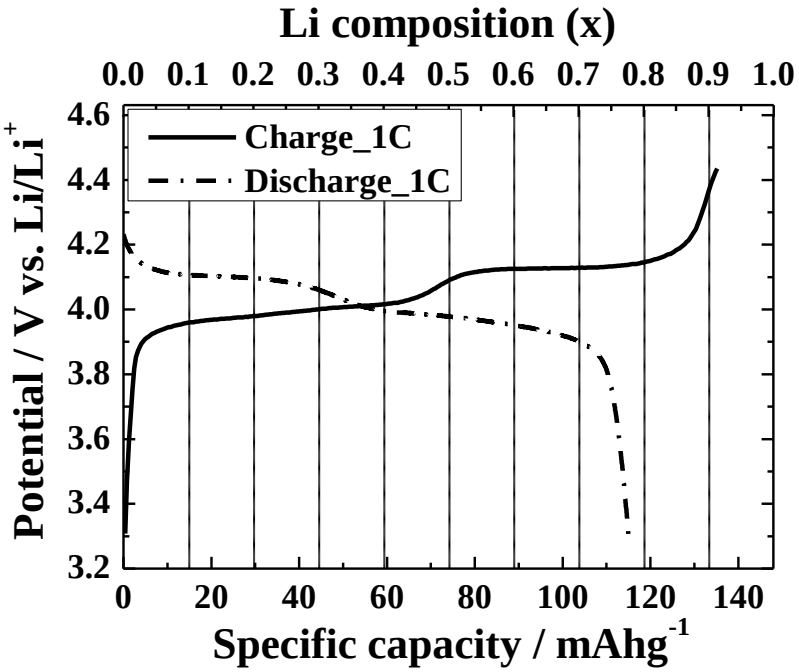

Figure 1-5. Two distinguishable regions at the potential-content curve vs Li in $Li_xMn_2O_4$ spinel phase

1.2.1.2 Layered structure cathode

$LiMO_2$ type lithium transition metal oxide with layered structure exhibits the densest arrangement of forming ionic bonding crystal structure. The closest packing structure composed of lithium ion, transition metal (M) ion and oxygen have a structure with the highest packing density by filling the lithium ion and M ion into the space of the frame layer with large size of oxygen ions in regular sequence. The oxide ions form a cubic-close packed structure with (111) close-packed octahedral site planes alternately filled with Li^+ and M^{3+} ion, as shown in figure 1-6, which is a hexagonal unit cell with $R\bar{3}m$ space group, signifying a rhombus-like unit cell with threefold improper rotational symmetry and a mirror plane.[26] This arrangement leads an ordered strictly two dimensional structure as shown in figure 1-6, where MO_2 slab and the LiO_2 slab are also marked. The lithium ion is located in the crystallographic 3a site, the transition metal M^{3+} ion is located in the 3b site, and the oxide ion resides in the 6c site with a ionic distribution of $[Li]_{3a}(M)_{3b}\{O_2\}_{6c}$. In this structure, both the lithium and transition metal ions occupy the octahedral sites. In a 'nonideal' layered $LiMO_2$ cathode, there will be some transition metal ions present in the lithium layer due to cation disorder, which can raise serious implications on the rate capability of the cathode and the observed phase relationships on lithium extraction process. [27, 28]

$LiCoO_2$

The commercially used $LiCoO_2$ is the most popular cathode in the layered oxide system, because of its favorable stoichiometric synthesis, excellent reversibility and a high electrochemical potential at the lithium contents x from 1 to 0.5 in terms of Li_xCoO_2. [29-32] It consists of layers of lithium that lie between slabs of octahedron formed by cobalt and oxygen atoms. Both lithium and cobalt are octahedraly coordinated by oxygen. These octahedrons are edge-sharing, and tilted relative to the layered structure. The major drawbacks of $LiCoO_2$ are toxicity, high cost, and the limited capacity of $140mAhg^{-1}$. Although most of the lithium can be extracted from $LiCoO_2$, only about half can be extracted reversibly. Removal of greater amounts of lithium beyond extraction limit attribute to phase transitions, large changes in unit cell volume, and the evolution of oxygen at voltage in excess of 4.2V vs. Li due to a large $O^{-2}p$ character of the holes. [32-35]

$LiNiO_2$

The nickel based $LiNiO_2$ offers a less expensive alternative to $LiCoO_2$, and it can

exhibits about 190 $mAhg^{-1}$ of discharge capacity. However, $LiNiO_2$ cathode has several serious drawbacks. It was known that it is difficult to prepare stoichiometric $LiNiO_2$. In addition, the consequent presence of nickel ions in the lithium plane (cation disorder of lithium and nickel ion), Jahn-Teller distortion associated with the presence of low-spin Ni^{3+}:d^7 ion, irreversible phase transitions upon lithium extraction process, and the loss of oxygen at elevated temperature are main reason interrupting its commercialization. [36] Recently, partially cobalt-substituted $LiNi_xCo_{1-x}O_2$ cathode achieves a better, stable reversible capacity of about $180mAhg^{-1}$. The partial substitution of cobalt exhibits the effect of stabilizing the layered structure with better ordering as well. [37]

$LiNi_xCo_{1-2x}Mn_xO_2$

Three transition metal system of Ni-Co-Mn exhibits excellent electrochemical properties combined with various merit like high capacity of $LiNiO_2$, stable electrochemical properties of $LiCoO_2$ and thermal stability and cost-effectiveness in manganese of $LiMnO_2$.[38-40] According to a first-principles study reported by Ohzuku et al, $LiNi_{1/3}Co_{1/3}Mn_{1/3}O_2$ consists of Ni^{2+}, Mn^{4+}, and low-spin state of Co^{3+} and is crystallized as the super-lattice by improving preparation methods.[40]

The structural variation during charge/discharge process in $Li_xNi_{1/3}Co_{1/3}Mn_{1/3}O_2$ appears that lattice constant c is totally increase with the decrease of lithium content x, but in $x<0.35$ it decrease due to increase of interlayer repulsion by oxygen loss. The lattice constant a exhibits opposite trend with c. [41] As a result, volume change during charge/discharge process almost constant, which means great advantage as cathode material. Therefore, $Li_xNi_{1/3}Co_{1/3}Mn_{1/3}O_2$ is able to realize superior charge/discharge properties, cyclability and long lifespan during battery operation.[42, 43] Although this cathode material is similar with $LiCoO_2$, the reason for regarding as an alternative to $LiCoO_2$ is having competition in cycle performance, stability and cost-effectiveness. [39-41] To improve its capacity property with remaining these merits, in addition, recently the development for materials increasing nickel contents x in $LiNi_xCo_{1-2x}Mn_xO_2$ system have been conducted. [44, 45]

1.2.1.3 Olivine type cathode

One of the most abundant metal elements, iron is not only much low price than cobalt, but also environmentally friendly. According to this point, cathode materials containing iron has been developed from the past, of them the most well-known is $LiFePO_4$ with olivine structure. $LiM(PO_4)$ compounds form the olivine structure as shown in figure 1-7, which exhibits a nearly close-packed-hexagonal oxide array. The Li^+ and M^{2+} ions

are located at octahedral sites and are arrayed into alternate (001) planes, which allow two dimensional conduction of lithium ion. Electrochemical lithium extraction give electromotive force, $Fe^{3+}/Fe^{2+} \approx 3.5V$ vs. Li.[7] A small, but first-order displaced structural change of framework cause a two phase separation over most of lithium contents range $0<x<1$ of $Li_xFe(PO_4)$ with a flat potential plateau. [46]

$LiFeO_2$, beginning model of $LiFePO_4$, has not been used due to the poor electrochemical properties, which has small gap of E_f between Fe^{3+}/Fe^{2+} and lithium so that exhibits the low operation voltage of 3.2V vs. Li in battery. By substituting from oxygen in $LiFeO_2$ to polyanion XO_{y-4}(X=S, P, As, y=2, 3), however, the operation voltage increased to approximately 3.4V vs. Li. Moreover, $LiFePO_4$ shows high structural and chemical stability. On the other hand, poor electronic conductivity and slow diffusion velocity for lithium ion are issues to be overcome with $LiFePO_4$ cathode material. The theoretical capacity of $170mAhg^{-1}$, a flat potential plateau at 3.4V, cost-effectiveness of iron-based composition and the excellent chemical stability makes $LiFePO_4$ cathode attractive for wide-scale battery applications such as in electric vehicles(EV). Recently, its electronic conductivity has been improved by doping or adding with conductive material (carbon, nano-sized particle silver) [47]

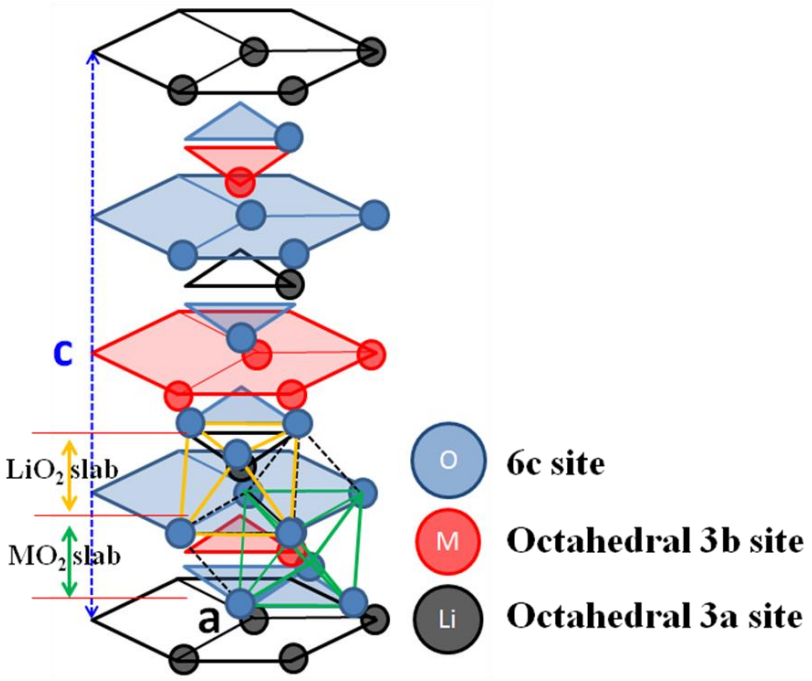

Figure 1-6. Crystallographic hexagonal unit cell of an ideal layered $LiMO_2$ oxide

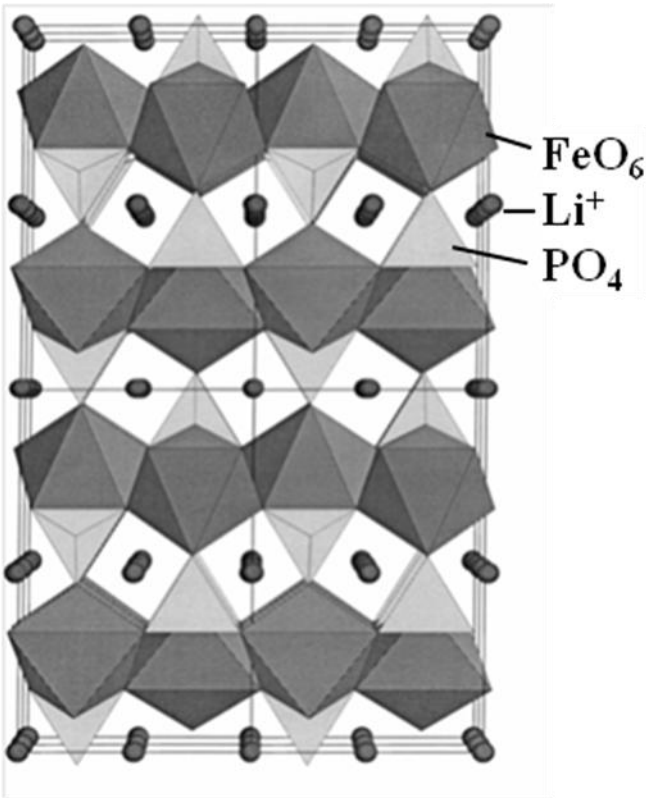

Figure 1-7. Crystal structure of $LiFePO_4$

1.2.2 Anodes

Anode and cathode material at discharge process in LIBs raises spontaneous oxidation and reduction reaction, respectively. That is, lithium ions are inserted into anode material during charge process, whereas they are extracted from anode material during discharge process. During the charge reaction, the electrolyte decomposes on the anode surface due to its relatively higher reduction potential than lithium potential. The electrolyte decomposition reaction leads to form solid electrolyte interphase (SEI) film on the electrode surface, which plays a role to prevent the additive electrolyte decomposition by suppressing electron transfer occurring at reaction between anode and electrolyte. Therefore, various fundamental properties such as capacity, electric power and lifespan largely depend on anode material. In case of anode material, lithium insertion/extraction is relatively difficult than in cathode material because of large capacity per unit weight, thus the anode design considering the lithium diffusion efficiency is the key to improve battery performance.

The high cost-effectiveness of carbon is one of the main reasons for the commercialization of carbon-based anodes. Also, when graphite anode is polarized to negative potential during initial lithium insertion step in an ethylene carbonate (EC) based electrolyte, the organic compound decomposes to form the stable SEI film.[48] This SEI film effectively passivates the anode surface and restrains further co-insertion of solvent, allowing only the migration of lithium ion. However, the major disadvantage of carbon anode is the limitation in volumetric capacity (theoretical volumetric capacity limit of 833Ah/L) and a large irreversible capacity loss during the first cycle. The alternative being considered in anode materials are the alloys and composites of Al, Si, Ge, Sn, Pb, Sb and Bi.[49] However, further research developments in the chemistry of these alloys are necessary prior to their commercialization.

1.2.3 Electrolyte

In LIB, the cell operation voltage given by electrochemical reaction are generally larger than the potential at which aqueous solutions are electrolyzed, in addition since lithium is very reactive to water, non-aqueous solutions are mainly used. Liquid electrolytes for LIB consist of lithium salts such as $LiPF_6$, $LiClO_4$ or $LiBF_4$, and an organic solvent such as ethylene carbonate (EC), dimethyl carbonate (DMC), 1,2-dimethoxyethane (DME) and diethyl carbonate (DEC), etc.. Physicochemical properties of typical organic solvent and lithium salt for LIB are indicated in table 1-1 and table 1-2, respectively.[50, 51]

A liquid electrolyte plays the role as a lithium ion carrier between the cathode and the

anode when electric current passes through an external circuit. Although organic solvents easily decompose on anode material during charge process, when appropriate organic solvent is used as the electrolyte, the solvent decomposes at initial charge process and forms a SEI film, which exhibits sufficient ionic conductivity and prevents the electrolyte to decompose after the second charge process.

Recently, electrolytes based on solvent mixtures of ethylene carbonate (EC) with dimethyl carbonate (DMC) and/or diethyl carbonate (DEC) are widely used in combination with 4V-level cathodes for LIB such as $LiCoO_2$, $LiMn_2O_4$, or $LiNiO_2$, due to the high oxidation potential value of the mixtures.[52, 53] The oxidation/reduction stability and conductivity of electrolytes are the most required properties for electrolyte systems of LIBs.

Table 1-1. Physicochemical properties of typical organic solvent for LIB [50]

solvent (Abbreviation)	MP (℃)	BP (℃)	dielectric constant	viscosity (cP)	E_{ox}^{*} (V vs. Li/Li+)
ethylene carbonate(EC)	39	248	89.6	1.86	6.2
propylene carbonate(PC)	-49.2	241.7	64.4	2.53	6.6
dimethyl carbonate(DMC)	0.5	90	-	0.59	6.7
diethyl carbonate(DEC)	-43	126.8	2.8	0.75	6.7
ethylmethyl carbonate(EMC)	-55	108	2.9	0.65	6.7
1,2-dimethoxyethane(DME)	-58	84.7	7.2	0.46	5.1

* oxidation potential (voltage supply rate : 5mV/s, Reference electrode : lithium)

Table 1-2. Physicochemical properties of lithium salt for LIB[51]

lithium salt	MP (℃)	anion radius(nm)	Λ_{ox}^{*} in PC (Scm^2/mol)	E_{ox} in PC (V vs. SCE)
$LiBF_4$	>300	0.229	28.9	3.6
$LiClO_4$	236	0.237	27.4	3.1
$LiPF_6$	194	0.254	26.3	3.8
$LiAsF_6$	>300	0.260	26.0	3.8
$LiCF_3SO_3$	>300	0.270	25.3	3.0
$Li(CF_3SO_2)_2N$	228	0.325	22.8	3.3
$LiC_4F_9SO_3$	>300	0.339	21.5	3.3
$Li(CF_3SO_2)_3C$	263	0.375	20.2	3.3

* Λ_{ox} : limit molar conductivity

1.2.4 Separator

Separator is an essential part not only in separating physical contact between cathode and anode, but also in serving path way for lithium ion transfer in cell, although it does not contribute to electrochemical reaction itself, it has an effect on battery performance and stability.

Separator is made of thin (10~20μm) polymer film with micro-porous to electrically isolate the anode and the cathode. Most of the commercial cells use polyolefin system separator materials, such as polyethylen (PE), polypropylene (PP), etc., due to its high mechanical strength (high machine direction strength, should not yield or shrink in width), chemical stability(resistance to puncture by electrode materials), wettability for the electrolyte and cost-efficiency.[54, 55] Commercialized products usually have 0.03~1μm of pore size, 30~50% of porosity and low thermal shutdown temperature (PE:~135°C, PP:~165°C). During the cell operation, therefore, the thermal stability to the rapid temperature rise by internal short circuit state inside the battery is able to be secured by the way to impede the exothermic reaction by inducing the micro-porous blockage by melt of polymer separator.

1.3 X-ray diffraction

Crystal can be defined as a solid with a regularly repeated internal structure. The unit cell is basic block of a crystal and is presented by three axis a, b, c and three interaxial angles α, β, γ. To describe the crystal face, it needs to consider intercepts of the three axes, h, k, l. The crystal face makes intercepts a/h, b/k, c/l with the three axes. The regularity of crystals is exhibited in the crystal lattice, which is a three dimensional array of points. The contents of the unit cell are arranged with infinite repetition in the crystal structure. There are seven systems (triclinic, monoclinic, orthorhombic, tetragonal, trigonal/rhombohedral, hexagonal, and cubic), in which rotational symmetry can express the infinitely repeated unit cells. These seven crystal lattices are classified as the four crystal lattice types (primitive P, face-centered F, single-face-centered A or B or C, and body-centered I), which gives 14 Bravais lattices. Symmetry elements (center of symmetry, mirror planes, glide planes, rotation axes, and screw axes) combined with the 14 Bravais lattices are classified as 230 space groups that makes possible a crystal to define regular arrange of three dimension.

Most of unit cells have a complex assembly of atoms, in which the distances between each atoms is comparable to the wavelength of X-ray.[56] The diffraction angle would depend on the various periodic relationships between atoms in the crystal. In figure 1-8,

crystallographic planes with the Miller indices (hkl) are described. The incident beam 2 reflecting at the second plane must pass farther distance ABC than the incident beam 1 reflecting at the top plane. Similarly, the incident beam 3 reflecting at the third pane must pass DEF farther. That is, all X-ray beams reflecting from planes below the surface will be retarded with respect to the first X-ray beam 1, causing interference. Considering crystal planes geometrically, if the distance ABC is exactly equal to one wavelength λ of X-ray and the distance DEF is equal 2λ, the reflection from all planes at any depth will emerge in the crystal, causing the constructive interference known as diffraction. The Bragg equation is readily driven from an analysis of the triangle OAB. The distance AB is obtained by taking the sine of θ.[57]

$$AB=d_{hkl}\sin\theta$$

When diffraction occurs in ABC=nλ, thus from such considerations, the Bragg equation can be driven,

$$n\lambda=2d_{hkl}\sin\theta$$

where λ is the wavelength of X-ray beam, n is an integer (nλ is the total path difference between waves scattered from adjacent lattice planes with equivalent indices), d is the lattice plane spacing (d-spacing) in the crystal. Therefore, when this equation is satisfied (when the relation of wavelength, inter-planar spacing, and angle of incidence beam is appropriate), thus X-ray diffraction maxima occur. When X-ray is diffracted by a crystal, the X-ray scattering intensity at any angle results from the combination of waves scattered from different atoms, which is modified by various degrees of constructive and destructive interference.

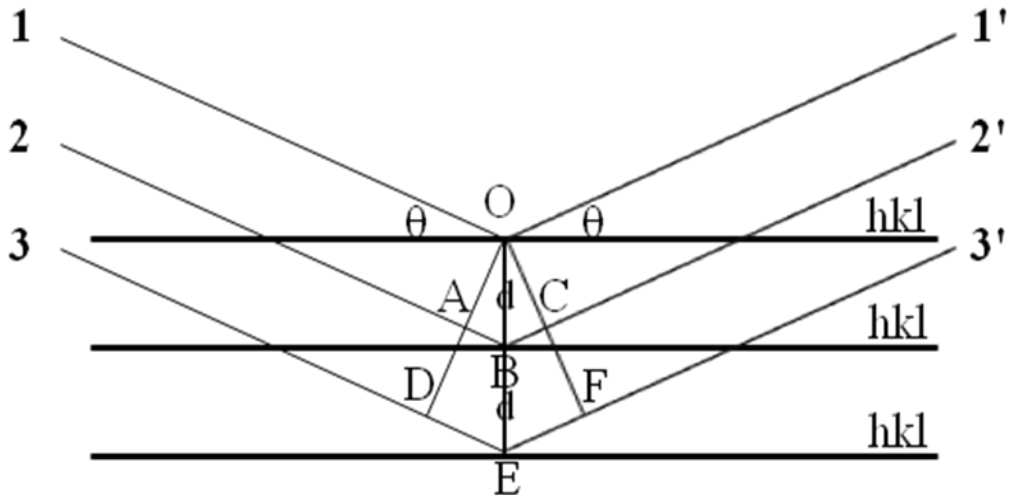

Figure 1-8. Crystallographic planes reflecting X-rays.

1.4 The Rietveld method

With the recent rapid advance in the use of versatile, inexpensive personal computers, it becomes easier to solve the complicated mathematics involved in working with all of the lines in the pattern, or even the total pattern including the background. The wide acceptance techniques of the Rietveld method [58] have provided the analyst with most tools for works with total data. The Rietveld analysis is conducted by minimizing the sum of the squared differences between measured and calculated patterns. The Rietveld method requires knowledge of the approximate crystal structure of all phases of mixture. [59, 60] The input data for the Rietveld method need to be enough similar to the required data to calculate a diffraction pattern, i.e., space group, atomic positions, occupancies on each site, and lattice constants for each phase. In order to fit the calculated value with the observed value, in addition, parameters determining the peak shape, a background profile, and scale factors for each phase are also required. In the sufficiently optimized cases, the atomic positions and occupancy on each site could also be successfully determined. A powder diffraction of crystalline material may be thought of as a collection of individual reflection profiles. The full pattern (equation 1-2) of X-ray diffraction can be driven by summing the assigned value of individual diffraction peaks (equation 1-1) that are obtained by multiplying the diffraction intensity $I(hkl)$ related to crystal structure and waveform function $\Omega_{hkl}(2\theta)$ related to the shape of diffraction peak. That is, the Rietveld method optimizes various parameters associated with the crystal structure and peak shape to match the patterns calculated by equation 1-2 with the experimentally obtained diffraction pattern by means of the least squares method, as written in equation 1-3. Here, i and w_i indicate any arbitrarily chosen point in the pattern and measured point, and the inverse number of observed intensity at the ith step $Y_{obs}(2\theta_i)$, respectively. [61]

$$I(hkl) \cdot \Omega_{hkl}(2\theta) \quad \text{..... (1-1)}$$

$$Y_{calc}(2\theta) = \sum_{hkl} I(hkl) \cdot \Omega_{hkl}(2\theta) + \varrho(2\theta) \quad \text{..... (1-2)}$$

$$\Delta = \sum_{i} w_i [Y_{obs}(2\theta_i) - Y_{calc}(2\theta_i)]^2 \quad \text{..... (1-3)}$$

Where, $\varrho(2\theta)$ indicates the background, which is experimental function presented as a polynomial of equation 1-4. Here, q_0, q_1, q_2, q_3, q_4 and q_5 are unknown parameters.

$$\varrho(2\theta) = q_0 + q_1 2\theta + q_2 2\theta^2 + q_3 2\theta^3 + q_4 2\theta^4 + q_5 2\theta^5 \cdots \quad \text{..... (1-4)}$$

When the sample consists of plural crystal species, the calculated value $Y_{calc}(2\theta)$ of XRD pattern can be indicated as equation 1-5, and optimized by equation 1-3. Therefore, the Rietveld analysis of mixed crystal phases is simultaneously optimized. Where, *n* presents crystal phase.

$$Y_{calc}(2\theta) = \sum_n \left[\sum_{hkl} I(hkl)_{,n} \cdot \Omega_{hkl,n}(2\theta) \right] + \varrho(2\theta) \quad \text{..... (1-5)}$$

The accuracy of fit in the Rietveld analysis is evaluated by R-value, as following equation 1-6, 1-7 and 1-8.

$$\mathrm{R_{wp}} = \frac{\sum_i w_i [Y_{obs}(2\theta_i) - Y_{calc}(2\theta_i)]^2}{\sum_i w_i [Y_{obs}(2\theta_i)]^2} \quad \text{..... (1-6)}$$

$$\mathrm{R_B} = \frac{\sum_{\mathrm{h}} |I_{obs,\mathrm{h}} - I_{calc,\mathrm{h}}|}{\sum_{\mathrm{h}} I_{obs,\mathrm{h}}} \quad \text{..... (1-7)}$$

$$\mathrm{R_F} = \frac{\sum_{\mathrm{h}} |\sqrt{I_{obs,\mathrm{h}}} - \sqrt{I_{calc,\mathrm{h}}}|}{\sum_{\mathrm{h}} I_{obs,\mathrm{h}}} \quad \text{..... (1-8)}$$

$\sum_{\mathrm{h}}$ means finding the value of diffraction line, $\mathrm{h} = \begin{pmatrix} h \\ k \\ l \end{pmatrix}$

1.5 Objective

Li-ion secondary batteries (LIBs) have received much attention as one of the next generation battery system due to its high energy density and operation power, and the research study to improve its performance have been proceeding actively with the recent drastic increase of demands for portable electronic devices and electric vehicle. The research on the crystal phase/structure of electrode materials is essential to understand the electrode behavior at the lithium insertion/extraction process and to design the advanced high efficiency electrode. With this approach to improvement in LIB, however, the relaxation analysis is important to make the transition of electrode material from kinetic state to equilibrium state clear. Especially, the most remarkable feature for this relaxation analysis is to focus on spontaneous change of electrode material itself without any side reaction such as the local cell reaction between the active material and the current collector or the supplemental conductor, and self discharge, etc. during the long relaxation time. In that regard, this differs from existing test methods using in-situ cell designed to reflect actual operation environment, considering that the side reactions considerably affect to electrode materials for long observation time.

The quantitative relaxation analysis on crystal phase/structure after the lithium insertion/extraction process for several electrode materials, such as γ-Fe_2O_3 and $LiFePO_4$ has previously conducted, however, the relaxation analysis of highly prospective other cathode materials, such as $LiMn_2O_4$ and $LiCoO_2$ have not been yet reported. Reminding previous relaxation analysis results, mainly two kinds of relaxation behavior which would be distinguished into the change of relaxation structure and relaxation phase are suggested, these relaxation mechanisms are considered depending on unique feature of each electrode material. Thus making the relaxation mechanism for each electrode material clear is the most attractive merit of relaxation analysis. Furthermore, of the relaxation behaviors, the relaxation phase change mechanism can be discussed from the reaction kinetics perspective in that the mole fraction of coexisting the Li-lean phase and the Li-rich phase changes with the elapsed time (the relaxation time), which is expected to make the initial state just after the electrochemical lithium extraction/insertion and the final state under thermodynamic equilibrium clear.

In this study, on the relaxation analysis of $LiMn_2O_4$ and $LiCoO_2$ cathode materials for LIBs was focused, the quantitative analysis data for relaxation phenomenon was obtained by means of XRD measurement and the Rietveld method. Especially to analyze the relaxation structure or phase for the electrode material itself, when the samples were characterized, the circuit was opened and immediately the working electrode was taken out of the cell in an argon-filled glove box to avoid the local cell

action between the active material and the current collector or the supplemental conductor.

In chapter 1, general information for lithium ion secondary battery and X-ray Rietveld method was introduced, and in chapter 2 the previous reports on the relaxation analysis and approach from kinetic perspective were introduced. In chapter 3 the relaxation phenomenon and behaviors for $LiMn_2O_4$ cathode material after lithium insertion process were investigated by means of XRD measurement and the asymmetry Lorentz function fitting program. In chapter 4 and 5, the relaxation analysis for $LiMn_2O_4$ and $LiCoO_2$ cathode materials after lithium extraction and/or insertion process was conducted by using XRD measurement and the Rietveld analysis, and their relaxation mechanisms were discussed. In chapter 6, finally the results of relaxation analysis for each cathode material were summarized, and suggested the contribution of this study in lithium ion secondary battery and future works.

References

1. J. Besenhard, *Handbook of Battery Materials*, WILEY-VCH (1998)
2. K. Mizushima, P. C. Jones, P. J. Wiseman and J. B. Goodenough, *Mater. Res. Bull.*, 15, 1159 (1993)
3. J. M. Tarascon and M. Armand, *Nature* 414(15), 359, (2001)
4. T. Sasaki, Y. Ukyo and T. Novak, *Nature materials*, vol.12 (2013)
5. D. Linden, T. B. Reddy, *Handbook of Batteries 3rd Edition*, McGraw-Hill, New York, Chapter 35 (2002)
6. M. Winter, J. O. Besenhard, M. E. Spahr and P. Novak, *Adv. Mater*. 10, 725 (1998)
7. A. K. Padhi, K. S. Nanjundaswamy and J. B. Goodenough, *J. Electrochem. Soc.* 144(4), 1188 (1997)
8. A. Deschanv, B. Raveau and Z. Sekkal, *Mater. Res.*, Bull., 6, 699 (1971)
9. T. Ohzuku, A. Ueda and N. Yamamoto, *J. Electrochem. Soc*., 142, 1431 (1995)
10. A.N. Jansen, A.J. Kahaian and K.D. Kepler, *J. Power Sources*, 902, 81-82 (1999)
11. M. M. Thackeray, W. I. F. David and J. B. Goodenough, *Mater. Res. Bull.* 17, 785 (1982)
12. M. M. Thackeray, W. I. F. David, P. G. Bruce and J. B. Goodenough, *Mater. Res. Bull.* 18, 461 (1983)
13. T. Ohzuku, M. Kitagawa and T. Hirai, *J. Electrochem. Soc.*, 137,769 (1990)
14. A. Mosbah, A. Verbaere and M. Tournoux, *Mater. Res. Bull.*, 18, 1375 (1983)
15. M. M. Thackeray, P. J. Johnson, L. A. de Picciotto, P. G. Bruce and J. B. Goodenough, *Mater. Res. Bull.*, 19, 179 (1984)
16. K. Kanamura, H. Naito, T. Yao and Z-I Takehara, *J. Mater. Chem*., 6(1), 33-36 (1996)
17. G. G. Amatucci, N. Pereira, T. Zheng and J. M. Tarascon, *J. electrochem. Soc.*, 148, A171 (2001)
18. M. M. Thackeray, Prog. *Solid State Chem.*, 25, 1 (1997)
19. C. Masquelier, M. Tabuchi, K. Ado, R. Kanno, Y. Kobayashi, T. Maki, O. Nakamura and J. B. Goodenough, *J. Solid State Chem.*, 123, 255 (1996)
20. D. H. Jang, Y. J. Shin and S. M. Oh, *J. Elctrochem. Soc.*, 143, 2204 (1996)
21. A. D. Pasquier, A. Bylr, P. Courjal, D. Larcher , G. Amatucci, B. Gerand and J. M. Tarascon, *J. electrochem. Soc*., 146, 48 (1999)
22. Y. Xia, T. Sakai, T. Fujieda, X. Q. Yang, X. Sun, S. F. Ma, J. McBreen, M. Yoshio, *J. Electrochem. Soc.*, 148, A723 (2001)
23. Y. Xia, N. Kumada and M. Yoshio, *J. Power Sources*, 90, 135 (2000)

24. G. G. Amatucci and J. S. Tarascon, *US Patent*, No. 5, 674, 645 (1997)
25. Y. K. Sun, G. S. Park, Y. S. Lee, M. Yoshio and K. S. Nahm, *J. Electrochem. Soc.*, 148, A994 (2001)
26. J. O. Bessenhard, Editor, *Handbook of Battery Materials*, Wiley-VCH, Weinheim(1999)
27. N. Igawa, T. Taguchi, H. Fukazawa, H. Yamauchi and W. Utsumi, *J. Am. Ceram. Soc.*, 93(8), 2144 (2010)
28. Y. Idemoto and T. Matsui, *Solid State Ionics*, 179, 625, 3 (2008)
29. M. S. Whittingham, *Chem. Rev.*, 104, 4271 (2004)
30. T. Ohzuku, A. Ueda, M. Nagayama, Y. Yasunou, and H. Komori, *Electrochim. Acta*, 38, 1159 (1993)
31. Y. Koyama, I. Tanaka, H. Adachi, Y. Makimura, and T. Ohzuku, *J. Power Sources*, 119-121, 644 (2003)
32. J. N. Reimers and J. R. Dahn, *J. Electrochem. Soc*., 139, 2091 (1992)
33. G. G. Amatucci, J. M. Tarascon and L. C. Klein, *J. Electrochem. Soc.*, 143, 1114 (1996)
34. R. V. Chebiam, A. M. Kannan, F. Prado and A. Manthiram, *Electrochem. Commun*.,3, 624 (2001)
35. S. Venkatraman, Y. Shin, and A. Manthiram, *Electrochem. Solid State Lett*., 6, A9 (2003)
36. G. Dutta, A. Manthiram and J. B. Goodenough, *J. Solid State Chem*., 96, 123 (1992)
37. W. Li and J. C. Currie, *J. Electrochem. Soc.*, 144, 2773 (1997)
38. Y. Koyama, I. Tanaka, T. Ohuzuku, *J. Power Sources*, 644, 119 (2003)
39. J. Guo, L. Jiao, H. Yuan, H. Li, M. Zhang, Y. Wang, *Electrochim Acta*, 51, 3731 (2006)
40. Y. Koyama, N. Yabuuchi, I. Tanaka, H. Adachi and T. Ohzuku, *J. Electrochem. Soc.*, 151(10), A1545-A1551 (2004)
41. J. Choi and A. Manthiram, *J. Electrochem. Soc.*, 152(9), A1715 (2005)
42. H. Ren, X. Li and Z. Peng, *J. Electrochim. Acta*, 56, 7088 (2011)
43. H. Liu and L. Tan, *J. Mater. Chem. and Physics*, 129, 729 (2011)
44. K.-S. Lee, S.-T. Myung, K. Amine, H. Yashiro and Y.-K. Sun, *J. Electrochem. Soc.*, 154(10), A971-A977 (2007)
45. S. -W. Cho, J.-H. Ju, S.-H. Ryu and K.-S. Ryu, *J. Korean Electrochem. Soc.*, 13(4), 264-269 (2010)
46. N. Ravet, J. B. Goodenough, S. Besuer, M. Simoneau, P. Hovington and M. Armand, *196th Electrochem. Soc. Meet*. Honolulu, Hawaii.

47. S. Y. Chung , J. T. Bloking and Y. M. Chiang, *Nature Materials*, 1(2), 123 (2002)
48. E. Peled, *J. Electrochem. Soc.*, 126, 2047 (1979)
49. Y. Hamon, T. Brousse, F. Jousse, P. Topart, P. Buvat and D. M. Schle ich, *J. Power, Sources*, 97, 185 (2001)
50. B. E. Blomgren, Lithium Batteries, *Academic Press*, New York (1983)
51. M. Ue, A. Murakami and S. Nakamura, *J. Electrochem. Soc.*, 149, A1385 (2002)
52. K. Xu, S. P. Ding and T. R. Jow, *J. Electrochem. Soc.*, 146, 4172 (1999)
53. X. Zhang, J. K. Pugh and P. N. Ross, *J. Electrochem. Soc.*, 148, E183 (2001)
54. H. Sakaebe and H. Matumoto, *Electrochem. Commun.* 5, 594 (2003)
55. Z. Mao and R. E. White, *J. Power Sources*, 43, 181 (1993)
56. J. P. Glusker and K. N. Trueblood, in *Crystal Structure Analysis – A Primer*, 3rd Edition, 23, Oxford Univ. press, Oxford (2010)
57. R. Jenkins and R. L. Snyder, in *Introduction to X-ray powder diffractometry*, 47, Wiley Interscience (1996)
58. H. M. Rietveld, J. Appl. Crystallogr. 2, 65-71 (1969)
59. R. J. Hill and C. J. Howard, J. Appl. Crystallogr. 20, 467-474 (1987)
60. D. L. Bish and S. A. Howard, j. Appl. Crystallogr. 21, 86-91 (1988)
61. Roderick J. Hill, in *The Rietveld Method*, R. A. Young, Editor, P 95, Oxford Univ. press, Oxford (1995).

CHAPTER 2

RELAXATION ANALYSIS OF ELECTRODE MATERALS FOR LITHIUM-ION SECONDRY BATTERIES

2.1 Relaxation analysis

When lithium was inserted into γ-Fe_2O_3 electrochemically, prolonged potential change was observed after termination of the insertion, as shown in figure 2-1. It was considered that this phenomenon reflects some continuing crystal structure change even after lithium insertion. Lithium was inserted into γ-Fe_2O_3, then the circuit was opened and the change of electrode material was analyzed, where this analysis is named as "Relaxation Analysis", because material is analyzed at relaxation process. The relaxation analysis is important to make the transition of electrode material from kinetic state to equilibrium state clear.

The cell was charged or discharged electrochemically with electrode material. When the required conditions were attained, the circuit was opened and the working electrode was taken out of the cell immediately in a glove box to avoid the local cell action between the electrode material and the current collector or the supplemental conductor. Then, the sample for XRD measurement was obtained. XRD patterns were measured with various relaxation time. The XRD patterns were analyzed by the Rietveld method using RIEVEC program coded by T. Yao. [1,2] In the relaxation analysis, the crystal structure and relaxation phenomenon of the several electrode materials after lithium insertion and/or lithium extraction have been investigated by means of X-ray diffraction measurement and the Rietveld analysis. Recently, the relaxation analysis of γ-Fe_2O_3 and $LiFePO_4$ electrode material for LIB has been reported. In this chapter 2, I would like to elaborate the results of relaxation analysis.

2.2 Relaxation analysis for γ-Fe_2O_3

Lithium was chemically inserted into γ-Fe_2O_3 using n-butyl lithium hexane solution with various lithium ion concentrations and the crystal structure in the process of lithium insertion was examined.[3] X-ray Rietveld analysis found that the sample was a mixture of two phases both belonging to the space group of $Fd\bar{3}m$, one is lithium rich and another is lithium lean. It was revealed that, unlike electrochemically lithium inserted γ-Fe_2O_3, the chemical lithium insertion process into γ-Fe_2O_3 takes two phases reaction, i.e. inserted lithium forms the Li-rich phase in which the lithium amount is constant, and the overall lithium concentration is controlled by the mole fraction changes between Li-rich phase and Li-lean phase. Li-rich phase is thought to be the same phase previously reported by Bonnet et al. and Pernet et al.,[4, 5] in which the iron occupancy of 16c sites were not equalized with that of 16d sites. This phase belongs to $Fd\bar{3}m$ not to $Fm\bar{3}m$. Fast lithium insertion could form the two phases of Li-lean and Li-rich even for electrochemical lithium insertion process.

Lithium was inserted into γ-Fe_2O_3 with two ways, electrochemically and chemically, or extracted from electrochemically lithium inserted γ-Fe_2O_3, and the crystal structure was investigated at the relaxation process.[6, 7] As shown in figure 2-2, in the process of electrochemical lithium insertion into γ-Fe_2O_3, the iron occupancy of 8a sites decreased and that of 16c sites increased. After the lithium insertion, the iron occupancy of 8a sites increased and that of 16c sites decreased gradually with elapsed time. At lithium insertion process, it was indicated that iron migrated from 8a sites to 16c sites, and then it was considered that lithium was inserted at 8a sites and the iron at 8a sites migrated into 16c sites. After the lithium insertion, it was indicated that iron migrated from 16c sites to 8a sites, and then it was considered that lithium migrated from 8a sites to 16c sites and iron moved from 16c sites to 8a sites. For electrochemical lithium extraction form lithium inserted γ-Fe_2O_3, the iron occupancy of 8a sites increased and that of 16c sites decreased just after the lithium extraction. It was indicated that iron moved from 16c sites to 8a sites during lithium extraction process and it was considered that lithium was extracted from 8a sites and the iron at 16c sites moved into 8a sites. From these results, it was considered that lithium prefers 8a site to occupy kinetically and prefers 16c sites thermodynamically, and that 8a sites take a role as a diffusion path from both lithium insertion and extraction. For the chemical lithium insertion sample, after the termination of chemical lithium insertion, there is no significant changes on the crystal structure even after the long relaxation time. Difference between chemical and electrochemical lithium insertion into γ-Fe_2O_3 was the degree of iron occupancy

changes at 8a sites in the process of lithium insertion. It is considered that it is difficult for lithium to diffuse into γ-Fe_2O_3 crystal particles when lithium is rapidly inserted at 8a sites, and that chemical lithium insertion process takes two phases reaction between Li-lean phase and Li-rich phase.

2.3 Relaxation analysis for $LiFePO_4$

The relaxation process of $LiFePO_4$ cathode was investigated after the termination of lithium insertion or lithium extraction.[8] It was revealed that the amount of $LiFePO_4$ phase decreased and that $FePO_4$ phase increased with relaxation time after the lithium insertion, as indicated in figure 2-3. It was considered that $LiFePO_4$ phase including lithium defects favorable lithium insertion formed in the process of lithium insertion, and that the defective $LiFePO_4$ phase separated to $LiFePO_4$ phase without defects and $FePO_4$ phase at the relaxation process. The effect of particle size on relaxation process was observed that the formation of the defective $LiFePO_4$ phase just after lithium insertion and the decrease amount of $LiFePO_4$ phase on relaxation time were smaller for the sample with smaller particle size. It was considered that diffusion paths become shorter because the sample with smaller particle has more surface area to react with lithium during discharge process. For the lithium extraction sample, compared to lithium insertion process, less amount of the defective $LiFePO_4$ formed regardless of particle size. It was considered that, by volume reduction reaction from $LiFePO_4$ to $FePO_4$, diffusion paths outside the crystal particles can be formed, and that the defective $LiFePO_4$ phase created only at reaction interface.

In conclusion, the relaxation analysis presents dynamic changes in structures and/or phases of electrode materials according to the condition of lithium transfer. In the future, it is expected that the relaxation analysis will develop as the powerful method for analyzing electrode materials.

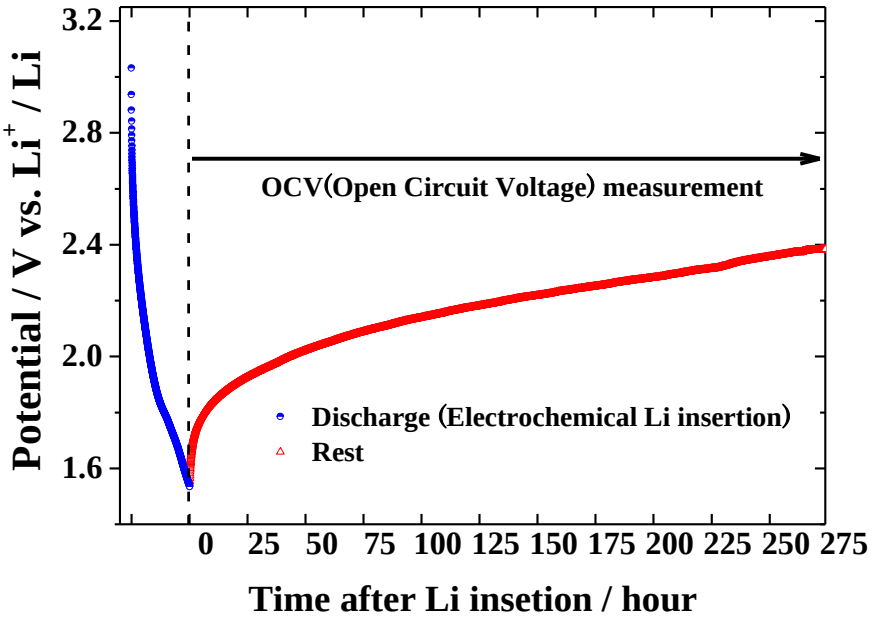

Figure 2-1. Result of OCV (Open Circuit Voltage) measurement after lithium insertion (Sample : $Li_{1.5}Fe_2O_3$).

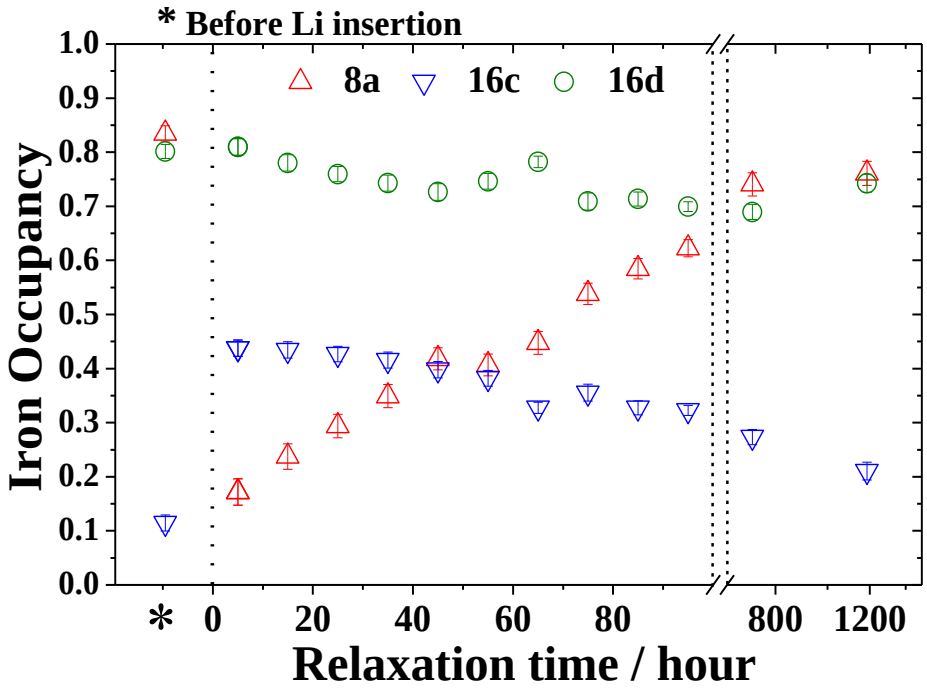

Figure 2-2. Relaxation of crystal structure of γ-Fe_2O_3 with elapsed time after lithium insertion: Site occupancy changes of iron at 8a, 16c and 16d sites. Asterisk mark (*) indicates the sample before lithium insertion.

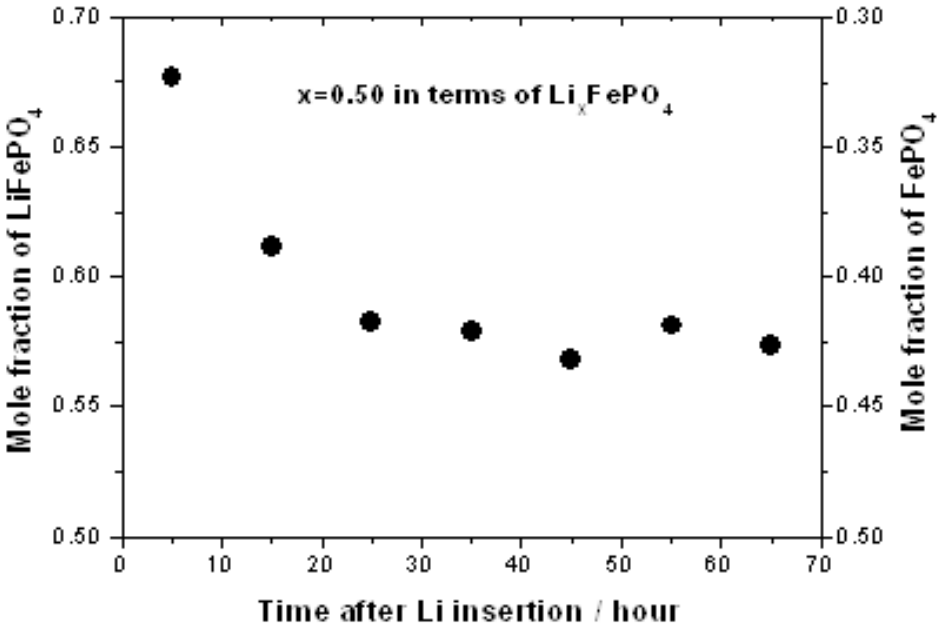

Figure 2-3. The relative mole fraction changes of $LiFePO_4$ phase with various elapsed time after termination of lithium insertion process in the sample x=0.5 in terms of Li_xFePO_4.[9]

References

1. T. Yao, T. Ito, and T. Kokubo, *J. Mater. Res.*, 10, 1079 (1995).
2. T. Yao, N. Ozawa, T. Aikawa, and S. Yoshinaga, *Solid State Ionics*, 175, 199 (2004).
3. S. Park, T. Matsui and T. Yao, *Zero-Carbon Energy Kyoto 2011, Edited by T. Yao, Green Energy and Technology, Springer*, 159-164 (2012)
4. B. Bonnet, P. Strobel, M. Ternet, M. Condrand, Y. Gros, C. Mouget and Y. *Mater. Sci. Forum*, 91-93, 345 (1992)
5. M. Pernet, P. Strobel, B. Bonnet, P. Bordet and Y. Chabre, *Solid State Ionics*, 66, 259 (1993)
6. S. Park, M. Oda and T. Yao, *Solid State Ionics*, 203, 29-32 (2011)
7. S. Park, S. Ito, K. Takasu and T. Yao, *Electrochem*, 80(10), 804-807 (2012)
8. S. Park, K. Kameyama and T. Yao, *Electrochem. and Solid-State Lett*. 15(4), A49-A52 (2012)
9. T. Yao, *Energy Procedia*, 34, 9-12 (2013)

CHAPTER 3

RELAXATION PHASE CHANGE OF ELECTROCHEMICALLY LITHIUM INSERTED SPINEL $LiMn_2O_4$

Lithium were firstly extracted till x≈0 electrochemically, then inserted till x=0.1 in terms of $Li_xMn_2O_4$ electrochemically at a rate of 1C, and stopped the lithium insertion. X-ray diffraction (XRD) patterns were measured as a function of elapsed time after lithium insertion and investigated phase change of $LiMn_2O_4$ material after lithium insertion. From the asymmetric Lorentz peak fitting result of the XRD patterns, it was found that the two phases, Li-rich phase and Li-lean phase, coexist. It is found that the lattice constants of both phases were almost constant and that the amount of Li-lean phase decreased and Li-rich phase increased with the elapsed time.

3.1 Introduction

Various kinds of transition metal oxides have been investigated as an electrode material for secondary lithium ion battery. As an example, $LiCoO_2$ has already been utilized in a practical rechargeable lithium battery. Spinel $LiMn_2O_4$ is one of the promising cathode materials for lithium ion secondary batteries because of relatively high energy density, cost effectiveness and low toxicity.[1-4] Spinel $LiMn_2O_4$ with structural complexity of three-dimensional octahedron arrangement shown in figure 3-1 (a) differs from many other layered cathode materials with two-dimensional octahedron arrangement shown in figure 3-1(b) in exhibiting a rich variety of electrochemical properties caused by electronic and structural phenomenon such as Jahn–Teller distortions [2, 5–7], charge ordering [8,9] and magnetic ordering [10].

Spinel $LiMn_2O_4$ composition belongs to the $Fd\bar{3}m$ space group [11, 12], where oxygen ion locate cubic closed packed 32e sites as the structural frame, lithium and manganese ion occupy tetrahedral 8a sites and octahedral 16d sites, respectively. The number 32 of "32e" is multiplicity and e is the Wyckoff letter in $Fd\bar{3}m$. The oxygen atom is surrounded by one lithium and three manganese atoms tetrahedrally.

In Mn_2O_4 structure, lithium ions can occupy both of the tetrahedral 8a and octahedral 16c site.[13] A slice parallel to (-110) in $Fd\bar{3}m$ is shown in figure 3-2, which indicate that the chains of edge-sharing MnO_6 octahedron parallel and LiO_4 tetrahedron are attached. These tetrahedrons form a zigzagging chain presented as the dotted line. The zigzagging chains lie on the octahedral 16c sites which are the largest vacancy in the spinel structure. These zigzagging chains are connected with each other with

three-dimensional pathway, as shown in figure 3-1(a). For the lithium diffusion in $LiMn_2O_4$, it is suggested that the lithium ions pass the 8a and 16c sites with a driving force by the difference of lithium concentration [14].

It has been known that the electrochemical reactions during the charge/discharge process of secondary lithium ion battery have a considerable effect on the crystal structure of electrode material. Many previous studies have proposed that the structural changes take place when lithium ions are inserted into or extracted from $LiMn_2O_4$. Kanamura et al. have refined the detailed structural changes of $Li_xMn_2O_4$ in the region from $LiMn_2O_4$ to $Li_{0.13}Mn_2O_4$ by using the X-ray diffraction measurement and the Rietveld analysis, as shown in figure 3-3 and follows.[2, 5, 6, 11, 15]

In terms of $Li_xMn_2O_4$,

1) The phase transition from a cubic phase to a tetragonal phase in the region of $1 \leqq x \leqq 2$.

2) The homogeneous spinel phase reaction with a continuous lattice parameter change in the region of $0.5 \leqq x \leqq 1$.

3) Two spinel phase coexistence with different lattice parameter in the region of $0.15 \leqq x \leqq 0.5$.

Generally, the electrochemical reactions of cathode material by the charge/discharge process are closely related with its crystal phase or structure transformation. That is, the research on the crystal phase/structure of electrode materials is essential to understand the electrode behavior at the lithium insertion/extraction process and to design the advanced high efficiency electrode. However unfortunately, at the rest stage after charge/discharge process the investigation for the crystal structure or phase change of only electrode material has not yet been reported, which would be also quite crucial in maintaining the stable performance of LIBs, moreover, predicting lithium diffusion mechanism in electrode material. In that regard, the relaxation analysis is important to make the transition of electrode material from kinetic state to equilibrium state clear. The relaxation analysis of changing their crystal phase/structure after the lithium insertion/extraction process for various electrode materials have been conducted such as γ-Fe_2O_3[16-18], $LiMn_2O_4$[19-21], $LiCoO_2$[22], $LiFePO_4$[23] and $LiNi_{1/3}Co_{1/3}Mn_{1/3}O_2$ [24], by using powder X-ray diffraction (XRD) measurement and the Rietveld analysis

method.

In chapter 3 and 4 described on $LiMn_2O_4$ cathode material, it was elaborated on the phase change of $LiMn_2O_4$ with relaxation time after the termination of lithium insertion. In this chapter 3, firstly all amount of lithium were extracted electrochemically and inserted till x=0.1 in terms of $Li_xMn_2O_4$ electrochemically at a rate of 1C then stopped the insertion. X-ray diffraction measurement was conducted as a function of elapsed time after termination of lithium insertion process and the relaxation phase change of $LiMn_2O_4$ cathode material investigated by means of the Lorentz function fitting program using least square method. From the asymmetric Lorentz peak fitting result of all the XRD pattern, it was found that the two phases, the Li-rich phase and the Li-lean phase, coexist. It is found that the lattice constants of both phases were almost constant and that the amount of the Li-lean phase decreased and the Li-rich phase increased during the relaxation time.

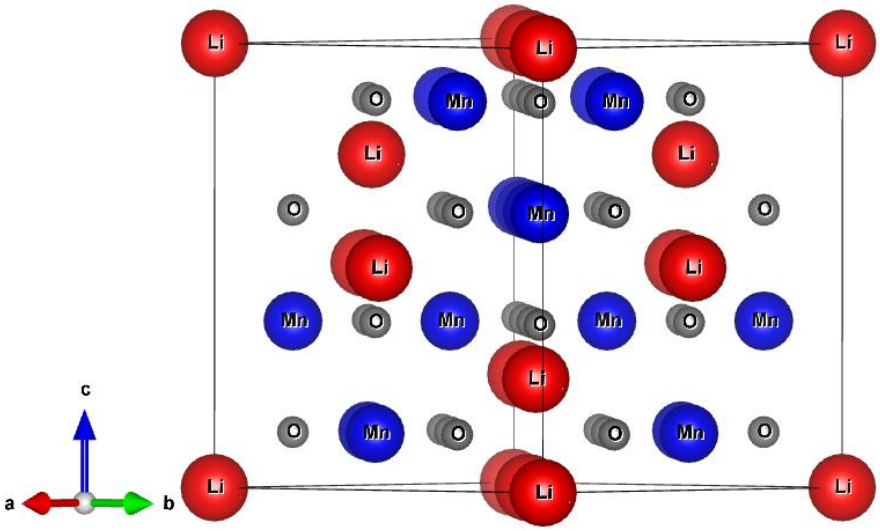

(a) Three-dimensional octahedron arrangement in Fd$\bar{3}$m

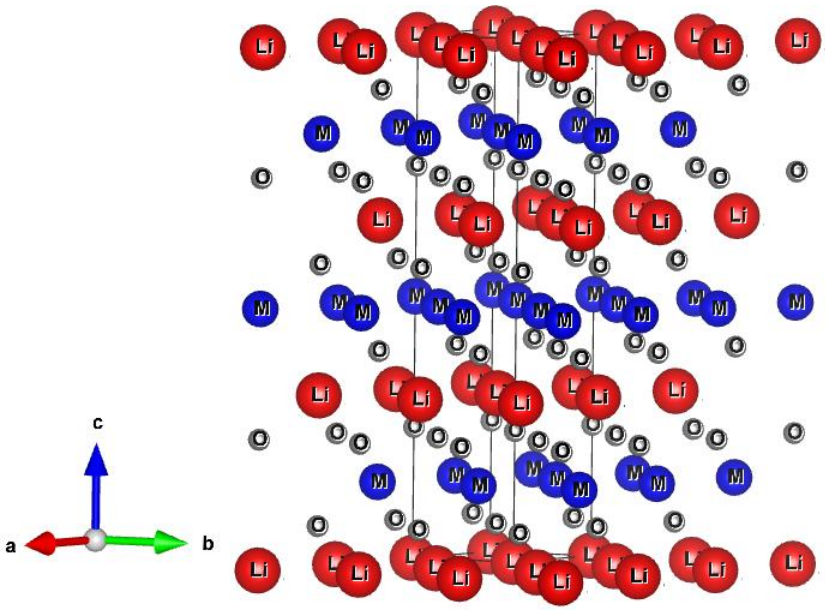

(b) Two-dimensional octahedron arrangement in R$\bar{3}$m

Figure 3-1. Structural arrangement of Fd$\bar{3}$m and R$\bar{3}$m

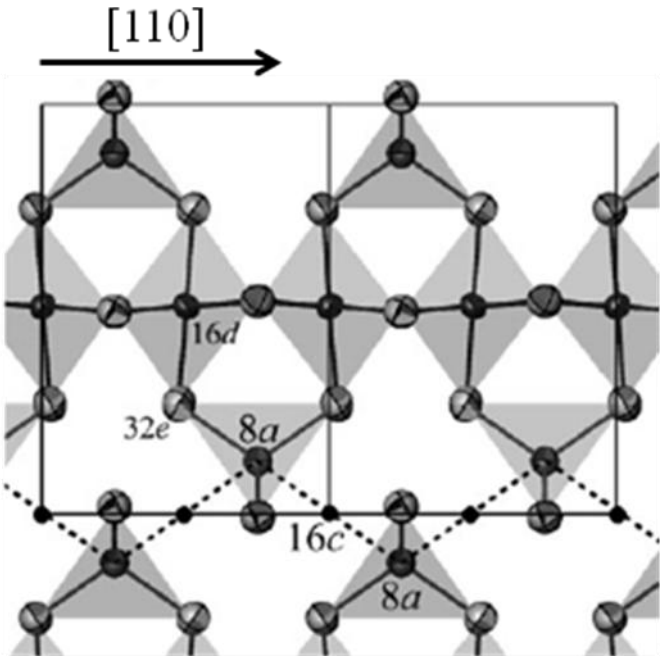

Figure 3-2. A slice parallel to (-110) in Fd$\bar{3}$m. The chains of edge-sharing MnO_6 octahedron parallel and LiO_4 tetrahedron are attached with lithium at 8a sites, manganese at 16d sites and oxygen at 32e sites in the space group Fd$\bar{3}$m. The lithium diffusion pathway is indicated as a dotted line connecting tetrahedral 8a sites and octahedral 16c site.[13]

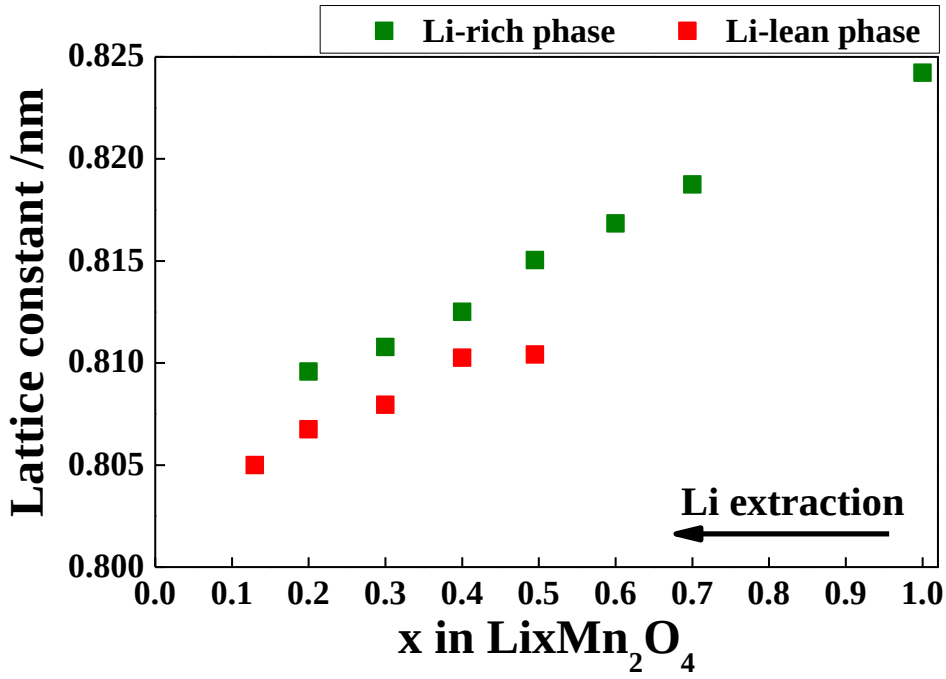

Figure 3-3. Two phase coexistence of $LiMn_2O_4$ [15]

3.2 Experimental

3.2.1 Materials synthesis

$LiMn_2O_4$ was synthesized by solid-state reaction between the starting materials Li_2CO_3 and MnO_2, as flow chart shown in figure 3-4. Li_2CO_3 and MnO_2 were weighed in a mole ratio of 1:4 and grounded by electric mortar for 5 h, then calcinated at 823 K for 12 h in air. The mixture was pressed to a disk by 9.8 MPa, sintered at 1073 K for 4 h. $LiMn_2O_4$ powder was prepared by grounding thus obtained pellet. Thus obtained $LiMn_2O_4$ powder was identified by X-ray diffraction (XRD) measurement with Cu-Kα radiation, figure 3-5 indicates XRD pattern of a well synthesized $LiMn_2O_4$ according to the JCPDS data.

3.2.2 Electrochemical lithium extraction/insertion

Electrochemical lithium extraction and insertion for $LiMn_2O_4$ was performed by using an argon-sealed three electrode type glass cell as shown in figure 3-6. The working electrode material consist of $LiMn_2O_4$, acetylene black (AB) and polytetrafluoro ethylene (PTFE) with the weight ratio of 0.80:0.15:0.05, which was spread on a nickel mesh current collector. Typically cathodes contained 12 mg of $LiMn_2O_4$. The electrolyte solution was Ethylene carbonate (EC) / dimethoxyethane (DME) (1:1 volume ratio) containing 1.0 mol dm^{-3} $LiClO_4$. Lithium metal foil was used as the counter electrode and reference electrode. The cells are charged and discharged at constant current while the voltage is monitored. The amount of extracted/inserted lithium was controlled by integrating the given constant current. Firstly all amount of lithium were extracted from $LiMn_2O_4$ electrochemically and the rest time was assigned for 20 min, then lithium was inserted to x=0.10, 0.15, 0.25 and 0.5 in terms of $Li_xMn_2O_4$ electrochemically at a rate of 1C, respectively. The details of electrochemical test are presented in table 3-1. When the samples were characterized, the circuit was opened and immediately the working electrode was taken out of the cell in an argon-filled glove box to avoid the local cell reaction between the active material and the current collector or the supplemental conductor, as drawn in figure 3-7.[16-24] The working electrode was washed in EC/DME (1:1 v/v, Kishida chemical Corp., Ltd.) solution then DME (Kishida chemical Corp., Ltd.) solution and dried at 35 °C in argon atmosphere.

3.2.3 X-ray diffraction (XRD) measurement

The sample was set in a sealed holder (2391A201, Rigaku Corp., Ltd.) with beryllium window in an argon-filled glove box, which was set to a Model Ultima powder X-ray diffractometer (UltimaIV, Rigaku Corp., Ltd.) with copper Kα radiation. In order to

investigate the relaxation phase change, XRD measurements were repeatedly carried out at the various relaxation times after termination of lithium insertion. The detailed conditions for XRD measurement are indicated in table 3-2. The tube voltage and current were adjusted to 40 kV and 40 mA. To focus on 311 peak that exhibits apparent two-phase coexistence, the scanning technique with sampling steps of $2\theta = 0.01°$ and scanning speed of $0.2° \text{ min}^{-1}$ were used over the range $35° \leq 2\theta \leq 40°$.

3.2.4 Lorentz function fitting

The XRD profiles obtained during the relaxation time were fitted by asymmetric Lorentz function program under the condition of two phases, the Li-lean phase and the Li-rich phase, and coexistence. From the fitting results, X-ray diffraction position and XRD intensity of the Li-lean phase and the Li-rich phase for 311 peak in space group $Fd\bar{3}m$ were precisely obtained, respectively.

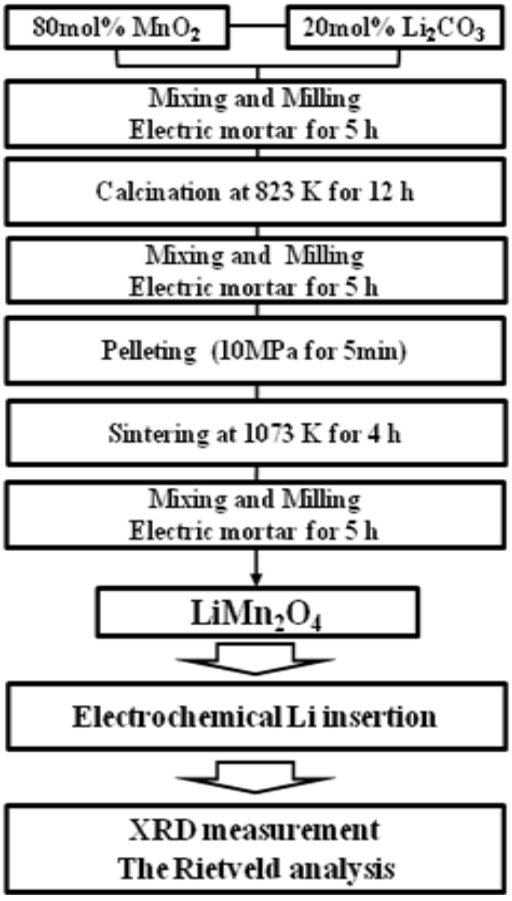

Figure 3-4. Flow chart of solid state reaction for $LiMn_2O_4$ synthesis

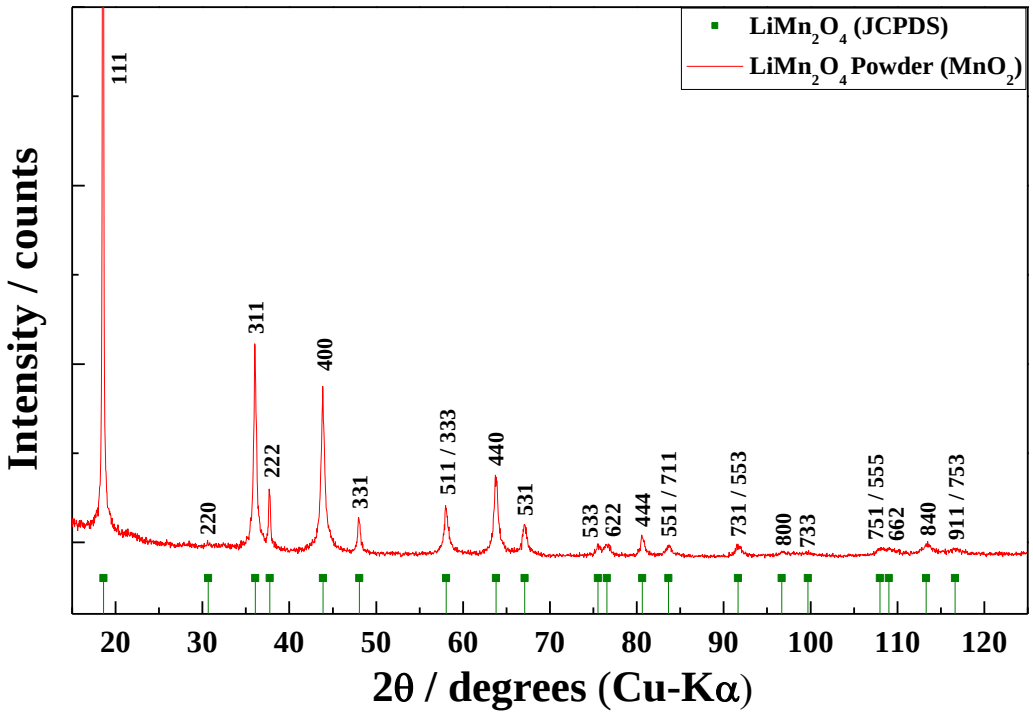

Figure 3-5. XRD pattern of $LiMn_2O_4$ powder

Table 3-1. Cell preparation condition

Cell	Three electrodes type glass cell (Argon-sealed)
W.E.	80wt%$LiMn_2O_4$ + 15wt%AB + 5wt%PTFE
C.E., R.E.	Lithium metal
Collector	Nickel mesh
Electrolyte	1 mol dm^{-3} $LiClO_4$ in EC/DME (1/1 v/v)
Lithium insertion (Procedure)	Lithium extraction to x=0 in $Li_xMn_2O_4$ at 1C
	24 h rest
	Lithium insertion to x=0.10, 0.15, 0.15 and 0.50 in $Li_xMn_2O_4$ at 1C
Relaxation	Argon atmosphere

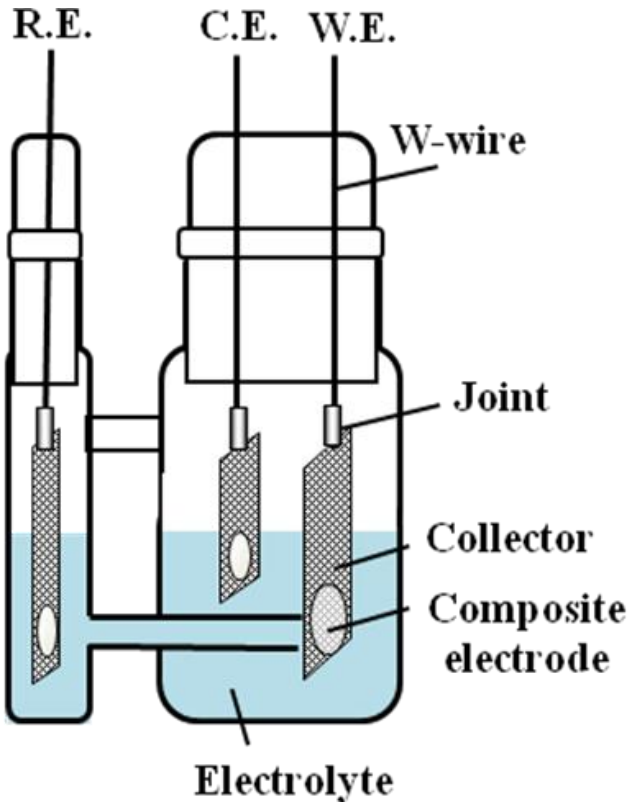

Figure 3-6. Three electrode type glass cell. The working electrode material consist of $LiMn_2O_4$, acetylene black (AB) and polytetrafluoro ethylene (PTFE) with the weight ratio of 0.80:0.15:0.05, which was spread on a nickel mesh current collector. The electrolyte solution was Ethylene carbonate (EC) / dimethoxyethane (DME) (1:1 volume ratio) containing 1.0 mol dm^{-3} $LiClO_4$. Lithium metal foil was used as the counter electrode and reference electrode.

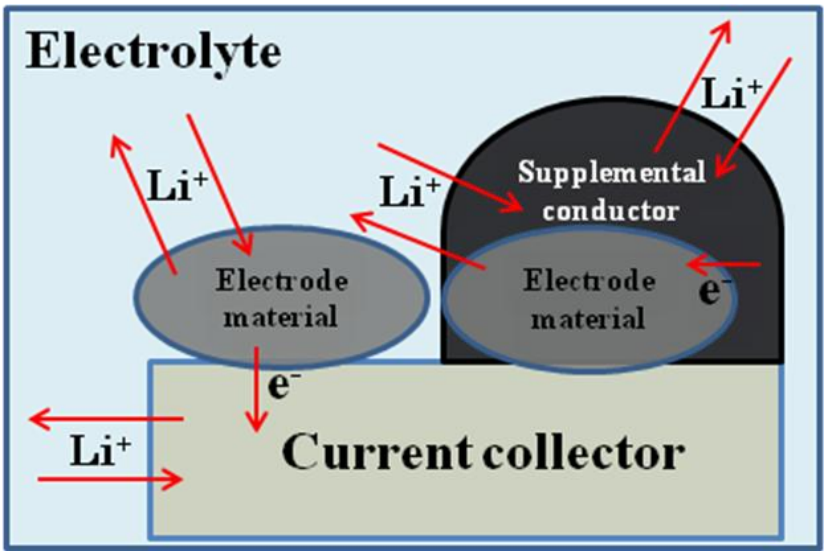

Figure 3-7. Schematic diagram of local cell reaction. When the samples were characterized, the circuit was opened and immediately the working electrode was taken out of the cell in an argon-filled glove box to avoid the local cell reaction between the active material and the current collector or the supplemental conductor

Table 3-2. XRD measurement condition

Method	2θ/θ
Source radiation	CuKα
Tube voltage & current	40 kV, 40 mA
Measured angle (2θ)	$15^{o} \leqq 2\theta \leqq 90^{o}$
Step width (2θ)	0.04^{o} (2θ)
Scanning speed	2^{o}/min
Divergence slit	$1 / 2^{o}$
Scattering slit	Open
Relaxation atmosphere	Argon gas
Data integration	5
Fitted angle (2θ)	$15^{o} \leqq 2\theta \leqq 90^{o}$

3.3 Results and discussion

3.3.1 Potential profile

Figure 3-8 shows potential profiles at 1 cycle for sample preparation. Firstly, most lithium was electrochemically extracted at a rate of 1C in each sample and then various amounts of lithium were inserted. Indicated numbers in the figure 3-8 are potentials where circuits were opened and the working electrodes were taken out of the cell for XRD measurement after the termination of lithium insertion.

3.3.2 XRD measurement

To find the lithium content for the two-phases coexistence in $Li_xMn_2O_4$, various amount of lithium was inserted to x=0.10, 0.15, 0.25 and 0.50 in $Li_xMn_2O_4$ with $x \approx 0$ by full charge. The XRD patterns for four kinds of samples characterized by electrochemical lithium insertion are represented in figure 3-9. XRD peaks shift to low angle area in 2θ with the increase of inserted lithium amount. Of indicated four patterns, $Li_{0.10}Mn_2O_4$ sample only exhibited apparent two-phase coexistence of the Li-lean phase and the Li-rich phase. In that regard, XRD patterns for $Li_{0.10}Mn_2O_4$ sample with the elapsed time was measured to investigate the relaxation phenomenon of the two-phase coexistence related to potential plateau. Figure 3-10 and 3-11 show the XRD patterns of $Li_{0.1}Mn_2O_4$ after 1h and 25h from termination of lithium insertion in 2θ from 35° to 40° (Cu-Kα), respectively. It is confirmed that the Li-lean phase and the Li-rich phase coexist and that XRD intensity of them had changed during the relaxation time.

3.3.3 Lorentz function fitting

XRD positions of 311 peaks for each relaxation sample of $Li_{0.1}Mn_2O_4$ with the Li-lean phase and the Li-rich phase were precisely obtained by asymmetric Lorentz function fitting, i.e. 36.98° and 36.61° in 2θ, which were converted into 0.8056nm and 0.8134nm in lattice constant, respectively. The relaxation phase change with elapsed time was investigated by using asymmetric Lorentz function fitting program.

Figure 3-12 shows the observed and fitted XRD patterns of $Li_{0.1}Mn_2O_4$ for 1h, 14h and 25h of relaxation time, respectively. The observed pattern agreed well with the fitted pattern obtained from the asymmetric Lorentz function; such good agreement between the observed and fitted patterns was also obtained at all XRD pattern.

3.3.4 Relaxation phenomenon of lithium inserted $LiMn_2O_4$

Figure 3-13 shows the lattice constant change of the Li-lean phase and the Li-rich

phase in $Li_{0.1}Mn_2O_4$ at the relaxation time after lithium insertion. Both the lattice constants of the Li-lean phase and the Li-rich phase were almost constant with approximately 0.8056nm and 0.8134nm during the relaxation time, respectively.

The XRD intensity ratio of the two-phases, the Li-rich phase and the Li-lean phase, was calculated by the following equation.

$$I_2 = I_2 \Big/ \sum_{i=1}^{2} I_i$$

Where i = 1 and 2 represent the Li-rich phase and the Li-lean phase, respectively. I is XRD intensity obtained from the asymmetric Lorentz function fitting. Figure 3-14 shows the change of XRD intensity ratio for the Li-lean phase and the Li-rich phase. It is indicated that the amount of the Li-lean phase decreased and that of the Li-rich phase increased with the elapsed time. It is considered that the Li-lean phase has more defects than the Li-rich phase because of its lithium deficiency, so that the Li-lean phase is kinetically favorable for lithium to diffuse during lithium insertion process. Therefore, the Li-lean phase was preferably produced at the lithium insertion process. On the other hand, the Li-rich phase is thermodynamically more stable than the Li-lean phase because of its more stoichiometric composition. Therefore the Li-lean phase decreased and the Li-rich phase increased with the relaxation time after lithium insertion in $Li_{0.1}Mn_2O_4$.

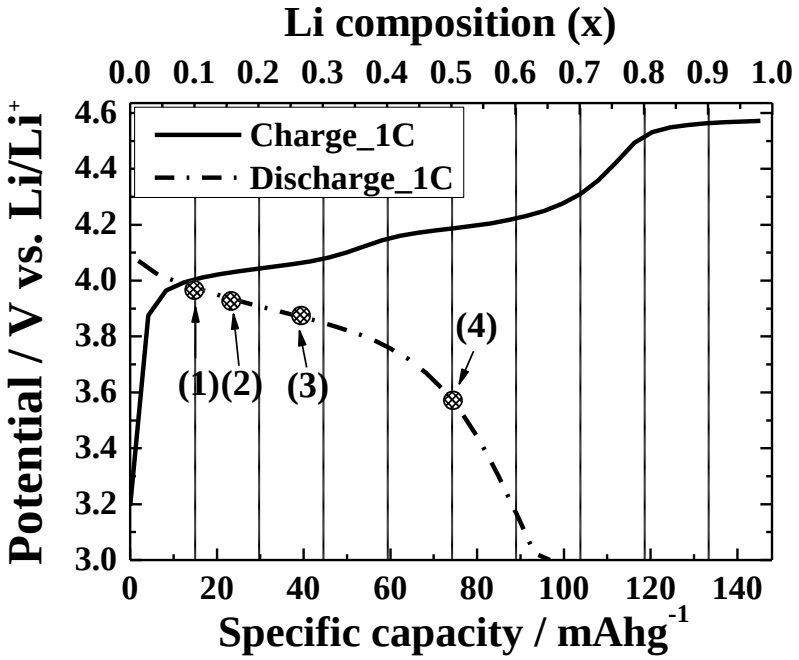

Figure 3-8. Potential profiles at 1 cycle for each sample. Indicated numbers in the figure are potentials where circuits were opened and the working electrodes were taken out of the cell for XRD measurement after the termination of lithium insertion. Lithium insertion condition is (1) x to 0.10 in $Li_xMn_2O_4$ at 1C, (2) x to 0.15 in $Li_xMn_2O_4$ at 1C, (3) x to 0.25 in $Li_xMn_2O_4$ at 1C and (4) x to 0.5 in $Li_xMn_2O_4$ at 1C.

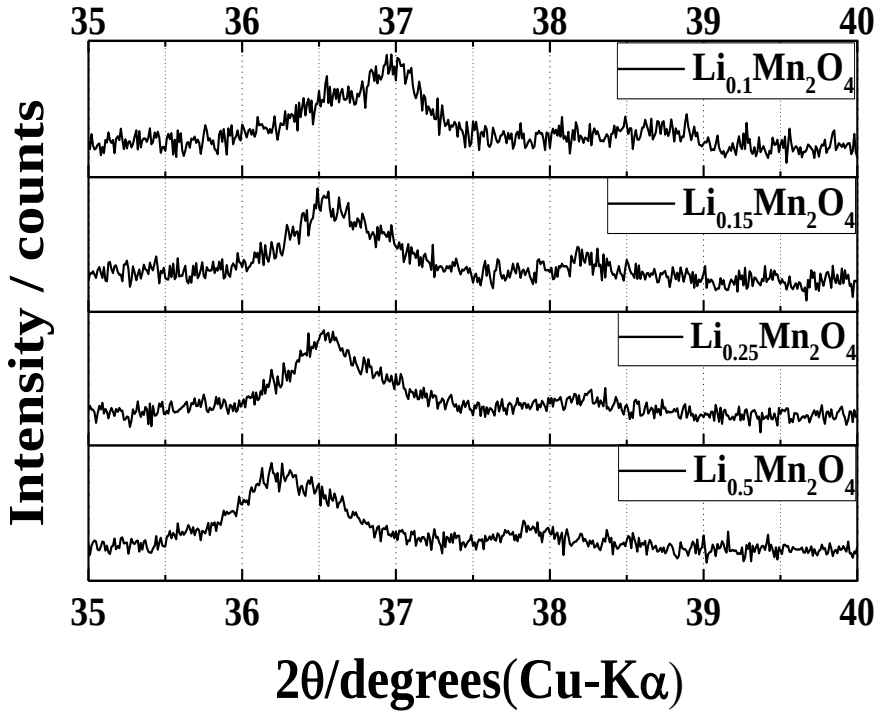

Figure 3-9. XRD patterns for $Li_xMn_2O_4$ after termination of lithium insertion (x=0.1, 0.15, 0.25 and 0.5)

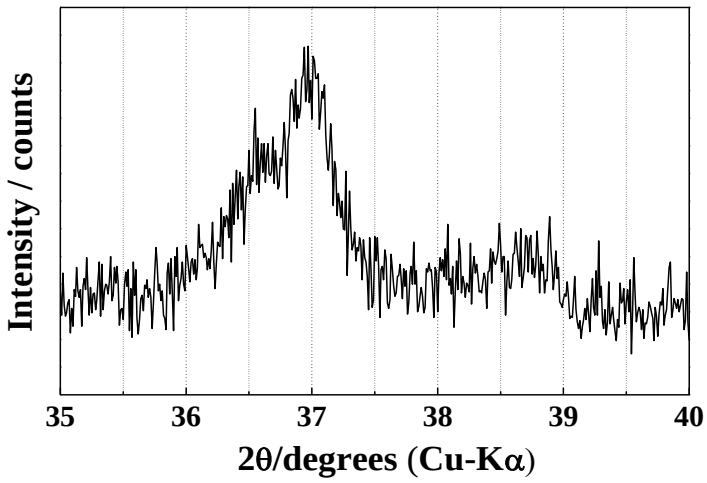

Figure 3-10. XRD pattern of $Li_{0.1}Mn_2O_4$ after 1h from termination of lithium insertion.

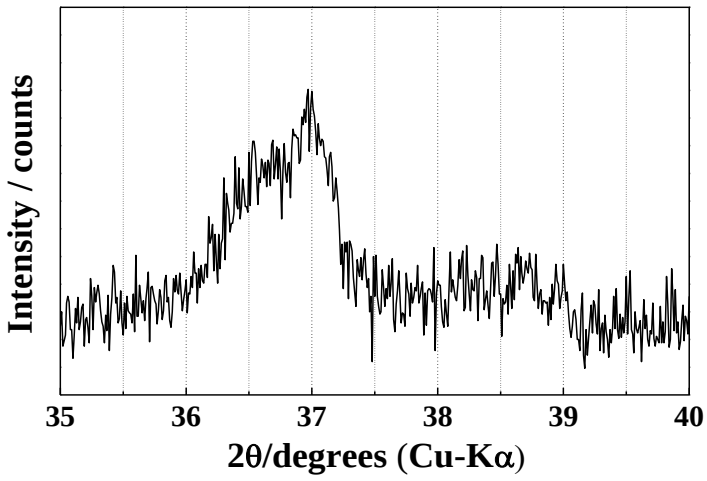

Figure 3-11. XRD pattern of $Li_{0.1}Mn_2O_4$ after 25h from termination of lithium insertion.

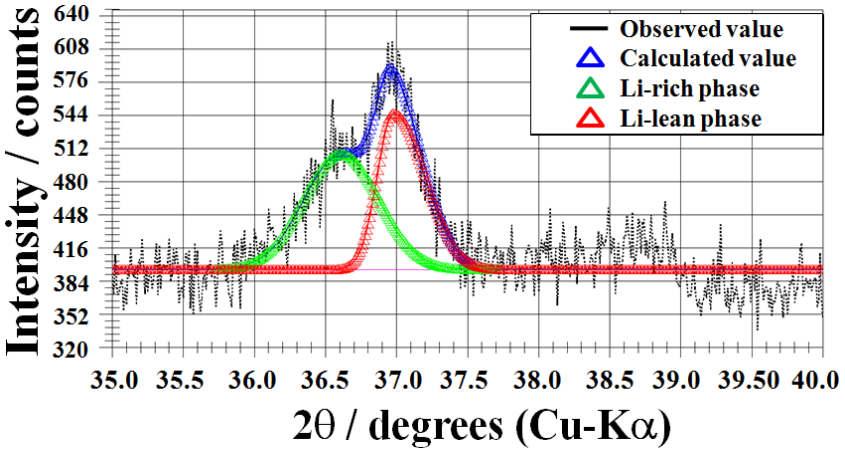

(a) After 1h

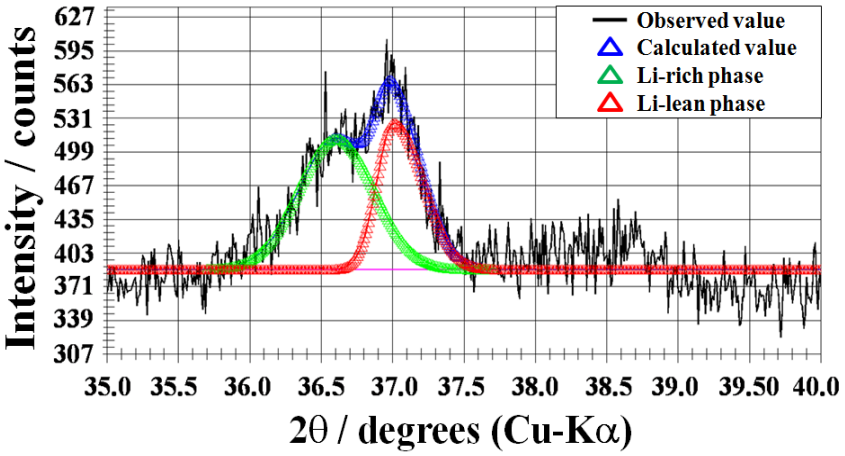

(b) After 14h

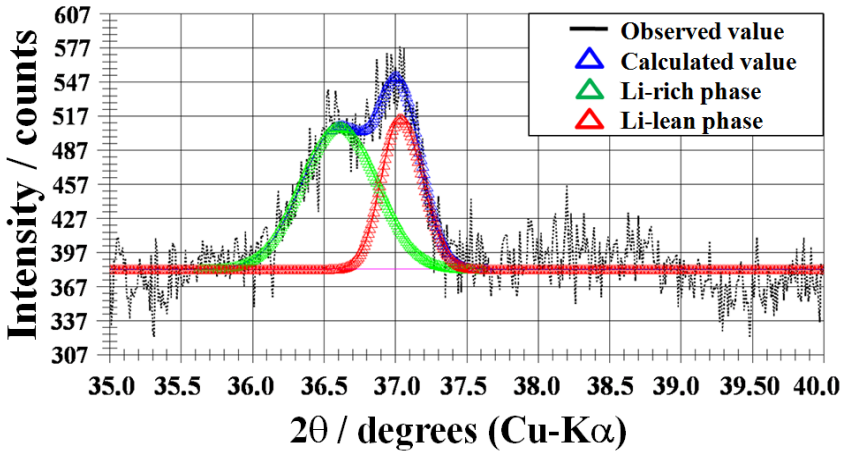

(c) After 25h

Figure 3-12. The asymmetric Lorentz function fitting to XRD patterns at 1h, 14h and 25 h elapsed time after lithium insertion

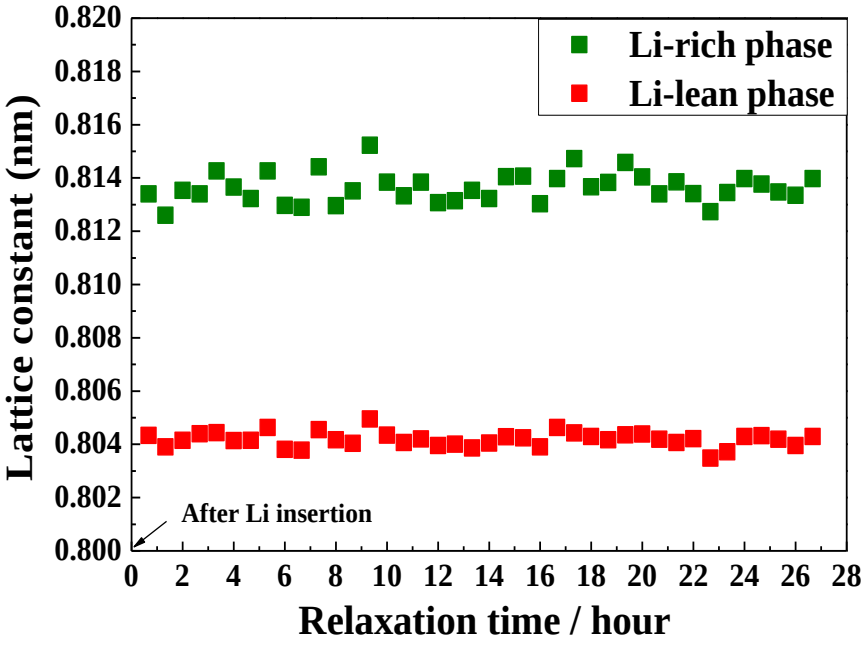

Figure 3-13. Lattice constant changes of the Li-lean phase and the Li-rich phase in $Li_{0.1}Mn_2O_4$ after termination lithium insertion.

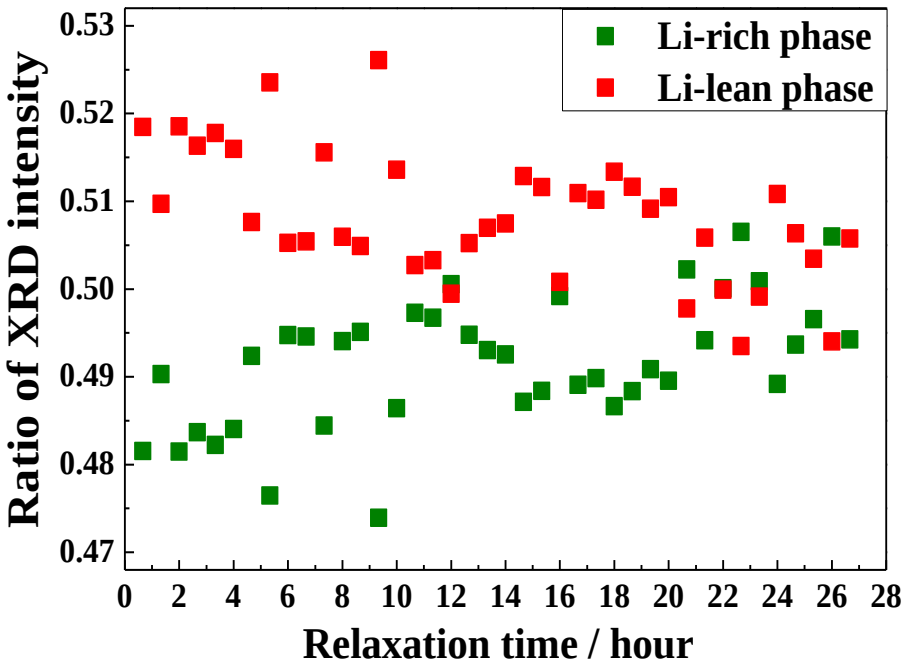

Figure 3-14. Ratio of XRD intensity of the Li-lean phase and the Li-rich phase in $Li_{0.1}Mn_2O_4$ after termination lithium insertion.

3.4 Conclusions

The relaxation phase change of $LiMn_2O_4$ cathode was investigated with the elapsed time after lithium insertion. Firstly most amount of lithium were extracted from $LiMn_2O_4$ electrochemically and took a rest for 20 min, then lithium were inserted to x=0.1 in terms of $Li_xMn_2O_4$ electrochemically at a rate of 1C. In order to investigate the crystal phase change, XRD was measured as a function of elapsed time.

Two phases, the Li-rich phase with lattice constant 0.8136nm and the Li-lean phase with lattice constant 0.8042nm, coexist in $Li_{0.1}Mn_2O_4$. Both two lattice constants were almost constant with the elapsed time. The Li-lean phase decreased and the Li-rich phase increased with elapsed time. It is considered that Li-lean phase has more defects than Li-rich phase because of its lithium deficiency, that Li-lean phase is kinetically favorable for lithium to diffuse. Therefore, the Li-lean phase was preferably produced at the lithium insertion process. On the other hand, the Li-rich phase is thermodynamically more stable than the Li-lean phase because of its more stoichiometric composition, therefore the Li-lean phase decreased and the Li-rich phase increased after the lithium insertion.

Reference

1. J. B. Goodenough, M. M. Thackery, W. I. F. David and P. G. Bruce, *Rev. Chim. Miner*, 21, 435-455 (1984).
2. T. Ohzuku, M. Kitagawa and T. Hirai, *J. Electrochem. Soc.*, 137(3), 769-774 (1990).
3. J. M. Tarascon, E. Wang, F. K. Shokoohi, W. R. Mckinnon and S. Colson, *j. Electrochem. Soc.*, 138(10), 2859-2863 (1991).
4. D. Guyomard and J. M. Tarascon, *J. Electrochem. Soc.*, 138(10), 2864-2868 (1991).
5. M.M. Thackeray, W.I.F. David, P.G. Bruce, J.B. Goodenough, *Mat. Res. Bull.* 18, 461–472 (1983).
6. M.M. Thackeray, P.J. Johnson, L.A. de Picciotto, P.G. Bruce,J.B. Goodenough, *Mat. Res. Bull*. 19, 179 (1984).
7. A. Yamada, M. Tanaka, *Mater. Res. Bull* 30, 715 (1995).
8. J. Rodr´ıguez-Carvajal, G. Rousse, C. Masquelier, M. Her- MRSEC Program of the National Science Founda- vieu, *Phys. Rev. Lett*. 81, 4660–4663 (1998).
9. G. Rousse, C. Masquelier, J. Rodr´ıguez-Carvajal, M. Hervieu, *Electrochem. Solid-State Lett*. 2, 1–3 (1999).
10. J.E. Greedan, N.P. Raju, A.S. Will, C. Morin, S.M. Shaw, J.N. Reimers, *Chem. Mater*. 10, 3058–3067 (1998).
11. A. Mosbah, A. Verbaere and M. Tournoux, *Mat. Res. Bull.*, 18(11), 1375-1381 (1983).
12. M.M. Thackeray, Prog. *Solid. State Chem.* 25, 1–71 (1997).
13. N. Ishizawa, K. Tateishi, *J. Ceramic Soc. Of Japan.*, 117(1), 6-14 (2009).
14. M. Wakihara, *Materials Science and Engineering*, R33, 109-134 (2001).
15. K. Kanamura, H. Naito, T. Yao and Z. I. Takehara, *J, Mater. Chem*., 6(1), 33-36 (1996)
16. S. Park, M. Oda, and T. Yao, *Solid State Ionics*, 203, 29 (2011).
17. M. Oda, S. Park, T. Yabutsuka, M. Hibino, and T. Yao, Meet. Abstr. - *Electrochem. Soc*., Abstract 49 (2010).
18. S. Park,M. Oda, T. Yabutsuka, and T. Yao, Meet. Abstr. - *Electrochem. Soc.*, Abstract 42 (2011).
19. I. S. Seo, S. Park, and T. Yao, *ECS Electrochem. Lett*., 2(1), A6 (2013).
20. I. S. Seo, S. Park, and T. Yao, *Zero-Carbon Energy Kyoto 2011, T. Yao, Editor, Springer*, 165 (2012).
21. I. S. Seo, S. Park, and T. Yao, Asian-core University Program on Advanced Energy Science, *International Symposium on Advanced Energy Systems and Materials*,

Abstract 11 (2011).
22. I. Seo, S. Nagashima, S. Takai, and T. Yao, *ECS Electrochem. Lett*., 2(7), A72-A74 (2013)
23. S. Park, K. Kameyama, and T. Yao, *Electrochem. Solid-State Lett.*, 15(4), A49 (2012).
24. I. Seo, S. Park, and T. Yao, Meet. Abstr. - *Electrochem. Soc*., Abstract 176 (2012).

CHAPTER 4

RELAXATION PHASE ANALYSIS OF ELECTROCHEMICALLY LITHIUM INSERTED SPINEL $LiMn_2O_4$

After electrochemical lithium extraction to $x \approx 0$ in terms of $Li_xMn_2O_4$, various amounts of lithium were electrochemically inserted to into $Li_xMn_2O_4(x \approx 0)$, then the relaxation structure after termination of lithium insertion was investigated by using X-ray diffraction measurement and the Rietveld analysis. The mole fraction of the Li-lean phase decreased and that of the Li-rich phase increased with the relaxation time after lithium insertion. It is considered that the Li-lean phase containing excess lithium formed during the lithium insertion process separated into two phases, the Li-lean phase without excess lithium and the Li-rich phase, during the relaxation process after termination of lithium insertion.

4.1 Introduction

Li-ion secondary batteries (LIBs) with high energy density and high power are expected for applications in energy storage systems and power sources for electric vehicles. Electrode materials are crucial for battery performance in LIBs and it is important to understand the electrode behavior in terms of lithium insertion/extraction process. Recently, it have been reported on the relaxation process of several electrode materials for lithium ion secondary batteries by using X-ray diffraction (XRD) measurement and the Rietveld analysis.[1-8] As an example of the relaxation analysis, the crystal structure changes of γ-Fe_2O_3 after termination of electrochemical lithium insertion were investigated, as a result it was found that the iron occupancy of 8a sites decreased and that of 16c sites increased with lithium insertion, while the iron occupancy of 8a sites increased and that of 16c sites gradually decreased after lithium insertion. In that regard, it is concluded that lithium preferentially occupies the 8a site kinetically, whereas the 16c site is favored thermodynamically.[1-3] It was also reported on the phase change of $LiFePO_4$ cathode material during the relaxation process after lithium insertion.[4] From the Rietveld analysis result, it was found that the amount of $LiFePO_4$ decreased while that of $FePO_4$ increased after lithium insertion. It was considered that $LiFePO_4$ including lithium defects were preferable for lithium diffusion during the insertion process and that the defective $LiFePO_4$ separated into $LiFePO_4$ without lithium defects and $FePO_4$ at the relaxation process after the termination of

lithium insertion.

Spinel $LiMn_2O_4$ is an attractive cathode material for lithium ion secondary batteries due to its cost-effectiveness, low toxicity, excellent thermal stability, relatively high operating voltage and energy density.[9-11] Various research studies on structural attributions of spinel $LiMn_2O_4$ have been conducted to improve its electrochemical performance.[10, 12-15] Kanamura et al. investigated the structural change of spinel $LiMn_2O_4$ induced by lithium extraction by using the Rietveld analysis method, and reported on the coexistence of two spinel phases in the region of $x < 0.5$ in terms of $Li_xMn_2O_4$ during the lithium extraction process.[16] They reported that the Li-lean phase had smaller lattice constant and more vacancies than the Li-rich phase, and that the amount of the Li-lean phase increased while the Li-rich phase decreased with the decrease of lithium content x.

In the previous chapter 3, with XRD data based on the intensity change of the 311 peak in $Li_{0.1}Mn_2O_4$ after termination of lithium insertion and discussed on the relaxation phenomenon of the coexisting Li-lean phase and Li-rich phase by using the asymmetry Lorentz function fitting program. It was found that the Li-rich phase and the Li-lean phase presented by Kanamura et al. coexist and that the amount of the Li-lean phase decreased and the Li-rich phase increased with various elapsed time.[5]

In this chapter 4, various amounts of lithium (x=0.10, 0.15 and 0.20) were electrochemically inserted into $Li_xMn_2O_4$ ($x \approx 0$), and then investigated the change of the relaxation structure after termination of lithium insertion by using XRD measurement and the Rietveld analysis. The relaxation analysis for $Li_{0.40}Mn_2O_4$ lithium-extracted at various C rates was also carried out. Although in chapter 3 just discussed on the XRD intensity of 311 peak indexed at 35^{o}~40^{o} in 2θ range, in this chapter 4 by adopting the Rietveld method for full data of the XRD profile even around 15^{o}~90^{o} in 2θ range, it is able to discuss on more precise and detailed relaxation phenomenon such as change of lattice constant, scale factor, mole fraction of coexisting Li-lean phase and Li-rich phase.

4.2 Experimental

4.2.1 Materials synthesis

$LiMn_2O_4$ was synthesized from Li_2CO_3 and $MnCO_3$ by solid-state reaction, as flow chart shown in figure 4-1. Li_2CO_3 and $MnCO_3$ were prepared in a mole ratio of 1:4, mixed and grounded by electric mortar for 5 h. The mixture was calcined at 550 °C for 12 h in air, then pressed to a disk by 9.8 MPa, sintered at 1073 K for 4 h. $LiMn_2O_4$ powder was prepared by grounding thus obtained pellet. Thus obtained $LiMn_2O_4$ powder was identified by X-ray diffraction (XRD) measurement with Cu-Kα radiation.

For the working electrode, the thus obtained $LiMn_2O_4$ powder was mixed with acetylene black (AB, Acetylene Black, Surface area: 133 m^2g^{-1}, Denkikagaku Kogyo) as a supplemental conductor and polytetrafluoro ethylene (PTFE) as an adhesive agent in a weight ratio of 0.70:0.25:0.05, then spread onto a nickel mesh current collector. After drying the working electrode at 120 °C for 24 h, a three electrode type glass cell was assembled in an argon-filled glove box. Lithium metal was used for counter and reference electrode. The electrolyte was 1M $LiClO_4$ dissolved in a mixture of ethylene carbonate (EC) and a 1,2-dimethoxyethane (DME) solution (1M $LiClO_4$ in EC/DME, 1:1 v/v, Kishida chemical Corp., Ltd.).

4.2.2 Electrochemical lithium extraction/insertion

Electrochemical lithium extraction and insertion were galvanostatically conducted at a rate of various C rates at 25 °C. The lithium extraction/insertion amount for all samples was calculated by integrating the current. Firstly the cell was charged to extract all of the lithium from $LiMn_2O_4$, the rest time was assigned for 24 h, then discharged to insert lithium until x=0.10, 0.15 and 0.20 in terms of $Li_xMn_2O_4$, respectively, which of detailed conditions are shown in table 4-1. When the samples were characterized, the circuit was opened and immediately the working electrode was taken out of the cell in an argon-filled glove box to avoid the local cell reaction between the active material and the current collector or the supplemental conductor. The working electrode was washed in EC/DME (1:1 v/v, Kishida chemical Corp., Ltd.) solution and DME (Kishida chemical Corp., Ltd.) solution to remove the remaining lithium-salt, then it was dried at 35°C in argon atmosphere.

4.2.3 X-ray diffraction (XRD) measurement

Electrochemically characterized working electrode was set in a sealed holder (2391A201, Rigaku Corp., Ltd.) with beryllium window in an argon-filled glove box,

which was set to a Model Ultima powder X-ray diffractometer (UltimaIV, Rigaku Corp., Ltd.) with copper Kα radiation. In order to investigate the relaxation structure change, XRD measurements were successively and repeatedly carried out at the various relaxation times after termination of lithium insertion or extraction. The tube voltage and current were adjusted to 40 kV and 40 mA. The scanning technique with sampling steps of $2\theta = 0.04°$ and scanning speed of $2° \text{ min}^{-1}$ was used over the 2θ range from 15° to 90°. Table 4-2 indicates the conditions of XRD measurement.

4.2.4 The Rietveld analysis

The XRD profiles were analyzed by the Rietveld method using RIEVEC program. [1-4, 7, 17-19] Successive ten XRD patterns with the elapsed time were integrated to reduce noise and improve accuracy of the Rietveld analysis. The relaxation time was indicated by mean time of elapsed time for measurement of integrated ten XRD patterns. The Rietveld analysis was conducted under the condition of two-phase, the Li-rich phase and the Li-lean phase, and coexistence.[16] The crystal structure of both phases was represented by the space group $Fd\bar{3}m$ (space group No. 227). The ionic configuration was regulated as manganese at the 16d site and oxygen at the 32e site. The contribution of lithium was ignored. The peaks derived from the AB and the nickel collector in the XRD patterns were evaluated as background curves.[1-4, 7, 17] From the results of the Rietveld analysis, lattice constant, scale factor and mole fraction of two phase were obtained.

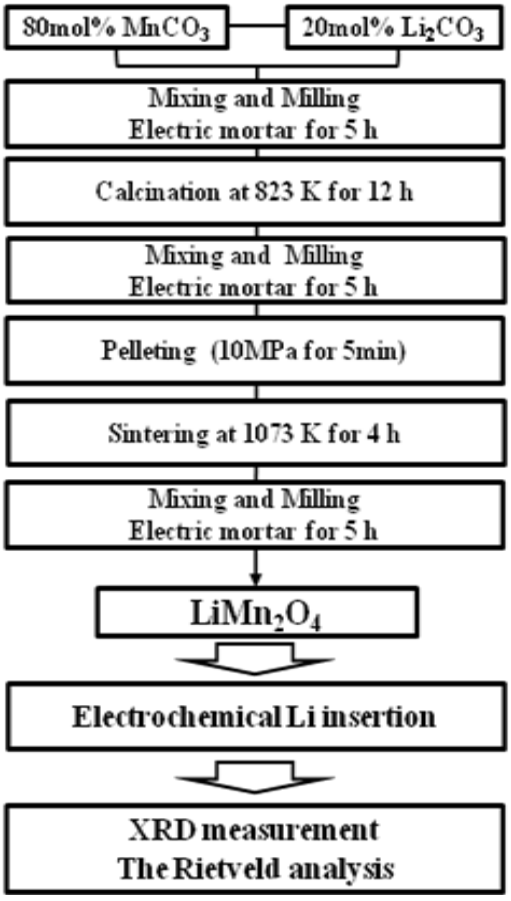

Figure 4-1. Flow chart for synthesis

Table 4-1. Cell preparation condition

Cell	Three electrodes type glass cell (Argon-sealed)
W.E.	70wt%$LiMn_2O_4$ + 25wt%AB + 5wt%PTFE
C.E., R.E.	Lithium metal
Collector	Nickel mesh
Electrolyte	1 mol dm^{-3} $LiClO_4$ in EC/DME (1/1 v/v)
Lithium insertion (Procedure)	Lithium extraction to x=0 in $Li_xMn_2O_4$ at 1C
	24 h rest
	Lithium insertion to x=0.10, 0.15 or 0.20 in $Li_xMn_2O_4$ at 1C
Lithium extraction	For $Li_{0.40}Mn_2O_4$ sample, Lithium extraction at 0.1C, 1C
Relaxation	Argon atmosphere

Table 4-2. XRD measurement condition

Method	2θ/θ
Source radiation	CuKα
Tube voltage & current	40 kV, 40 mA
Measured angle (2θ)	$15^{o} \leqq 2\theta \leqq 90^{o}$
Step width (2θ)	0.04^{o} (2θ)
Scanning speed	2^{o}/min
Divergence slit	$1 / 2^{o}$
Scattering slit	Open
Relaxation	Argon atmosphere
Data integration	10
Fitted angle (2θ)	$15^{o} \leqq 2\theta \leqq 90^{o}$

4.3 Results and discussion

4.3.1 Potential profile

Figure 4-2 shows potential profile of $LiMn_2O_4$ samples during one cycle of charge/discharge process at 1C. Solid line and dotted line indicate charge and discharge profile, respectively. Firstly, most lithium was electrochemically extracted at a rate of 1C in each sample and then various amounts of lithium were inserted. The three kinds of samples, (1) x=0.10, (2) x=0.15 and (3) x=0.20 at the discharge process, are indicated by circle mark in figure 4-2, respectively.

4.3.2 XRD measurement and the Rietveld analysis

Figure 4-3 indicates XRD patterns of a well synthesized $LiMn_2O_4$ according to the JCPDS data, which are also compared with XRD pattern of $LiMn_2O_4$ synthesized from Li_2CO_3 and MnO_2 in chapter 2. XRD peaks of $LiMn_2O_4$ synthesized from Li_2CO_3 and $MnCO_3$ are much sharper than that of $LiMn_2O_4$ synthesized from Li_2CO_3 and MnO_2. It is considered that this contributed to smooth lithium diffusion, and two apparent potential plateaus near 4V range related to two-phase coexistence for typical $LiMn_2O_4$ cathode were exhibited in figure 4-2, in that regards, the discharge capacity property was improved than that of $LiMn_2O_4$ in chapter 1.

In figure 4-4, 4-5 and 4-6, XRD profiles for each relaxation time of $Li_xMn_2O_4$ (x=0.10, 0.15 and 0.20) were indicated from 35^o to 40^o in the 2θ range, where the XRD intensity change of coexisting two phases is observed. Thus measured full XRD patterns were well-fitted with the patterns obtained by the Rietveld method. Figure 4-7, 4-8 and 4-9 show the fitting results of $Li_xMn_2O_4$ (x=0.10, 0.15 and 0.20) sample after 130 h from the termination of lithium insertion, respectively. The magnification plots of fitting result of two phases from 35° to 40° show well fitting of the Li-rich phase and Li-lean phase coexistence. Reliability values of R_{WP} (R-weighted pattern), R_F (R-structure factor) and R_B (R-Bragg) were sufficiently small. The Rietveld fittings were successfully conducted for all of the XRD patterns. From the Rietveld refinement results, lattice constant, scale factor and oxygen parameter of the Li-lean phase and the Li-rich phase at the relaxation time was obtained, respectively.

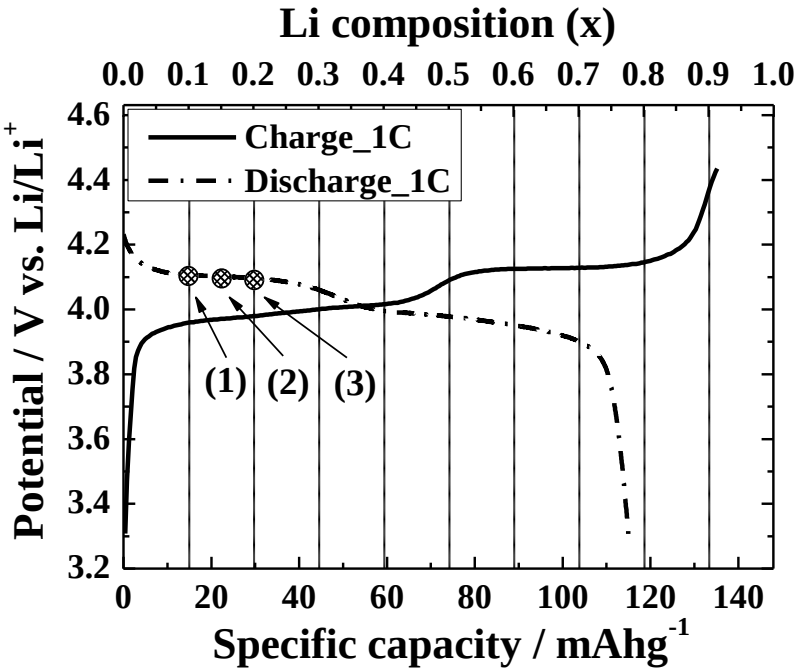

Figure 4-2. Potential profiles at 1 cycle for each sample. Indicated numbers in the figure are potentials where circuits were opened and the working electrodes were taken out of the cell for XRD measurement after the termination of lithium insertion. Lithium insertion condition is (1) x to 0.10 in $Li_xMn_2O_4$ at 1C, (2) x to 0.15 in $Li_xMn_2O_4$ at 1C, (3) x to 0.20 in $Li_xMn_2O_4$ at 1C.

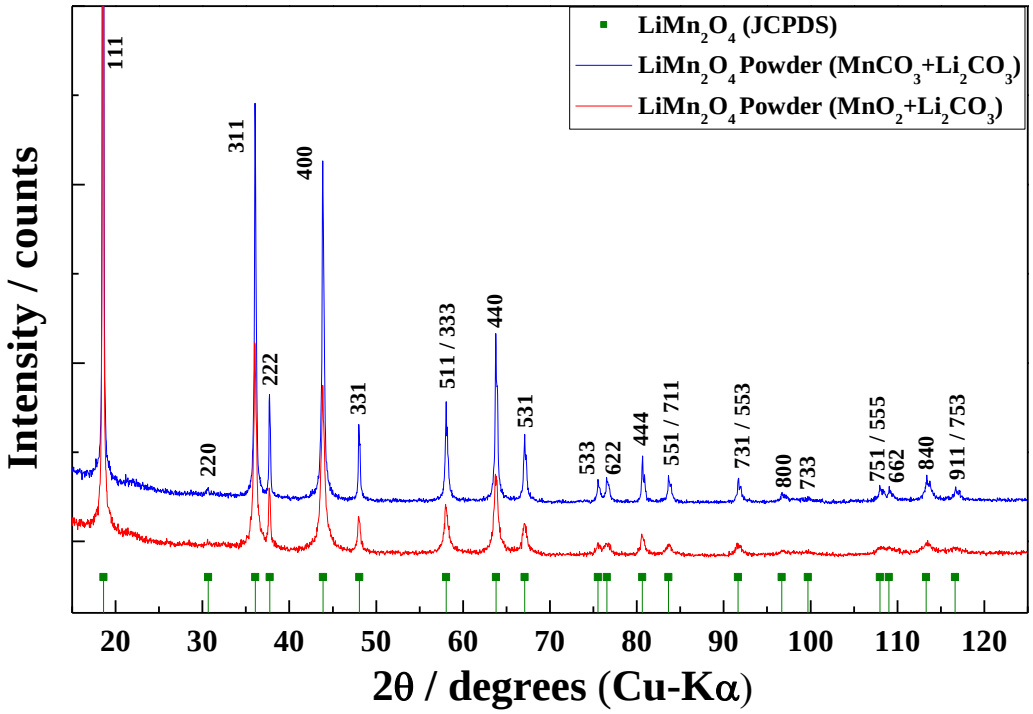

Figure 4-3. XRD pattern of $LiMn_2O_4$ powder

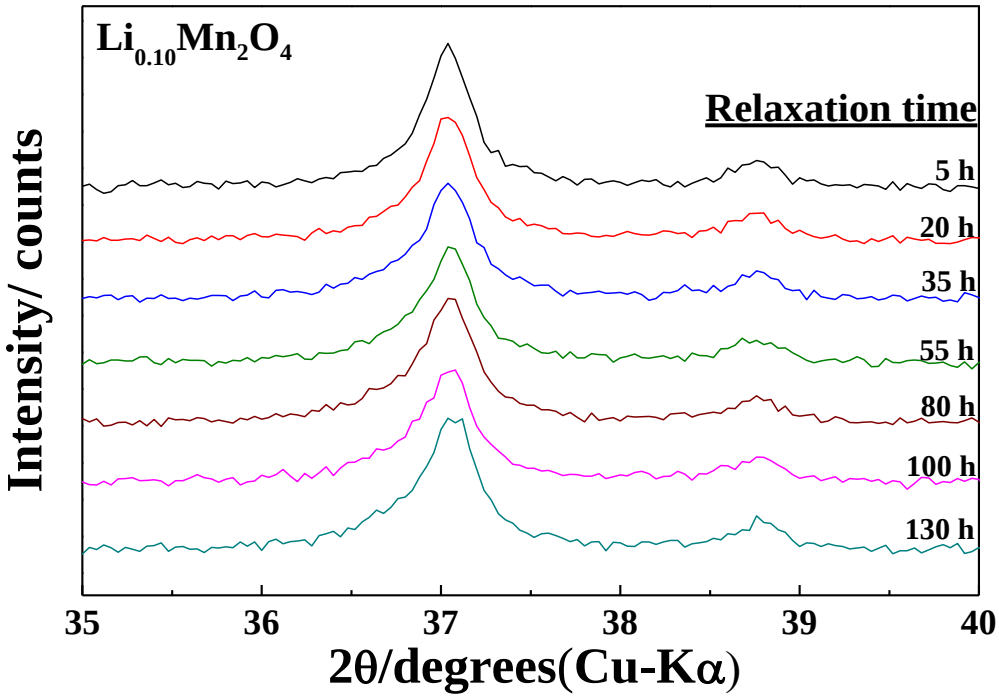

Figure 4-4. XRD patterns change of $Li_{0.10}Mn_2O_4$ with relaxation time

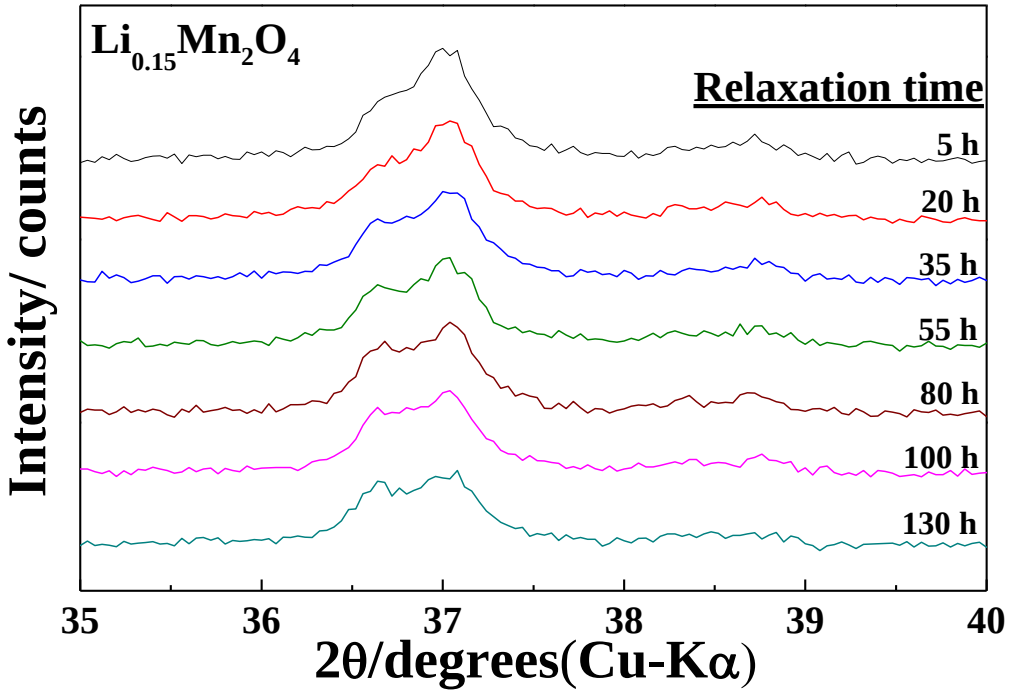

Figure 4-5. XRD patterns change of $Li_{0.15}Mn_2O_4$ with relaxation time

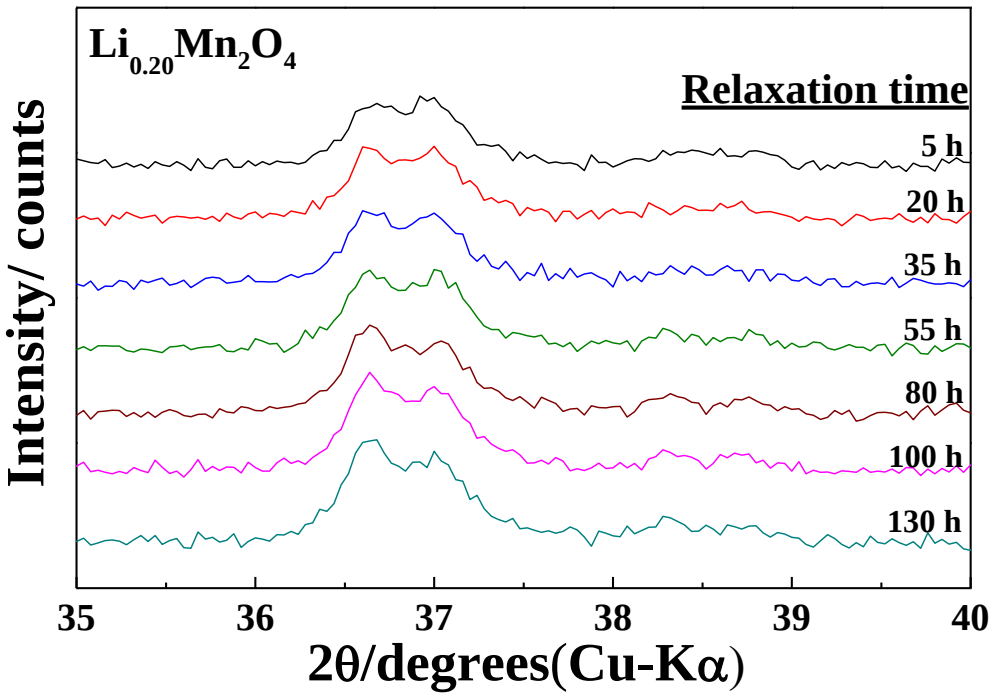

Figure 4-6. XRD patterns change of $Li_{0.20}Mn_2O_4$ with relaxation time

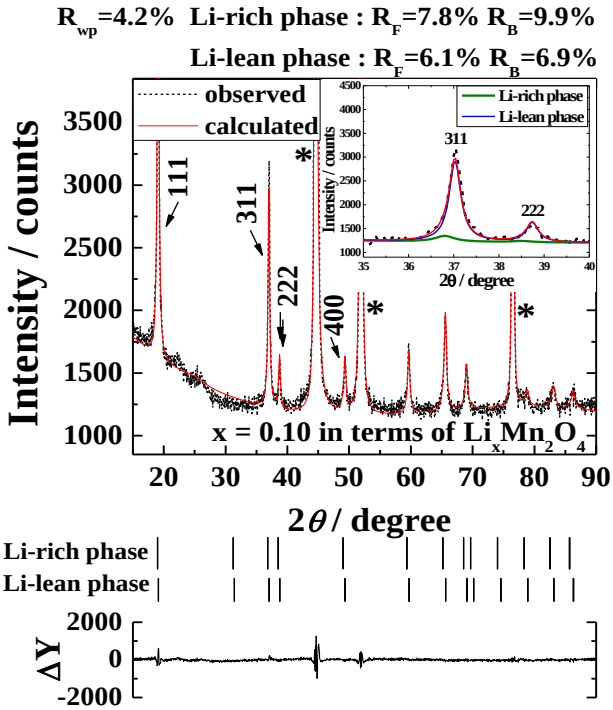

(a) 5h sample

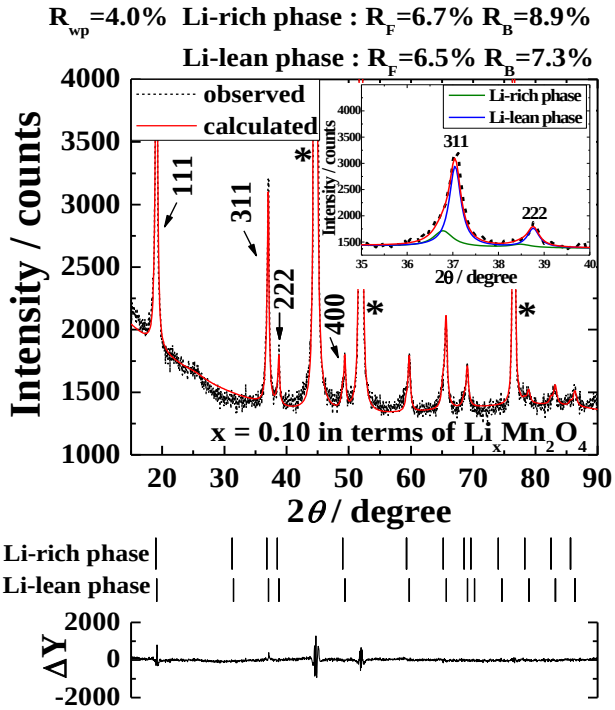

(a) 130h sample

Figure 4-7. Rietveld fitting result of $Li_xMn_2O_4$ x=0.10

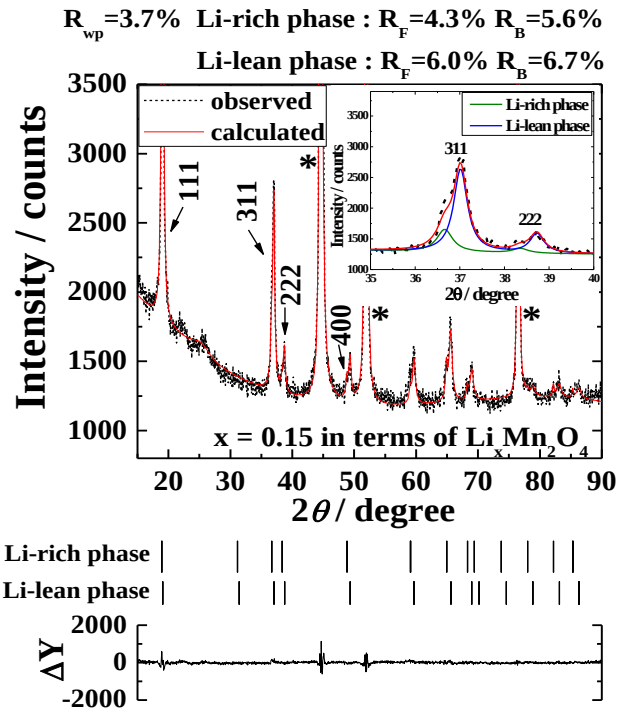

(a) 5h sample

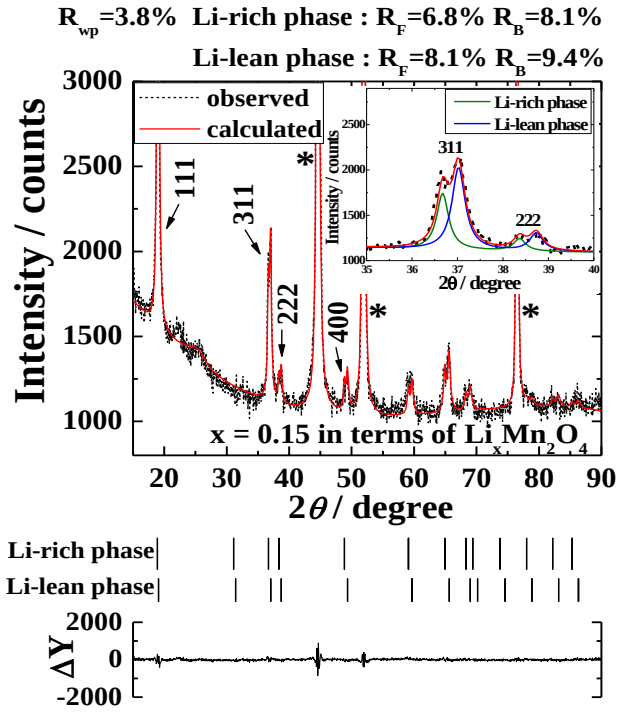

(a) 130h sample

Figure 4-8. Rietveld fitting result of $Li_xMn_2O_4$ x=0.15

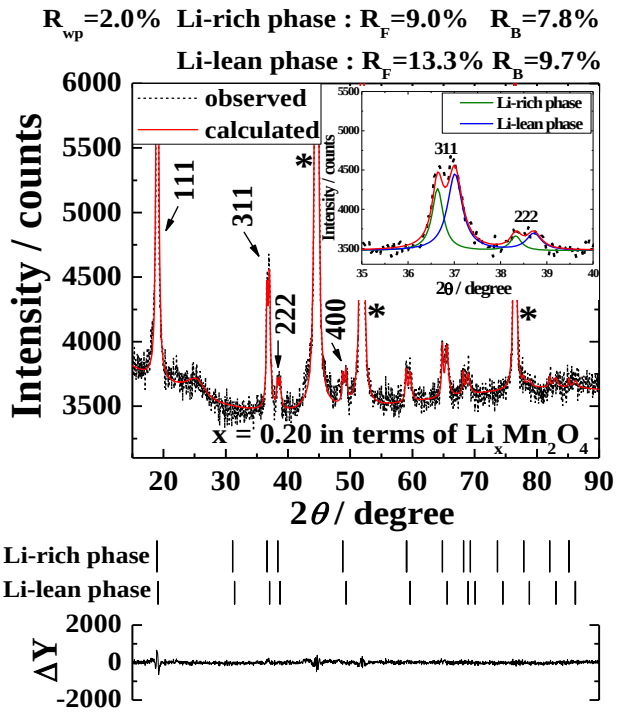

(a) 5h sample

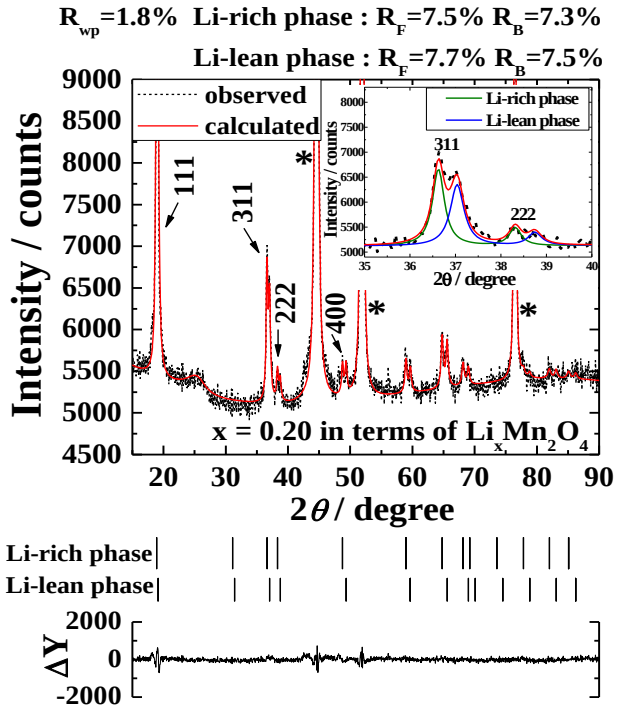

(b) 130h sample

Figure 4-9. Rietveld fitting result of $Li_xMn_2O_4$ x=0.20

4.3.3 Effect of the lithium insertion

The lattice constants obtained by the Rietveld analysis for the Li-rich phase and the Li-lean phase at the relaxation time after lithium insertion in $Li_xMn_2O_4$ (x=0.10, 0.15 and 0.20) are presented in figure 4-10, 4-11 and 4-12, respectively. Each of the lattice constants of the Li-rich phase and the Li-lean phase was almost constant during the relaxation time.

The mole fraction of the two-phases, the Li-rich phase and the Li-lean phase, was calculated by the following equation.[20]

$$M_2 = S_2 Z_2 V_2 \Big/ \sum_{i=1}^{2} S_i Z_i V_i$$

Where i = 1 and 2 represent the Li-rich phase and the Li-lean phase, respectively. M, S, Z and V are the mole fraction, the scale factor obtained by the Rietveld analysis, the number of formula units per unit cell and the unit cell volume, respectively. Figure 4-13, 4-14 and 4-15 show the mole fraction changes of the Li-rich phase and the Li-lean phase as a function of the relaxation time after lithium insertion in $Li_xMn_2O_4$ (x=0.10, 0.15 and 0.20), respectively. The mole fraction of the Li-rich phase increased and that of the Li-lean phase decreased with the relaxation time in $Li_xMn_2O_4$ (x=0.10, 0.15 and 0.20). It is considered that the Li-lean phase has more vacancies than the Li-rich phase due to lithium deficiency and that the structure of the Li-lean phase was maintained even containing excess lithium at the lithium insertion process in order to promote lithium diffusion. It is considered that the Li-lean phase containing excess lithium formed during the lithium insertion process separated into two phases, the Li-lean phase without excess lithium and the Li-rich phase, during the relaxation process. Therefore, the mole fraction of the Li-rich phase increased and that of the Li-lean phase decreased during the relaxation time after termination of lithium insertion.

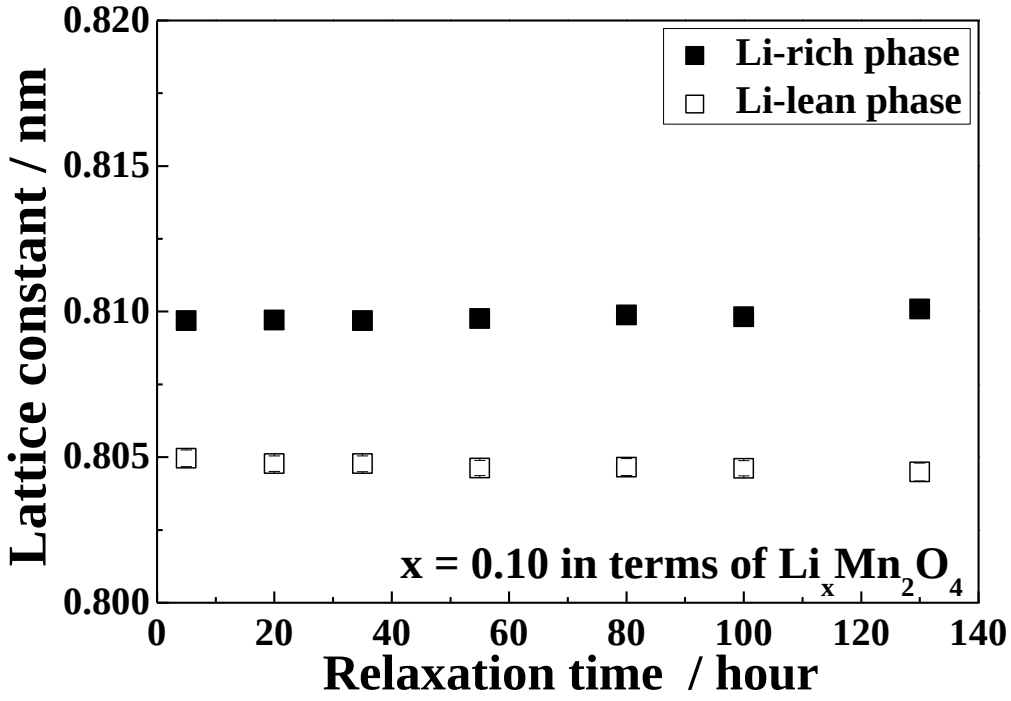

Figure 4-10. The lattice constant for the Li-rich phase and the Li-lean phase during the relaxation time in $Li_{0.10}Mn_2O_4$. Solid and open mark indicate the Li-rich phase and the Li-lean phase, respectively. The error bars were small enough to be included in each data's mark.

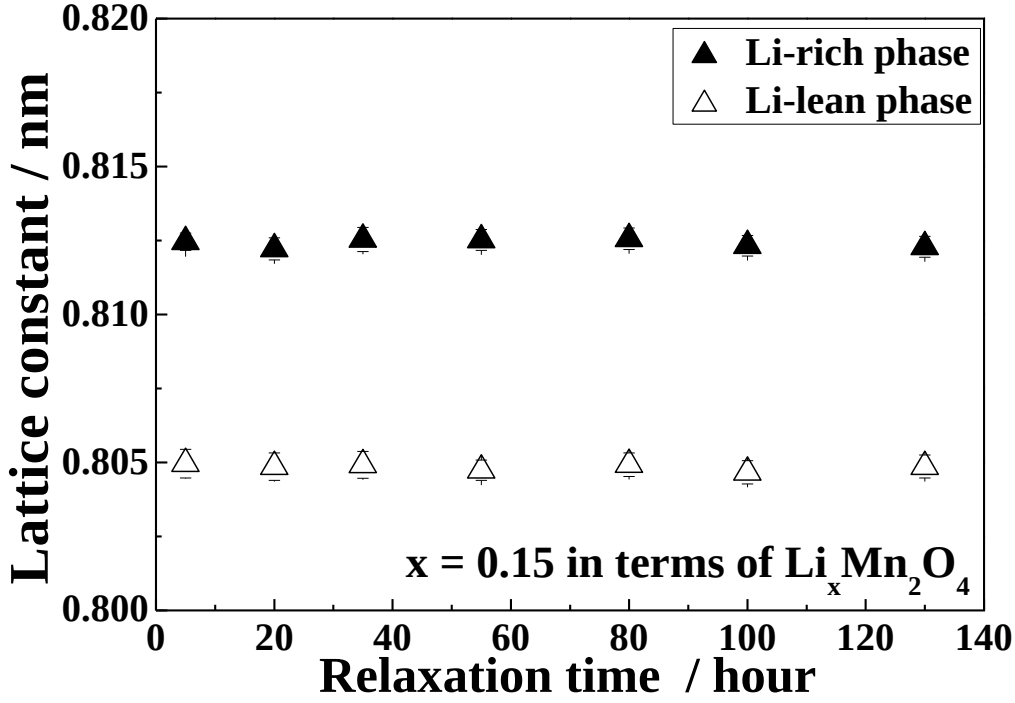

Figure 4-11. The lattice constant for the Li-rich phase and the Li-lean phase during the relaxation time in $Li_{0.15}Mn_2O_4$. Solid and open marks indicate the Li-rich phase and the Li-lean phase, respectively. The error bars were small enough to be included in each data's mark.

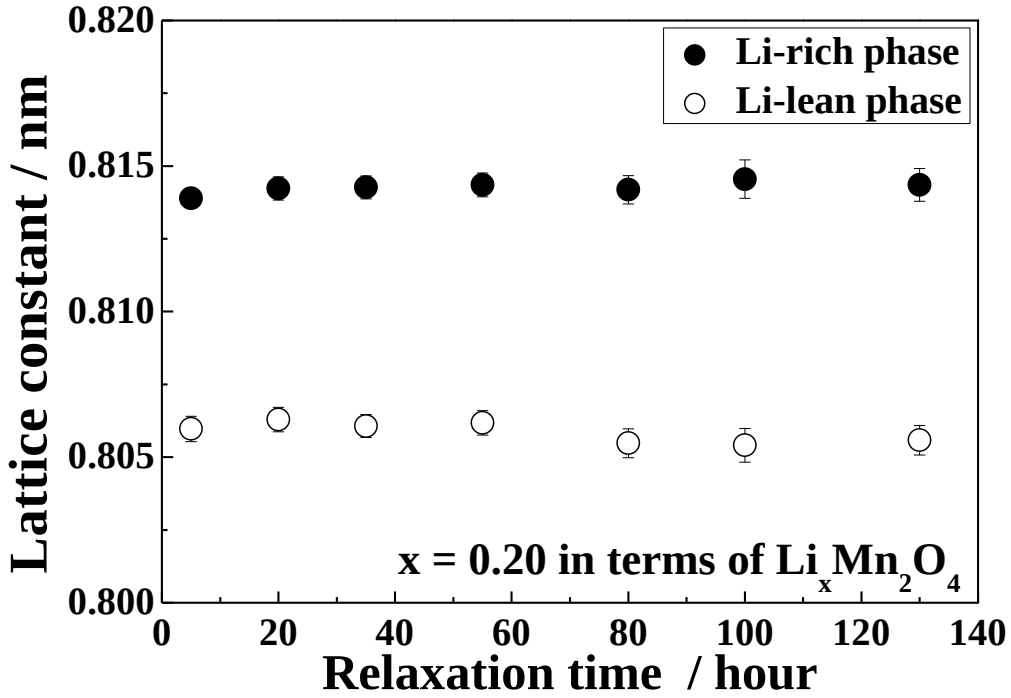

Figure 4-12. The lattice constant for the Li-rich phase and the Li-lean phase during the relaxation time in $Li_{0.20}Mn_2O_4$. Solid and open mark indicate the Li-rich phase and the Li-lean phase, respectively. The error bars were small enough to be included in each data's mark.

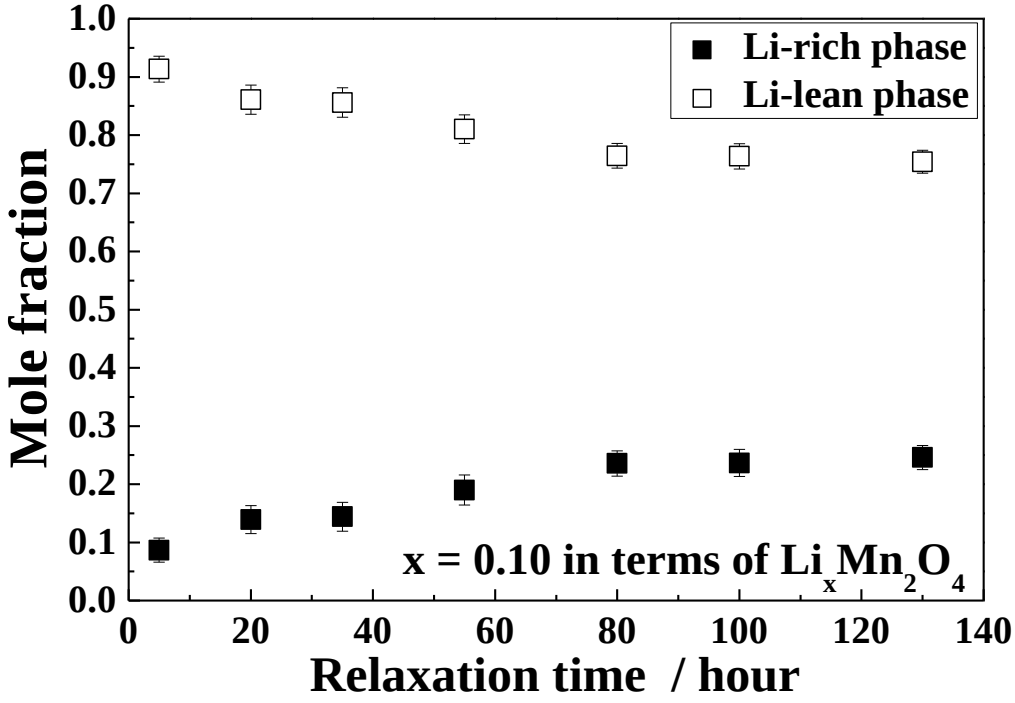

Figure 4-13. The mole fraction change of the Li-rich phase and the Li-lean phase during the relaxation time in $Li_{0.10}Mn_2O_4$. Solid and open mark indicate the Li-rich phase and the Li-lean phase, respectively. The error bars were small enough to be included in each data's mark.

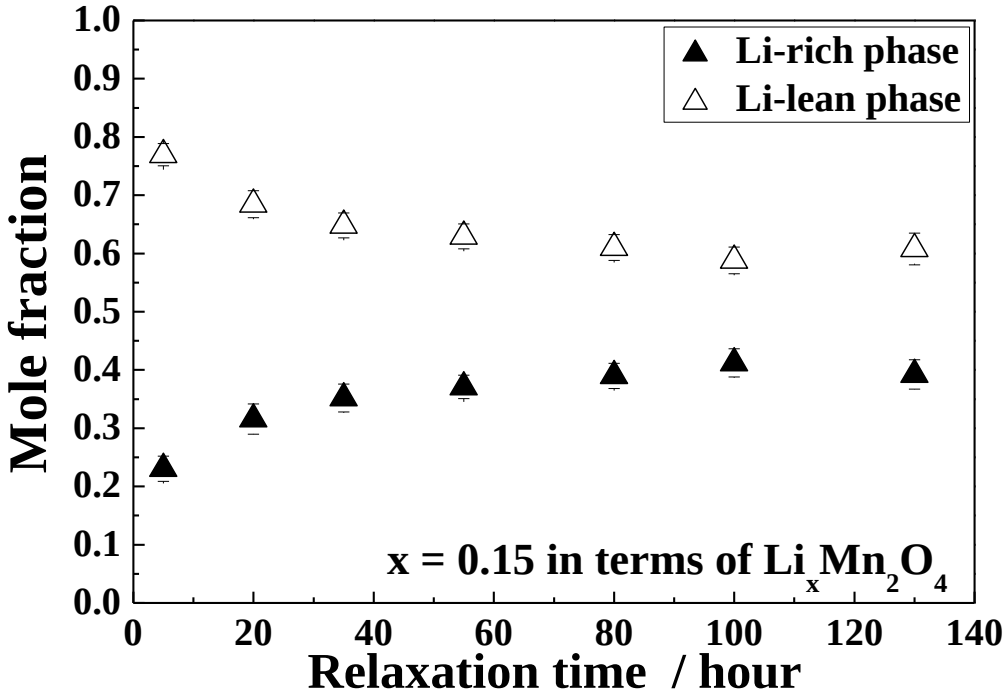

Figure 4-14. The mole fraction change of the Li-rich phase and the Li-lean phase during the relaxation time in $Li_{0.15}Mn_2O_4$. Solid and open mark indicate the Li-rich phase and the Li-lean phase, respectively. The error bars were small enough to be included in each data's mark.

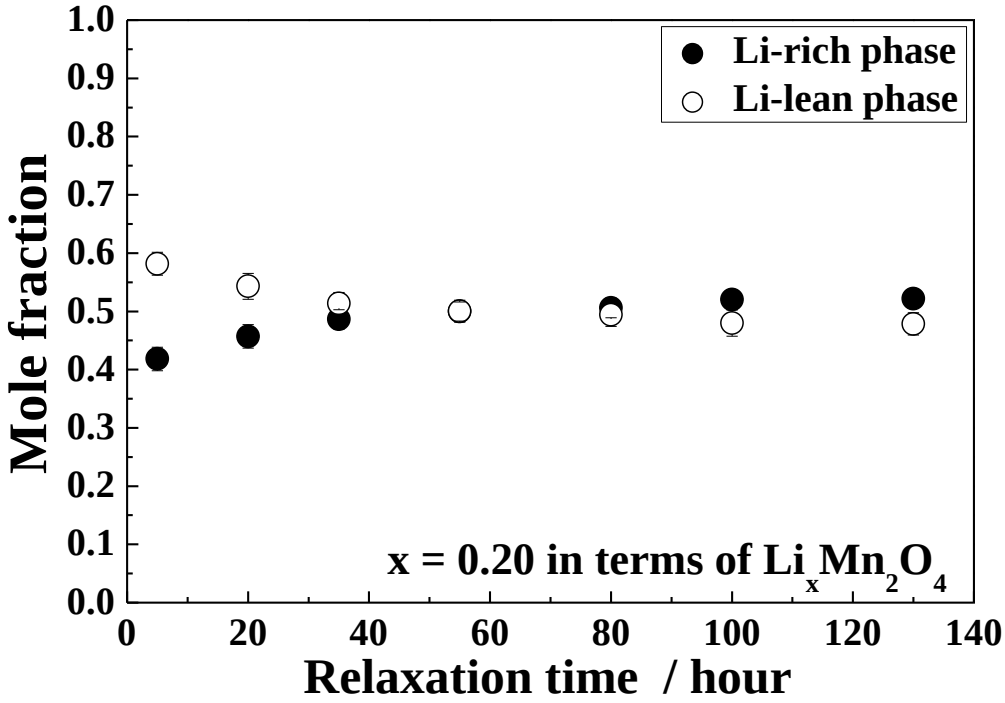

Figure 4-15. The mole fraction change of the Li-rich phase and the Li-lean phase during the relaxation time in $Li_{0.20}Mn_2O_4$. Solid and open marks indicate the Li-rich phase and the Li-lean phase, respectively. The error bars were small enough to be included in each data's mark.

4.4 Conclusions

After electrochemical lithium extraction to $x \approx 0$ in terms of $Li_xMn_2O_4$, various amounts of lithium were electrochemically inserted to into $Li_xMn_2O_4(x \approx 0)$, then the relaxation structure after termination of lithium insertion was investigated by using X-ray diffraction measurement and the Rietveld analysis. In case of lithium inserted, each of the lattice constants of the Li-rich phase and the Li-lean phase was almost constant during the relaxation time. The mole fraction of the Li-lean phase decreased and that of the Li-rich phase increased with the relaxation time after lithium insertion. It is considered that the Li-lean phase containing excess lithium formed during the lithium insertion process separated into two phases, the Li-lean phase without excess lithium and the Li-rich phase, during the relaxation process after termination of lithium insertion.

References

1. S. park, M. Oda, T. Yao, *Solid State Ionics*, 203, 29 (2011)
2. M. Oda, S. Park, T. Yabutsuka, M. Hibino, and T. Yao, Meet. Abstr. - *Electrochem. Soc.*, Abstract 49 (2010).
3. S. Park, M. Oda, T. Yabutsuka, and T. Yao, Meet. Abstr. - *Electrochem. Soc*., Abstract 42 (2011).
4. S. park, K. Kameyama, T. Yao, *Electrochem. Solid-State Lett.*, 15(4), A49 (2012).
5. I. S. Seo, S. Park, T. Yao, *Zero-Carbon Energy Kyoto 2011, T. Yao, Editor, Springer*, 165 (2012).
6. I. S. Seo, S. Park, and T. Yao, Asian-core University Program on Advanced Energy Science, *International Symposium on Advanced Energy Systems and Materials*, Abstract 11 (2011).
7. I. S. Seo, S. Park, and T. Yao, Meet. Abstr. - Electrochem. Soc., Abstract 23 (2011).
8. S. Uraki, S. Park, T. Yao, Symp. Abstr. - *Electrochem. Soc. of Japan*, Abstract 1C37 (2012)
9. M.M. Thackeray, Prog. *Solid State Chem.*, 25, 1 (1997).
10. T. Ohzuku, M. Kitagawa, T. Hirai, *J. Electrochem. Soc.*, 137(3), 769 (1990).
11. C. Masquelier, M. Tabuchi, K. Ado, R. Kanno, Y. Kobayashi, Y. Maki, O. Nakamura, J.B. Goodenough, *J. Solid State Chem.*, 123, 255 (1996).
12. J. M. Tarascon and D. Guyomard, *Electrochim. Acta*, 38(9), 1221 (1993)
13. J. M. Tarascon, E. Wang and F. K. Shokoohi, *J. Electrochem. Soc.*, 138(10), 2859 (1991).
14. D. Guyomard and J. M. Tarascon, *J. Electrochem. Soc.*, 139(4), 937 (1992).
15. A. Momchilov, V. Manev and A. Nassalevska, *J. Power Sources*, 41,305 (1993).
16. K. Kanamura, H. Naito, T. Yao and Z-i. Takehara, *J. Mater. Chem.*, 6(1), 33 (1996).
17. Yamauchi, M. Hibino, and T. Yao, *Solid State Ionics*, 191, 45 (2011).
18. T. Yao, T. Ito, and T. Kokubo, *J. Mater. Res.*, 10, 1079 (1995).
19. T. Yao, N. Ozawa, T. Aikawa, and S. Yoshinaga, *Solid State Ionics,* 175, 199 (2004).
20. Roderick J. Hill, in *The Rietveld Method*, R. A. Young, Editor, P 95, Oxford Univ. press, Oxford (1995).

CHAPTER 5

RELAXATION ANALYSIS OF ELECTROCHEMICALLY LITHIUM EXTRACTED OR/AND INSERTED LAYERED $LiCoO_2$

5.1 Introduction

Li-ion secondary batteries (LIBs) have received much attention as one of the next generation battery system due to its high energy density and operation power, and the research study to improve its performance have been proceeding actively with the recent drastic increase of demands for portable electronic devices and electric vehicle. The research on the crystal phase/ structure of electrode materials is essential to understand the electrode behavior at the lithium insertion/extraction process and to design the advanced high efficiency electrode. The relaxation analysis is important to make the transition of electrode material from kinetic state to equilibrium state clear. Recently, it has been reported on the relaxation phenomenon of changing their crystal phase/structure after the lithium insertion/extraction process for various electrode materials by using powder X-ray diffraction (XRD) measurement and the Rietveld analysis method.[1-8]

In the previous study on relaxation analysis of γ-Fe_2O_3 electrode material, it was found that the iron occupancy of 8a sites decreased and that of 16c sites increased with lithium insertion, then the iron occupancy of 8a sites increased and that of 16c sites gradually decreased at the relaxation process after the lithium insertion. It is considered that the lithium preferentially favored the 8a site kinetically, whereas the 16c site is occupied thermodynamically.[1-3]

It was also reported on the phase change of $LiFePO_4$ cathode material during the relaxation process after lithium insertion.[7] From the Rietveld analysis result, it was found that the amount of $LiFePO_4$ decreased while that of $FePO_4$ increased after lithium insertion. It was considered that $LiFePO_4$ including lithium defects were preferable for lithium diffusion during the insertion process and that the defective $LiFePO_4$ separated into $LiFePO_4$ without lithium defects and $FePO_4$ at the relaxation process after the termination of lithium insertion.

In chapter 3 and 4, we investigated the relaxation phenomenon of $LiMn_2O_4$ with the coexistence state of two phases, the Li-rich phase and the Li-lean phase, after the lithium insertion by using the Rietveld method,[4-6] and found that the mole fraction of the Li-rich phase increased and that of the Li-lean phase decreased with the relaxation time. It is considered that, at the lithium insertion process, the Li-lean phase has more

vacancies than the Li-rich phase due to lithium deficiency and that the structure of the Li-lean phase was maintained even containing excess lithium in order to promote lithium diffusion. It is considered that the Li-lean phase containing excess lithium formed during the lithium insertion process separated into the Li-lean phase without excess lithium and the Li-rich phase during the relaxation process.

$LiCoO_2$ with a layered rock-salt structure is the most widely used cathode material for LIBs due to its excellent reversibility and a high electrochemical potential at the lithium contents x from 1 to 0.5 in terms of Li_xCoO_2.[9-12] Reimers et al. reported that the phase of Li_xCoO_2 changes as single hexagonal phase for x=1.00-0.93, two hexagonal phases for x=0.93-0.75, single hexagonal phase for x=0.75 ~ near 0.5.[12] It consists of layers of lithium that lie between slabs of octahedron formed by cobalt and oxygen atoms. Both lithium and cobalt are octahedrally coordinated by oxygen. These octahedrons are edge-sharing, and tilted relative to the layered structure. The major drawbacks of $LiCoO_2$ are toxicity, high cost, and the limited capacity of $140mAhg^{-1}$. Although most of the lithium can be extracted from $LiCoO_2$, only about half can be extracted reversibly. Removal of greater amounts of lithium beyond extraction limit attribute to phase transitions, large changes in unit cell volume, and the evolution of oxygen at voltage in excess of 4.2V vs. Li due to a large $O^{-2}p$ character of the holes. [13-16]

In this chapter, Li_xCoO_2 samples (x = 0.90, 0.85 and 0.80) were prepared at the region of two hexagonal phases coexistence by charging/discharging the cell at the various C rate, then investigated the phase change of the two hexagonal phases with the elapsed time after the lithium extraction/insertion process by using XRD measurement and the Rietveld analysis method, it is able to discuss on more precise and detailed relaxation phenomenon such as change of lattice constant, scale factor, mole fraction change of coexisting the Li-lean phase and the Li-rich phase.

5.2 Experimental

5.2.1 Cell preparation

Commercial lithium cobalt oxide ($LiCoO_2$, Strem Chemicals Corp.) powder was used as the cathode material. After mixing the $LiCoO_2$ powder with acetylene black (AB, Acetylene Black, Surface area: 133 m^2g^{-1}, Denkikagaku Kogyo) as a supplemental conductor and polytetrafluoro ethylene (PTFE) as an adhesive agent in a weight ratio of 0.80:0.15:0.05, the mixture was spread onto a nickel mesh current collector. The electrode was dried to remove moisture at 120 °C for 24 h, then which was assembled as working electrode for a three electrode type glass cell in argon atmosphere. Counter and reference electrode were lithium metal, and the electrolyte was a 1M $LiClO_4$ in ethylene carbonate (EC) and a 1,2-dimethoxyethane (DME) solution (1M $LiClO_4$ in EC/DME, 1:1 v/v, Kishida chemical Corp., Ltd.) , as shown table 5-1.

5.2.2 Electrochemical lithium extraction/insertion

The electrochemical lithium extraction/insertion processes were galvanostatically conducted at various C rates at 25°C. The amount of extracted/inserted lithium was controlled by integrating the adjusted current. Table 5-2 lists thus obtained samples under the various electrochemical charge/discharge conditions, where the sample name indicates insertion(IN) or extraction(EX), lithium composition and charge or discharge rate. Each lithium-extracted sample was charged to x=0.80(EX80C1), 0.85(EX85C1) and 0.9(EX90C1) in terms of $LixCoO_2$, respectively. For the lithium-inserted samples, we firstly extracted lithium to x=0.50 at 1C in Li_xCoO_2 electrochemically, then inserted lithium to x=0.85 at 1C or 3C. When the samples were characterized, the circuit was opened and immediately the working electrode was taken out of the cell in an argon-filled glove box to avoid the local cell reaction between the active material and the current collector or the supplemental conductor. The working electrode was washed in EC/DME (1:1 v/v, Kishida chemical Corp., Ltd.) solution then DME (Kishida chemical Corp., Ltd.) solution to remove the remaining lithium-salt, then it was dried at 35°C in argon atmosphere.

5.2.3 X-ray diffraction (XRD) measurement

The working electrode was set in a sealed holder (Rigaku Corp., Ltd.) with beryllium window in an argon-filled glove box, which was mounted in a powder X-ray diffractometer (Model RINT – TTR, Rigaku Corp., Ltd.) with copper Kα radiation. In order to investigate the relaxation structure change, XRD measurements were

successively and repeatedly carried out at the various relaxation times after termination of lithium insertion or extraction. Tube voltage and current were adjusted to 40 kV and 200 mA. The sampling steps and scanning speed were set to 0.04° and 2° min^{-1} over from 15° to 75° in terms of 2θ, respectively. Table 5-3 indicates the conditions of XRD measurement.

5.2.4 The Rietveld analysis

Successive five XRD patterns with the elapsed time were integrated to reduce the noise and improve the fitting accuracy of the Rietveld analysis, which were analyzed by the Rietveld method using RIEVEC program.[1-8, 17, 18] The relaxation time was indicated by mean time of elapsed time for measurement of integrated five XRD patterns. The Rietveld analysis was conducted regarding to the coexisting two phases, the Li-rich phase and the Li-lean phase. The measured diffraction lines of the two phases were indexed according to the space group $R\bar{3}m$ (No. 166). The lithium, cobalt and oxygen atoms occupy 3a (0, 0, 0), 3b (0, 0, 1/2) and 6c (0, 0, z≈1/4) sites in the crystallographic position, respectively. The contribution of lithium was ignored. The peaks diffracted from the AB and the nickel collector in the XRD patterns were evaluated as background curves.

Table 5-1. The condition of prepared cell

Working electrode	$LiCoO_2$ 80wt% + AB 15wt% + PTFE 5wt%
Counter & reference Electrode	Lithium metal
Current collector	Nickel mesh
Electrolyte	1 mol dm^{-3} $LiClO_4$ in EC/DME (1/1 v/v)

Table 5-2. Samples prepared under various charge/discharge conditions.

Sample name	EX90C1	EX85C1	EX80C1	EX85C01	EX85C3	IN85C1	IN85C3
Li content x in Li_xCoO_2	x=0.90	x=0.85	x=0.80	x=0.85	x=0.85	x=0.85	x=0.85
C rate	1	1	1	0.1	3	1	3

Table 5-3. XRD measurement condition

Method	2θ/θ
Source radiation	CuKα
Tube voltage & current	40 kV, 200 mA
Measured angle (2θ)	$15^{o} \leqq 2\theta \leqq 70^{o}$
Step width (2θ)	0.04^{o} (2θ)
Scanning speed	2^{o}/min
Divergence slit	$1 / 2^{o}$
Scattering slit	Open
Relaxation	Argon atmosphere
Data integration	5
Fitted angle (2θ)	$15^{o} \leqq 2\theta \leqq 70^{o}$

5.3 Results and discussion

5.3.1 Potential profile

Figure 5-1 shows potential profiles of Li_xCoO_2 samples ($0.5 \leqq x \leqq 1$) during one cycle of charge/discharge process at various C rates. Solid line and dotted line indicate charge and discharge profile, black, blue and red lines indicate 1C, 0.1C and 3C rate, respectively. For the lithium inserted samples, lithium was firstly extracted to x=0.50 at 1C, then inserted to x=0.85 at 1C and 3C, respectively. Characterized samples are indicated by circle mark in figure 5-1, respectively. It is found that EX85C3 and IN85C3 samples charged/discharged at 3C exhibits apparent polarization induced by high C rate.

5.3.2 XRD measurement and the Rietveld analysis

Figure 5-2 indicates XRD patterns of pristine powder and lithium-extracted samples with various lithium contents x=0.90, 0.85 and 0.80 Li_xCoO_2, respectively, where EX90C1, EX85C1 and EX80C1, XRD peaks with two phase coexistence are appeared. Figure 5-3 shows the x=0.85 sample in terms of Li_xCoO_2 after various lithium extraction or insertion process. Although the lithium contents x are same each other as x=0.85, the XRD peak intensity of coexisting the Li-lean phase and the Li-rich phase is different, as shown in the comparison with 108 and 110 peak.

All the XRD patterns during the relaxation time were well-fitted with patterns obtained by the Rietveld method. From figure 5-4 to figure 5-8 show the Rietveld fitting result of several lithium extracted samples (lithium extraction to x=0.90, 0.85, 0.80 by 1C or 3C rate) after 2.5 h and 47.5 h from the termination of the electrochemical lithium extraction. Figure 5-9 and 5-10 show the Rietveld fitting result of several lithium inserted samples (lithium insertion to x= 0.85 by 1C or 3C rate) after 2.5 h and 47.5 h from the termination of the electrochemical lithium insertion. The illustration in the figure indicates the detailed fitting figure of the coexisting two phases from 37° to 40°. The Rietveld fittings for all the XRD patterns were successfully conducted with sufficiently small reliability values of R_{WP} (R-weighted pattern), R_B (R-Bragg) and R_F (R-structure factor). We obtained the mole fraction of the Li-rich phase and the Li-lean phase by using the following equation.[19]

$$M_2 = S_2 Z_2 V_2 \Big/ \sum_{i=1}^{2} S_i Z_i V_i$$

Where i = 1 and 2 represent the Li-rich phase and the Li-lean phase, respectively. M, S, Z and V are the mole fraction, the scale factor obtained by the Rietveld analysis, the number of formula units per unit cell and the unit cell volume, respectively. We describe the relaxation analysis results depending on the following three factors.

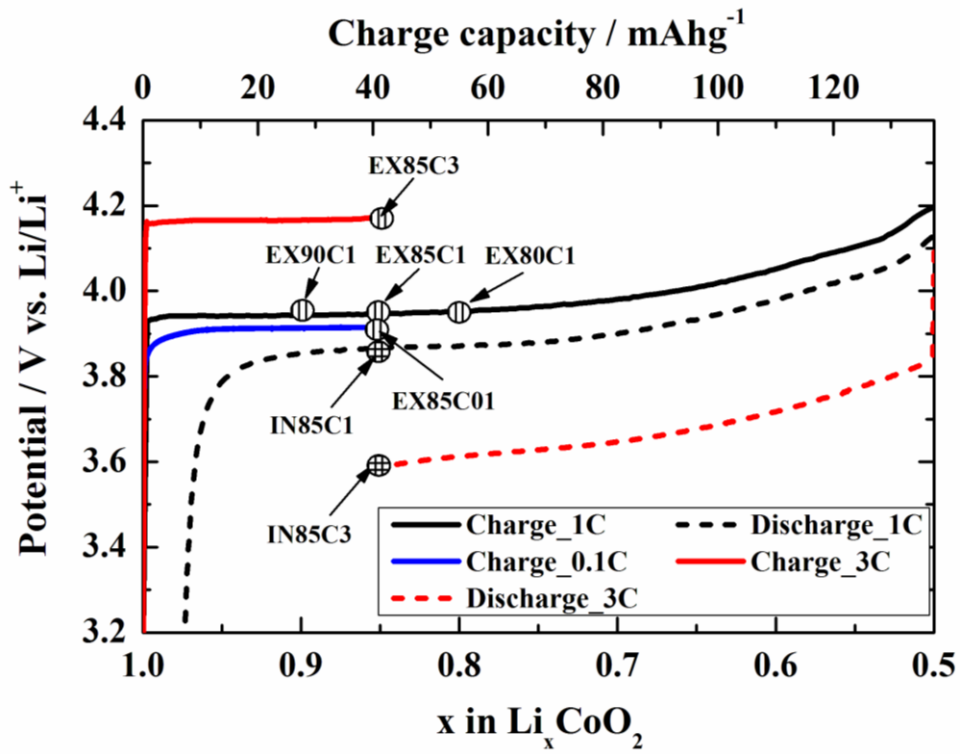

Figure 5-1. The potential profile of Li_xCoO_2 samples ($0.5 \leqq x \leqq 1$) at the charge/discharge process, where the sample name indicates insertion(IN) or extraction(EX), lithium composition and charge or discharge rate. The solid line and dots indicate charge and discharge process, respectively. Black, blue and red line present 1C, 0.1C and 3C of C rate, respectively. For the lithium inserted samples, lithium was firstly extracted to x=0.50 at 1C, then inserted to x=0.85 at 1C and 3C, respectively.

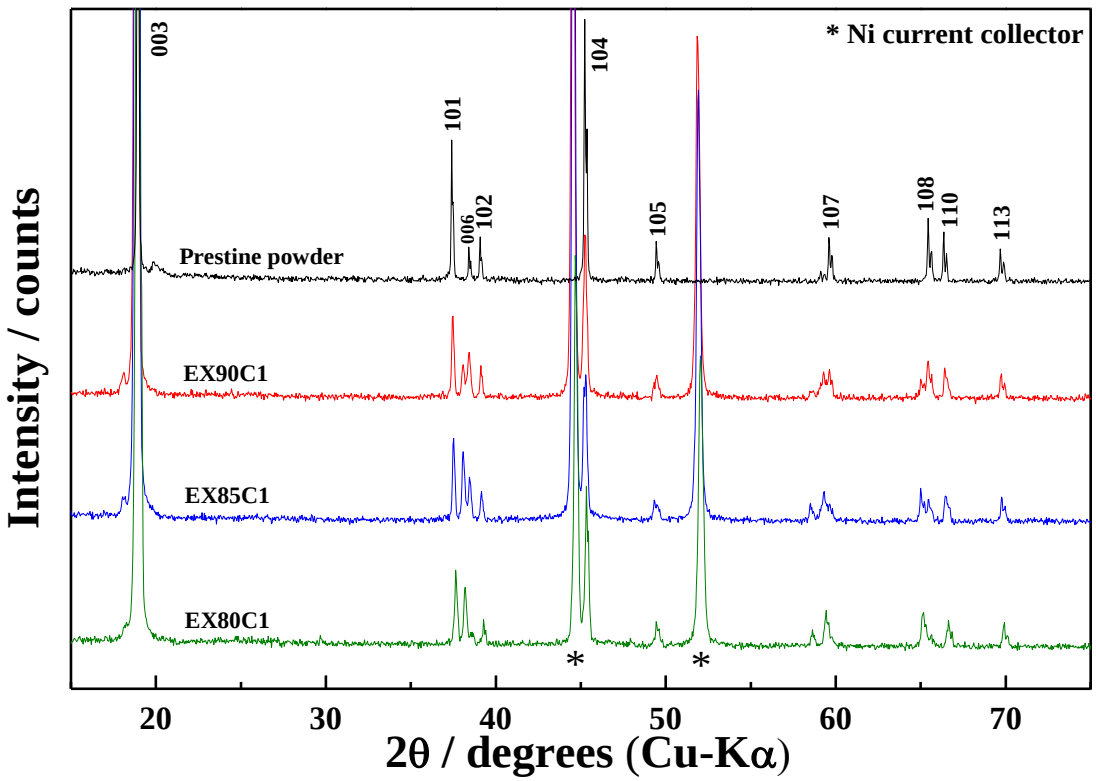

Figure 5-2. XRD patterns of lithium extracted samples

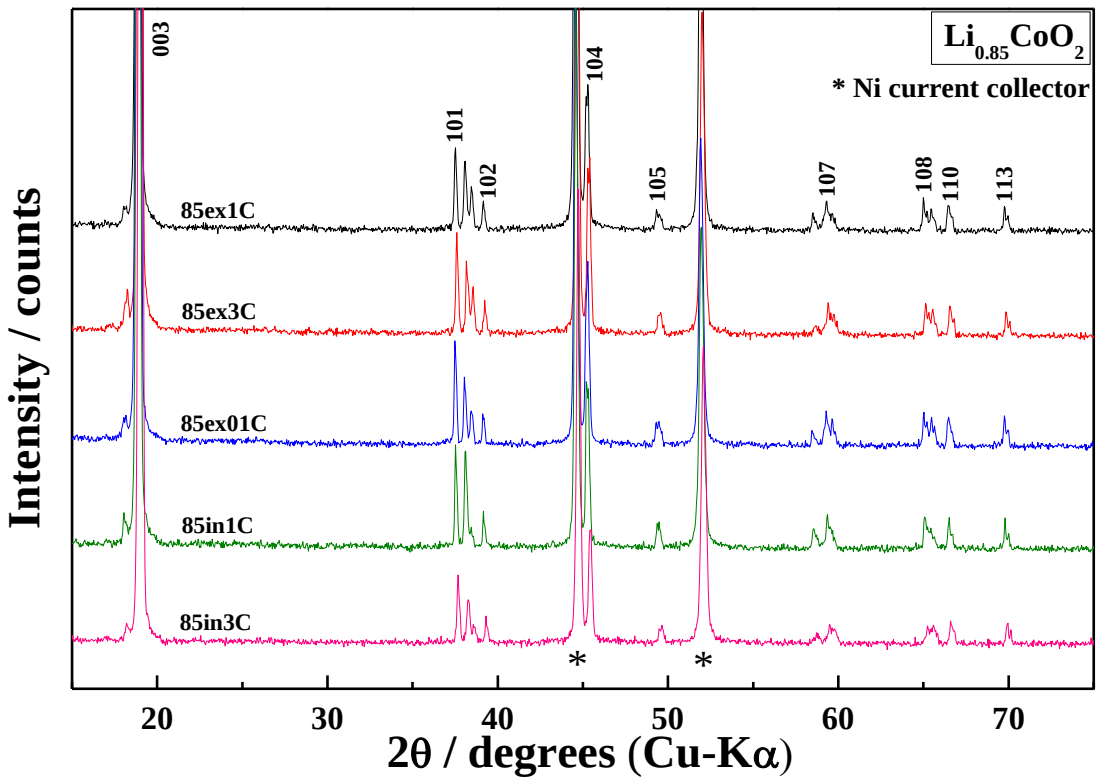

Figure 5-3. XRD patterns of Li extracted or inserted $Li_{0.85}CoO_2$

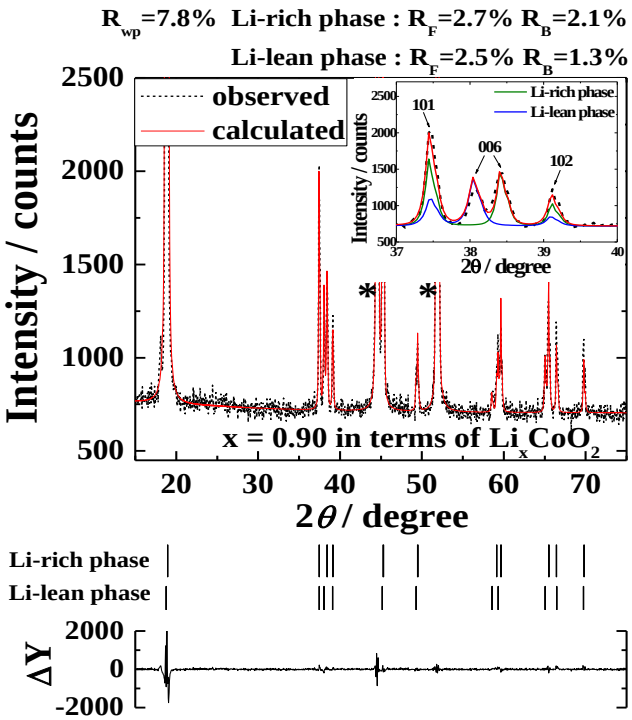

(a) 5h sample

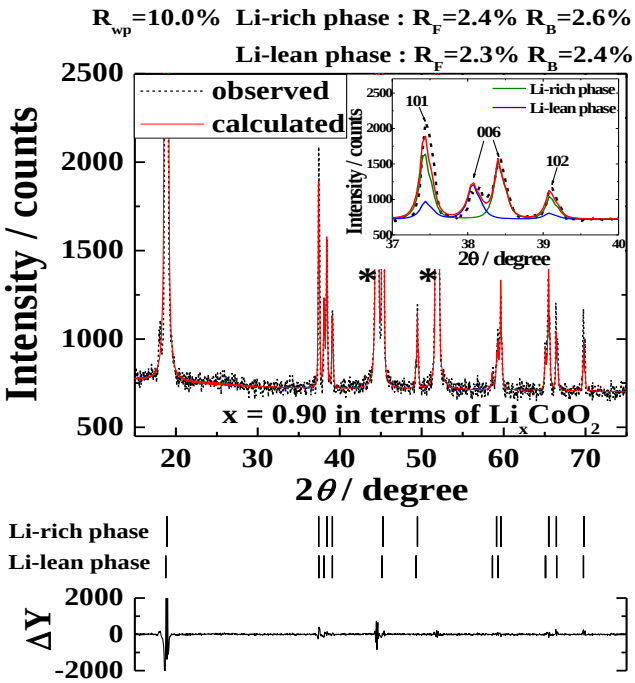

(b) 47.5h sample

Figure 5-4. The Rietveld fitting of EX90C1(lithium extraction to x=0.90 by 1C rate after the termination of electrochemical lithium extraction.

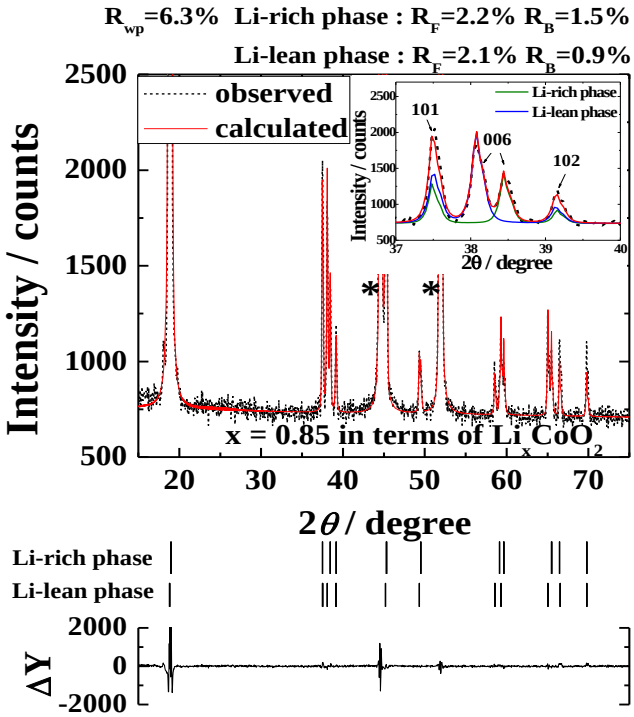

(a) 5h sample

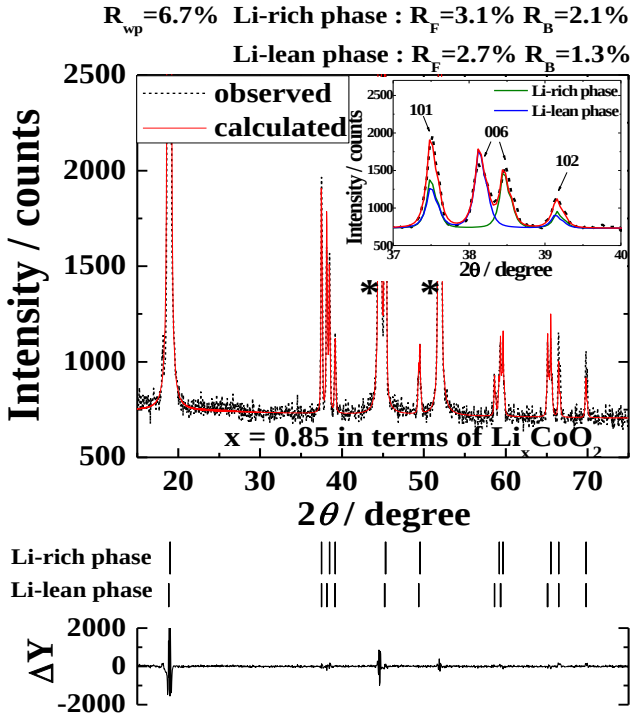

(b) 47.5h sample

Figure 5-5. The Rietveld fitting of EX85C1(lithium extraction to x=0.85 by 1C rate after the termination of electrochemical lithium extraction.

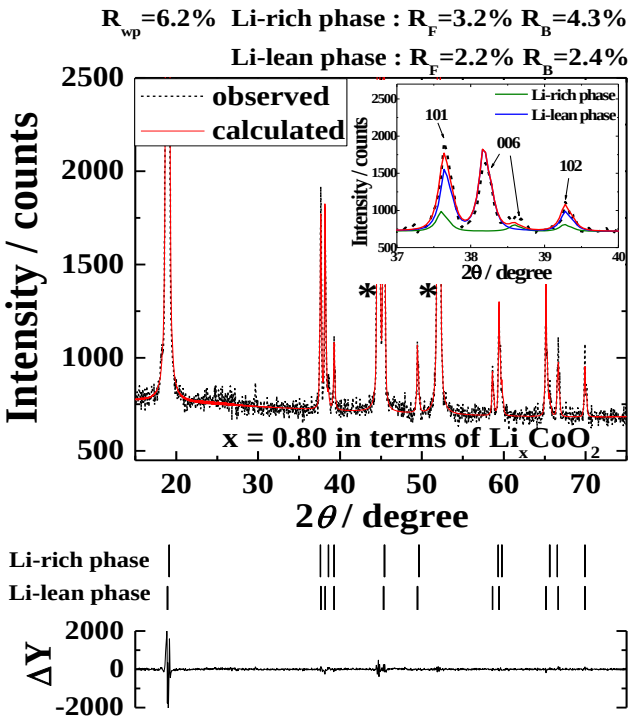

(a) 5h sample

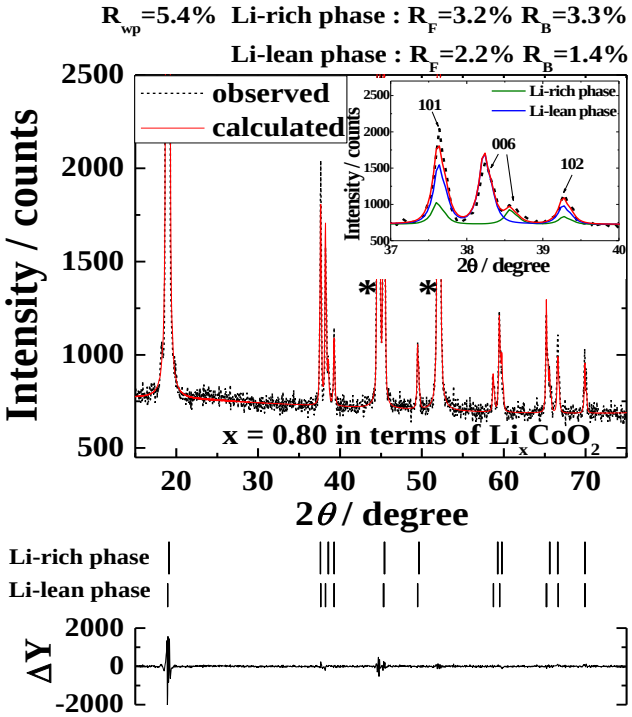

(b) 47.5h sample

Figure 5-6. The Rietveld fitting of EX80C1(lithium extraction to x=0.80 by 1C rate after the termination of electrochemical lithium extraction.

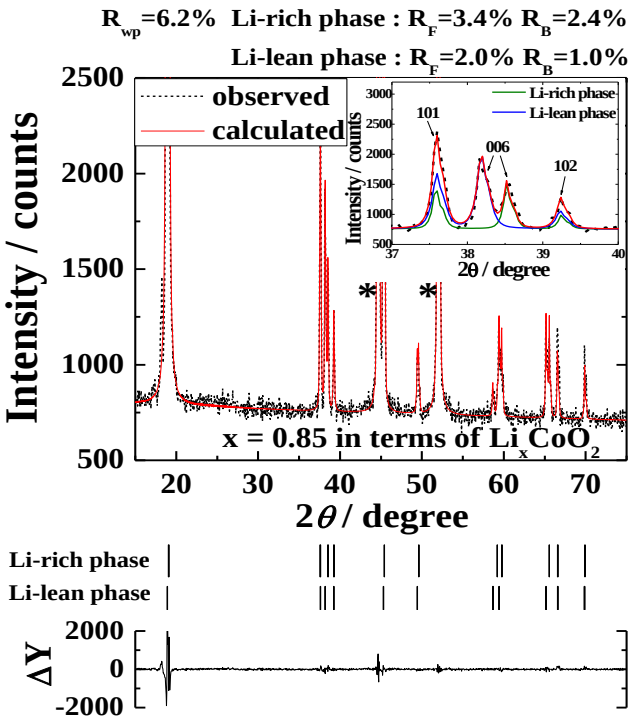

(a) 5h sample

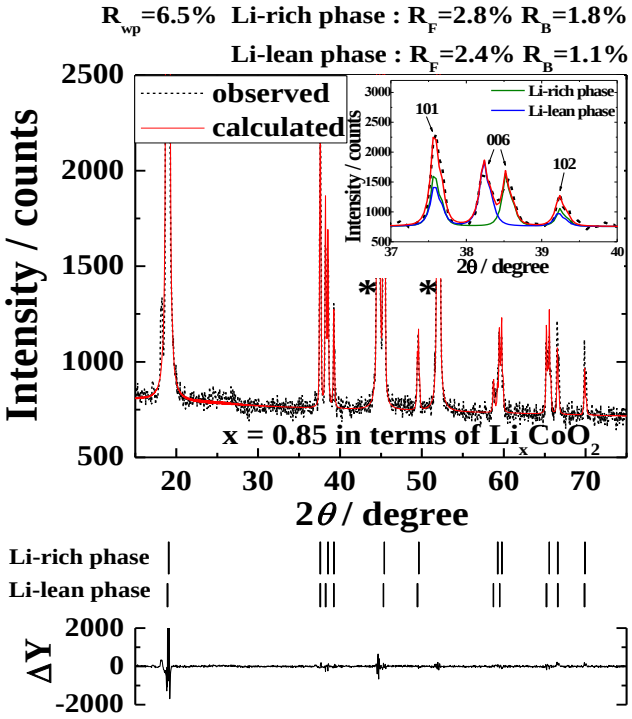

(b) 47.5h sample

Figure 5-7. The Rietveld fitting of EX85C3(lithium inserted to x=0.85 by 3C rate after the termination of electrochemical lithium extraction.

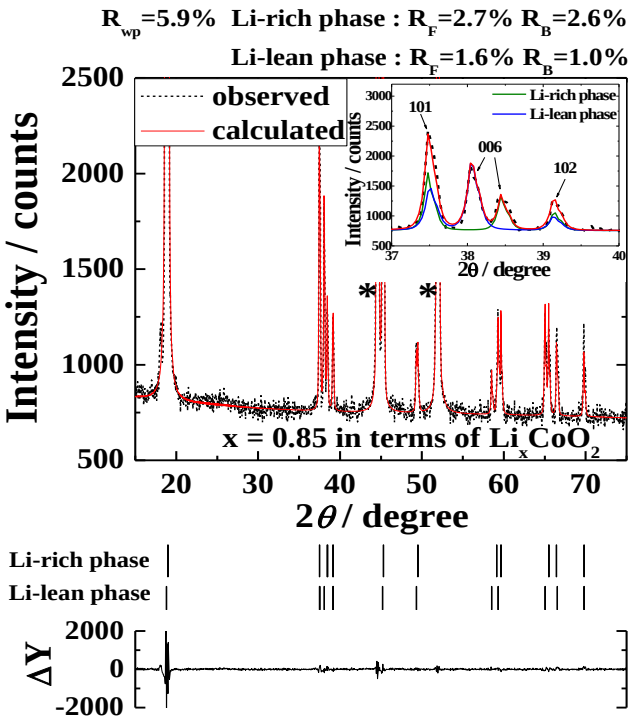

(a) 5h sample

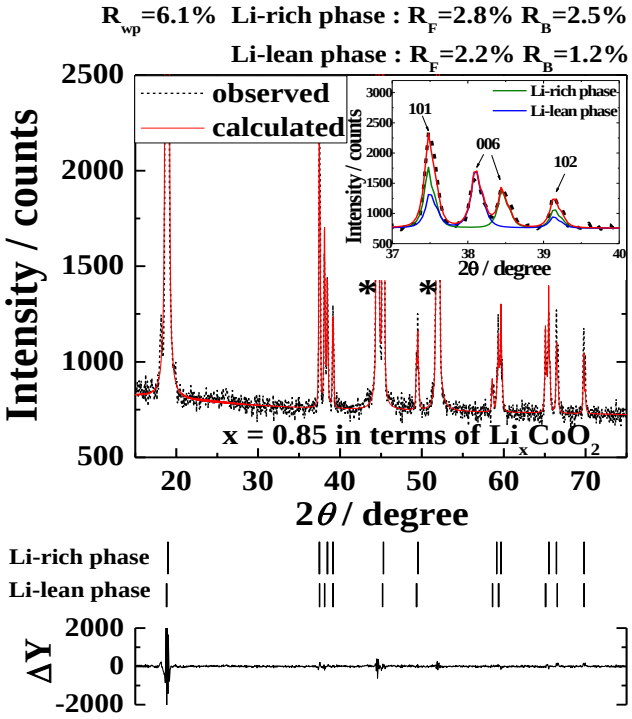

(b) 47.5h sample

Figure 5-8. The Rietveld fitting of EX85C01(lithium extraction to x=0.80 by 0.1C rate after the termination of electrochemical lithium extraction.

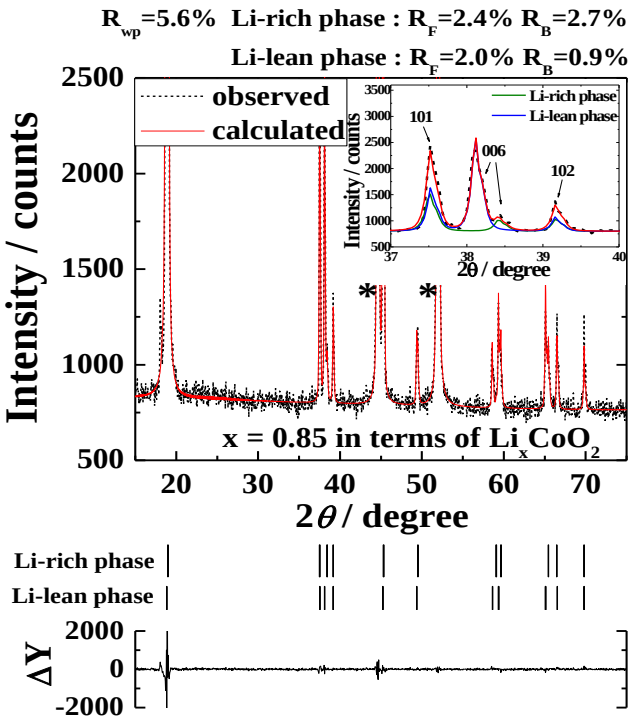

(a) 5h sample

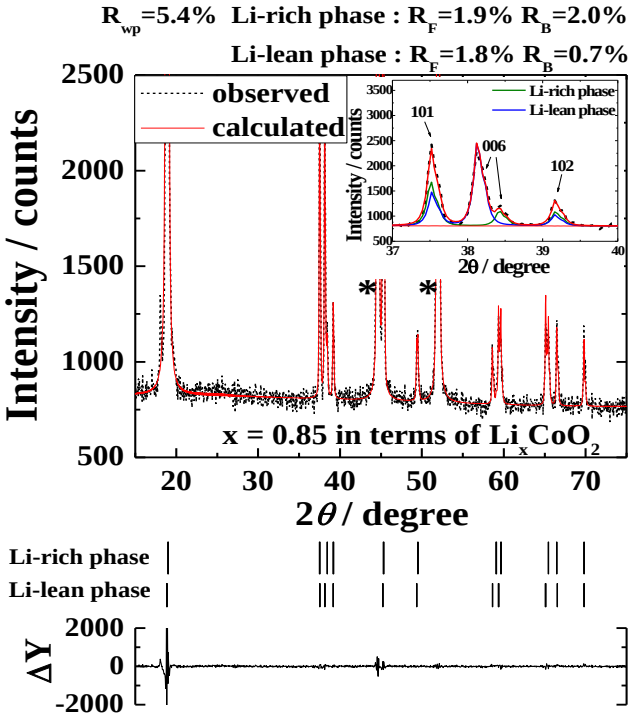

(b) 47.5h sample

Figure 5-9. The Rietveld fitting of IN85C01(lithium insertion to x=0.85 by 1C rate after the termination of electrochemical lithium extraction.

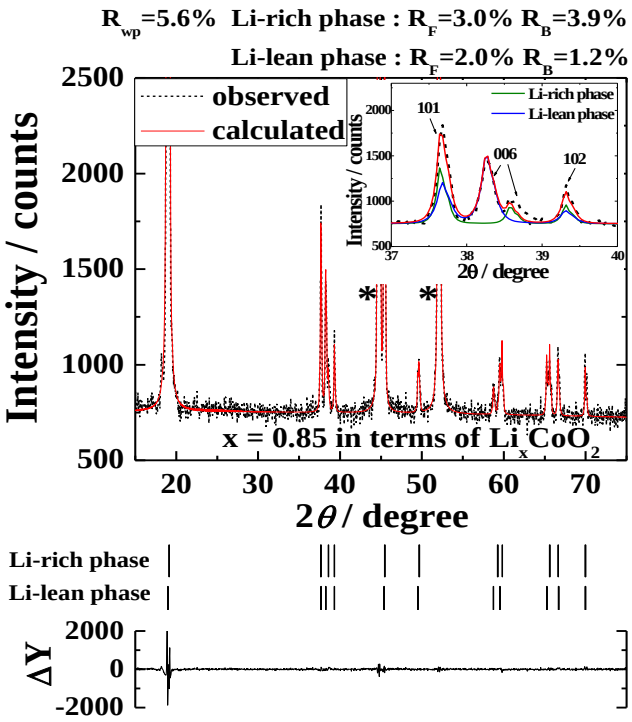

(a) 5h sample

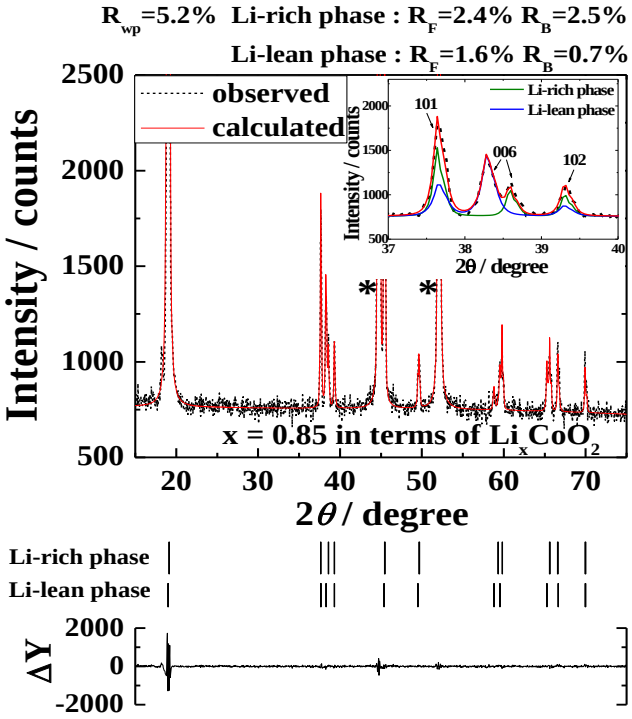

(b) 47.5h sample

Figure 5-10. The Rietveld fitting of IN85C3(lithium insertion to x=0.85 by 3C rate after the termination of electrochemical lithium extraction.

5.3.3 Effect of the lithium extraction

Figure 5-11 shows the mole fraction change of two phases, the Li-rich phase and the Li-lean phase at the relaxation time after the lithium extraction for EX90C1, EX85C1 and EX80C1, respectively. At the lithium extraction process, the mole fraction of the Li-lean phase increased and that of the Li-rich phase decreased with the increase of lithium extraction amount. During the relaxation time the mole fraction of the Li-rich phase increased and that of the Li-lean phase decreased for all the samples. It is considered that the Li-lean phase preferable for lithium diffusion was formed even containing excess lithium at the lithium extraction process then separated into the Li-lean phase without excess lithium and the Li-rich phase during the relaxation time.

5.3.4 Effect of the lithium extraction rate

Figure 5-12 shows the mole fraction change of the Li-rich phase and the Li-lean phase at the relaxation time for various lithium extraction rates. The mole fraction of the Li-lean phase in EX85C3 was larger than that of EX85C1 just after the lithium extraction then it rapidly decreased with the relaxation time. In case of EX85C01, the mole fraction of the Li-lean phase was the smallest and decreased most slowly with the relaxation time. It is considered that larger amount of the Li-lean phase was formed for faster lithium extraction to promote the lithium diffusion preferably. The faster lithium diffusion, larger amount of Li-lean phase formed and this made the driving force of phase change increase at the relaxation time.

5.3.5 Effect of the lithium insertion rate

To investigate the relaxation behavior after lithium insertion process, the mole fraction changes of the Li-lean phase and the Li-rich phase in IN85C1 and IN85C3 were investigated as a function of the relaxation time, as indicated in figure 5-13. The mole fraction of the Li-lean phase in IN85C1 and IN85C3 decreased with the relaxation time. It is considered that at the lithium insertion process, the Li-lean phase was maintained even containing excess lithium to promote the lithium diffusion, then at the relaxation process the Li-lean phase with excess lithium separated into the Li-lean phase without excess lithium and the Li-rich phase.

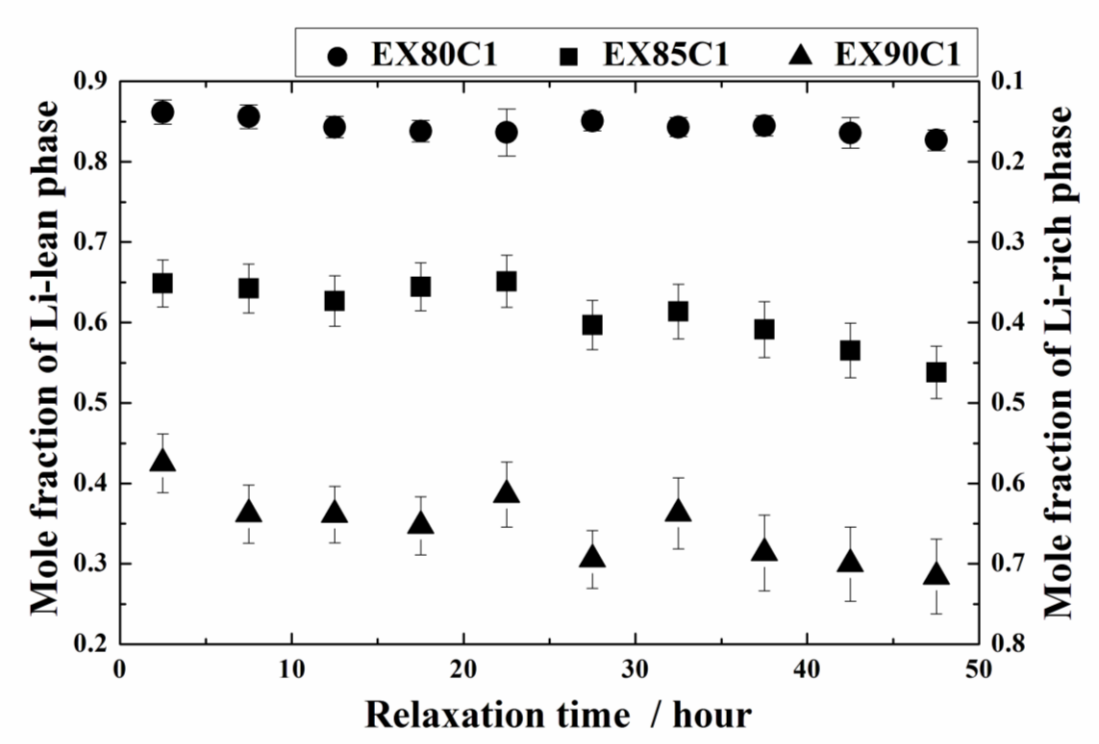

Figure 5-11. The mole fraction changes of the Li-rich phase and the Li-lean phase during the relaxation time after the lithium extraction, where each sample was charged to x=0.80(EX80C1), 0.85(EX85C1) and 0.9(EX90C1) in terms of Li_xCoO_2, respectively.

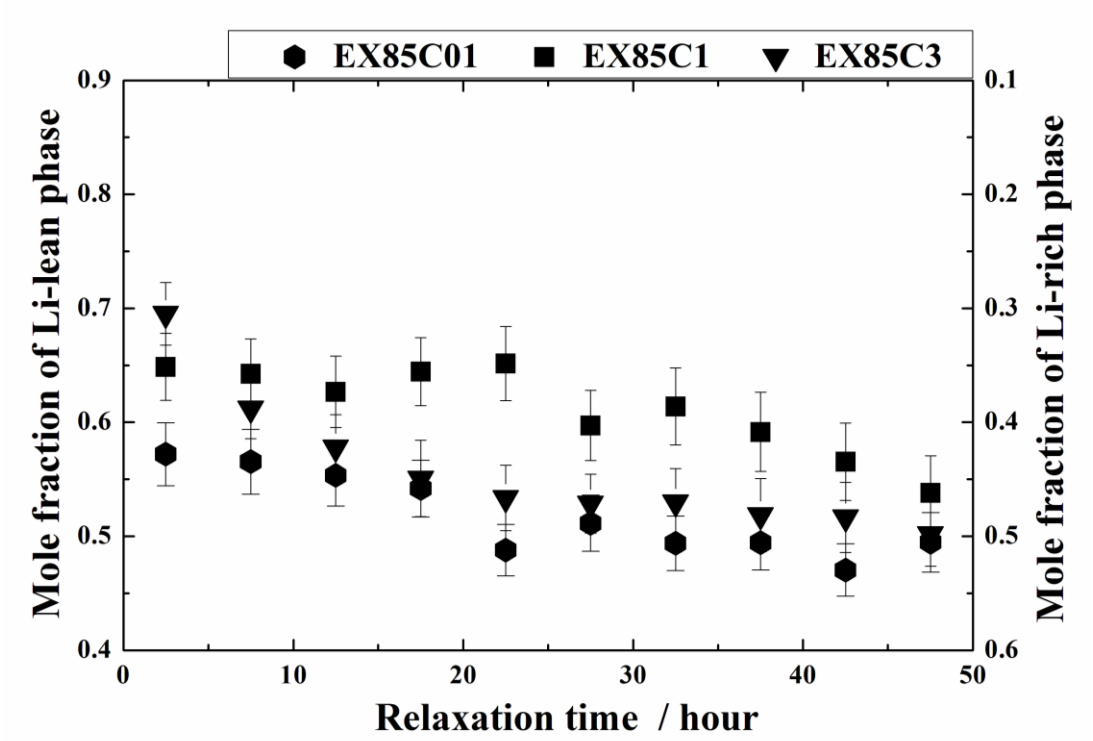

Figure 5-12. The mole fraction changes of the Li-rich phase and the Li-lean phase during the relaxation time after the lithium extraction, where each sample was charged to x=0.85 at 0.1C (EX85C01), 1C(EX85C1) and 3C(EX85C3) in terms of Li_xCoO_2, respectively.

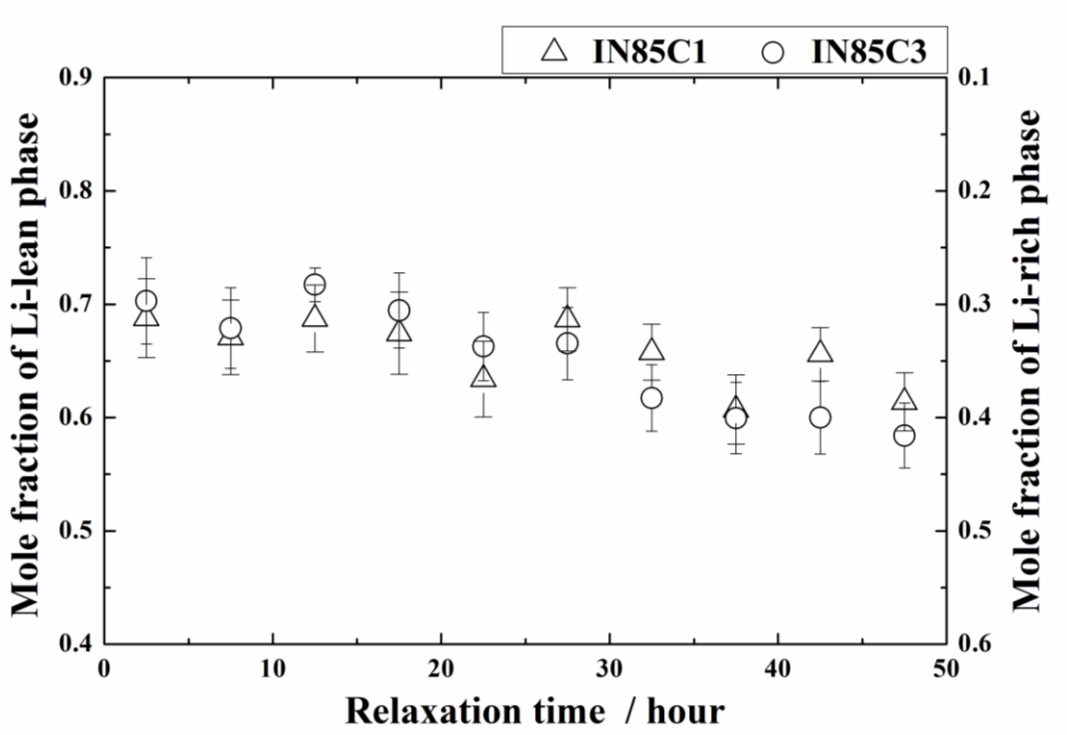

Figure 5-13. The mole fraction changes of the Li-rich phase and the Li-lean phase during the relaxation time after the lithium insertion, where each sample was firstly charged to x=0.5 at 1C, then discharged to x=0.85 at 1C(IN85C1) and 3C(IN85C3) in terms of Li_xCoO_2, respectively.

5.4 Conclusions

In this chapter, the crystal phase change with relaxation time of $LiCoO_2$ cathode after the termination of electrochemical lithium extraction or insertion was investigated by means of XRD measurement and the Rietveld analysis. Li_xCoO_2 samples (x = 0.90, 0.85 and 0.80) were prepared at the region of two hexagonal phases coexistence by charging and/or discharging the cell at the various C rate. It was discussed on more precise and detailed relaxation phenomenon such as change of lattice constant and mole fraction change of coexisting the Li-lean phase and the Li-rich phase.

After the lithium extraction process, the mole fraction of the Li-rich phase increased while that of the Li-lean phase decreased with the relaxation time. It is considered that the Li-lean phase was preferably produced even having excess lithium to promote lithium diffusion at the lithium extraction process, then the Li-lean phase separated into the Li-rich phase and the Li-lean phase with no excess lithium at the relaxation time after the lithium extraction. For faster lithium extraction, larger amount of the Li-lean phase was formed, then the non-equilibrium Li-lean phase decreased rapidly during the relaxation time due to the increase of driving force for phase change.

After the lithium insertion process, the mole fraction of the Li-rich phase increased and that of the Li-lean phase decreased with the relaxation time. It is considered that at the lithium insertion process, the Li-lean phase with excess lithium was maintained to promote the lithium diffusion, then at the relaxation process the Li-lean phase with excess lithium separated into the Li-lean phase without excess lithium and the Li-rich phase.

References

1. S. Park, M. Oda, and T. Yao, *Solid State Ionics*, **203**, 29 (2011).
2. M. Oda, S. Park, T. Yabutsuka, M. Hibino, and T. Yao, Meet. *Abstr. - Electrochem. Soc.*, Abstract 49 (2010).
3. S. Park, M. Oda, T. Yabutsuka, and T. Yao, Meet. *Abstr. - Electrochem. Soc.*, Abstract 42 (2011).
4. I. S. Seo, S. Park, and T. Yao, *ECS Electrochem. Lett.*, **2(1)**, A6 (2013).
5. I. S. Seo, S. Park, and T. Yao, *Zero-Carbon Energy Kyoto 2011*, T. Yao, Editor, Springer, 165 (2012).
6. I. S. Seo, S. Park, and T. Yao, *Asian-core University Program on Advanced Energy Science, International Symposium on Advanced Energy Systems and Materials*, Abstract 11 (2011).
7. S. Park, K. Kameyama, and T. Yao, *Electrochem. Solid-State Lett.*, **15(4)**, A49 (2012).
8. I. Seo, S. Park, T. Yao, Meet. *Abstr. - Electrochem. Soc.*, Abstract 176 (2012).
9. M. S. Whittingham, *Chem. Rev.*, **104**, 4271–4302 (2004)
10. T. Ohzuku. A. Ueda, M. Nagayama, Y. Yasunou, H. Komori, *Electrochim. Acta*, **38**, 1159 (1993).
11. Y. Koyama, I. Tanaka, H. Adachi, Y. Makimura and T. Ohzuku, *J. Power Sources*, **119–121**, 644–648 (2003).
12. J. N. Reimers and J. R. Dahn, *J. Electrochem. Soc.*, **139**, 2091–2097 (1992).
13. J. N. Reimers and J. R. Dahn, J. Electrochem. Soc., 139, 2091 (1992)
14. G. G. Amatucci, J. M. Tarascon and L. C. Klein, J. Electrochem. Soc., 143, 1114 (1996)
15. R. V. Chebiam, A. M. Kannan, F. Prado and A. Manthiram, Electrochem. Commun.,3, 624 (2001)
16. S. Venkatraman, Y. Shin and A. Manthiram, Electrochem. Solid State Lett., 6, A9 (2003)
17. T. Yao, T. Ito, and T. Kokubo, *J. Mater. Res.*, **10**, 1079 (1995).
18. T. Yao, N. Ozawa, T. Aikawa, and S. Yoshinaga, *Solid State Ionics*, **175**, 199 (2004).
19. Roderick J. Hill, in *The Rietveld Method*, R. A. Young, Editor, P 95, Oxford Univ. press, Oxford (1995).

CHAPTER 6

GENERAL SUMMARY

Li-ion secondary batteries (LIBs) have received much attention as one of the next generation battery system due to its high energy density and operation power, and the research study to improve its performance have been proceeding actively with the recent drastic increase of demands for portable electronic devices and electric vehicle. The research on the crystal phase/structure of electrode materials is essential to understand the electrode behavior at the lithium insertion/extraction process and to design the advanced high efficiency electrode. With this approach to improvement in LIB, the relaxation analysis is important to make the transition of electrode material from kinetic state to equilibrium state clear. With an aim to understand the relaxation mechanism various cathode materials for lithium ion secondary batteries lithium were electrochemically extracted and/or inserted, then the relaxation analysis was performed by means of X-ray powder diffraction measurement and the Rietveld method. Especially, the most remarkable feature for this relaxation analysis is to focus on spontaneous and dynamic changes in structures and/or phases of electrode materials according to the condition of lithium transfer during long relaxation time without any side reaction such as the local cell reaction between the active material and the current collector or the supplemental conductor, and self discharge, etc. In this study, the relaxation analysis of $LiMn_2O_4$ and $LiCoO_2$ cathode materials for LIBs was dealt with.

In chapter 3, on the relaxation phenomenon of spinel $LiMn_2O_4$, that is an attractive cathode material for lithium ion secondary batteries due to its cost-effectiveness, low toxicity, excellent thermal stability, relatively high operating voltage and energy density, was mainly discussed. Kanamura et al. investigated the structural change of spinel $LiMn_2O_4$ induced by lithium extraction by using the Rietveld analysis method, and reported on the coexistence of two spinel phases in the region of $x < 0.5$ in terms of $Li_xMn_2O_4$ during the lithium extraction process. They reported that the Li-lean phase had smaller lattice constant and more vacancies than the Li-rich phase, and that the amount of the Li-lean phase increased while the Li-rich phase decreased with the decrease of x. In that regard, to investigate relaxation phenomenon of coexisting the Li-rich phase and the Li-lean phase, after electrochemical lithium insertion, XRD was measured through the local 2θ region of from 35 to 40 with the elapsed time after termination of electrochemical lithium insertion. For thus obtained XRD pattern $Li_{0.1}Mn_2O_4$ sample, XRD intensity of 311 peaks was analyzed as function of the

relaxation time by means of the Lorentz function fitting program. From the result, it was found that the Li-rich phase and the Li-lean phase presented by Kanamura et al. coexist and that the amount of the Li-lean phase decreased and the Li-rich phase increased with various elapsed time.

In chapter 4, to analysis the relaxation process of lithium-inserted $LiMn_2O_4$, after electrochemically inserting various amounts of lithium (x = 0.10, 0.15 and 0.20) into $Li_xMn_2O_4$ ($x \approx 0$), full data of XRD measured, and then the change of the relaxation structure after termination of lithium insertion was investigated by using the Rietveld analysis. As a result, it was found that the mole fraction of the Li-lean phase decreased and that of the Li-rich phase increased with the relaxation time after lithium insertion. It is considered that, at the lithium insertion process, the Li-lean phase has more vacancies than the Li-rich phase due to lithium deficiency and that the structure of the Li-lean phase was maintained even containing excess lithium in order to promote lithium diffusion. It is considered that the Li-lean phase containing excess lithium formed during the lithium insertion process separated into the Li-lean phase without excess lithium and the Li-rich phase during the relaxation process.

Finally in chapter 5, relaxation analysis after electrochemical lithium extraction / insertion for $LiCoO_2$ cathode material was conducted with various elapsed times. Layered $LiCoO_2$ cathode material is the most widely used cathode material for LIBs due to its excellent reversibility and a high electrochemical potential at the lithium content x from 1 to 0.5 in terms of Li_xCoO_2. Reimers et al. reported that the phase of Li_xCoO_2 changes as single hexagonal phase for x=1.00-0.93, two hexagonal phases for x=0.93-0.75, single hexagonal phase for x=0.75 - near 0.5. In this chapter, Li_xCoO_2 samples (x = 0.90, 0.85 and 0.80) were prepared for the region of two hexagonal phases coexistence by electrochemical lithium extraction/insertion at the various C rate, then the relaxation phase change of the two hexagonal phases was investigated with the elapsed time after the lithium extraction/insertion by means of XRD measurement and the Rietveld analysis method. It was found that after the lithium extraction process, the mole fraction of the Li-rich phase increased while that of the Li-lean phase decreased with the relaxation time. It is considered that the Li-lean phase was preferably produced even having excess lithium to promote lithium diffusion at the lithium extraction process, then the Li-lean phase separated into the Li-rich phase and the Li-lean phase with no excess lithium at the relaxation time after the lithium extraction. For faster lithium extraction, larger amount of the Li-lean phase was formed, then the non-equilibrium Li-lean phase decreased rapidly during the relaxation time due to the increase of driving force for phase change. After the lithium insertion process, the mole

fraction of the Li-rich phase increased and that of the Li-lean phase decreased with the relaxation time. It is considered that at the lithium insertion process, the Li-lean phase with excess lithium was maintained to promote the lithium diffusion, then at the relaxation process the Li-lean phase with excess lithium separated into the Li-lean phase without excess lithium and the Li-rich phase.

In this study, the relaxation analysis featured to focus on spontaneous change of electrode material itself without any side reaction and self discharge, etc. during the long relaxation time. From this study on relaxation analysis, we found the relaxation behavior has two types of mechanism in level of crystal structure and crystal phase, obtained the quantitative data for relaxation change and considered the contribution of the Li-lean phase containing excess lithium for relaxation behavior. Thus obtained quantitative data for relaxation analysis are expected to be applied to various research and development fields for LIB as reliable basic data. Battery performance test sufficiently considering the relaxation effect would be able to provide reliable data to reduce the errors on operation of LIB, because the rest time at real battery operation process, especially relaxation time after partial charge/discharge process, accounts considerably large part for operation environment, and the charge/discharge system in LIB is generally controlled according to standard of its potential value on operation. Considering the relationship between charge/discharge rate and relaxation phenomenon, in addition, relaxation analysis would be essential in development of EVs with high charge capability.

Finally, it is thought that more various experiments and demonstrations for relaxation analysis are needed to apply for real battery field, because the battery system is highly complex in that various chemical reaction occurs in each part of LIB. In this study, relaxation analysis was performed by means of powder X-ray diffraction and the Rietveld method, which was very suitable to analyze the dynamics of the cathode materials from the viewpoint of crystal structure. Furthermore, if other powerful apparatus and advanced measurement techniques are combined and utilized with this relaxation analysis method, much more information data for relaxation behavior and mechanism can be obtained. In that regard, neutron diffraction measurement is one of the powerful techniques to analyze the real behavior of lithium diffusion in electrode material. To observe the local crystal structure at the relaxation process by means of transmission electron microscope (TEM) would be a good approach. In addition, X-ray absorption fine structure (XAFS) or nuclear magnetic resonance (NMR) would help information on more detailed local relaxation structure to determine. It is thought that optimized electrochemical test techniques are also essential to investigate the

contribution of relaxation effect to real battery operation, especially to high rate operation condition and downtime of battery.

LIST OF PUBLICATIONS

This dissertation entitled "Relaxation Analysis of Cathode Materials for Li-Ion Secondary Battery" is based on the following publications.

< Chapter 3 >

Im Sul Seo, Seungwon Park, and Takeshi Yao

"Relaxation Phase Analysis of $LiMn_2O_4$ Cathode for Secondary Li Ion Battery"

Zero-Carbon Energy Kyoto 2011, Edited by T. Yao, Green Energy and Technology, Springer, Pages 165-170 (2011)

< Chapter 4 >

Im Sul Seo, Seungwon Park, and Takeshi Yao

"Relaxation Phase Analysis of Li inserted Li-Mn-O Cathode for Secondary Li Ion Battery"

ECS Electrochemistry Letters, Volume 2, Issue 1, Pages A6-A9 (2013)

< Chapter 5 >

Im Sul Seo, Shota Nagashima, Shigeomi Takai, and Takeshi Yao

"Relaxation Analysis of Li-Co-O Cathode Material for Li Ion Secondary Batteries"

ECS Electrochemistry Letters, Volume 2, Issue 7, Pages A72-A74 (2013)

ACKNOWLEDGEMENT

For all those who provided encouragement and support in my research study and life of studying abroad, I would like to express my heartfelt thanks.

First of all, I express my deep gratitude to my supervisor, Professor Takeshi Yao of Department of Fundamental Energy Science, Graduate School of Energy Science, Kyoto University. His constant support and considerate guidance during the course of this work have allowed me to learn how to think about problems and how to solve them as a scientist. And his kind encouragements have been helpful in my learning and life.

I would like to express thanks to Professor Takashi Morii, Professor Takashi Sagawa and Professor Rika Hagiwara of Department of Fundamental Energy Science, Graduate School of Energy Science, Kyoto University for their helpful suggestions, discussions and comments for this study.

And I grateful to Professor Ki Woo Nam of Department of Materials Science and Engineering, Pukyong National University for his considerate encouragements and constant support for many a long year.

I am indebted to Professor Shigeomi Takai of Graduate School of Energy Science, Kyoto University for his helpful comments and discussions.

I would like to thank to Assistant Professor Takeshi Yabutsuka of Graduate School of Energy Science, Kyoto University for his kind encouragement and helpful advices.

I am grateful to be supported by “Energy Science in the Age of Global Warming” of Global Center of Excellence (G-COE) program (J-051) of the Ministry of Education, Culture, Sports, Science and Technology of Japan, and grant-in-Aid for Challenging Exploratory Research (24656581) of the Ministry of Education, Culture, Sports, Science and Technology (MEXT) that made this research study successfully possible in Japan.

I especially would like to express my gratitude to Dr. Seungwon Park and Mr. Shota Nagashima of Functional Solid State Chemistry Laboratory for their support on study and helps on the experiments.

I would like to express my deep appreciation to Ms. Ayaka Kotera, a secretary of Functional Solid State Chemistry Laboratory for a lot of helps and warm encouragement in my life of studying abroad.

I express my gratitude to Functional Solid State Chemistry Laboratory members, Mr. Hiroshi

Tsubouchi, Mr. Shota Uraki, Mr. Kaoru Takasu, Mr. Taichi Iwai, Mr. Yuya Kawai for their a lot of helps.

I am particularly grateful to my family for perpetual support and constant encouragement.

September, 2013

Imsul Seo